WL-TR-91-2073

PRELIMINARY DEVELOPMENT OF A THREE-DIMENSIONAL NONLINEAR APPROXIMATION PROCEDURE FOR TURBOMACHINERY DESIGN OPTIMIZATION APPLICATIONS

Stephen S. Stahara
Jasopin Lee
John R. Spreiter

RMA Aerospace, Inc.
883 North Shoreline Blvd., Suite B200
Mountain View, CA 94043

20 August 1991

Final Report for Period November 1985 to February 1991

AERO PROPULSION AND POWER DIRECTORATE
WRIGHT LABORATORY
AIR FORCE SYSTEMS COMMAND
WRIGHT-PATTERSON AIR FORCE BASE, OHIO 45433-6563

NOTICE

When Government drawings, specifications, or other data are used for any purpose other than in connection with a definitely Government-related procurement, the United States Government incurs no responsibility nor any obligation whatsoever. The fact that the government may have formulated, or in any way supplied the said drawings, specifications, or other data, is not to be regarded by implication or otherwise in any manner construed, as licensing the holder or any other person or corporation, or as conveying any rights or permission to manufacture, use, or sell any patented invention that may in any way be related thereto.

This report is releaseable to the National Technical Information Service (NTIS). At NTIS, it will be available to the general public, including foreign nations.

This technical report has been reviewed and is approved for publication.

Scott M. Richardson

SCOTT M. RICHARDSON
Project Engineer
Technology Branch

Francis R. Ostdiek

FRANCIS R. OSTDIEK
Chief, Technology Branch
Turbine Engine Division

FOR THE COMMANDER

Robert E. Henderson

ROBERT E. HENDERSON
Deputy for Technology
Turbine Engine Division
Aero Propulsion & Power Directorate

If your address has changed, if you wish to be removed from out mailing list, or if the addressee is no longer employed by your organization, please notify WL/POTX, Wright-Patterson AFB, OH 45433-6563 to help us maintain a current mailing list.

Copies of this report should not be returned unless return is required by security considerations, contractual obligations, or notice on a specific document.

SECURITY CLASSIFICATION OF THIS PAGE

REPORT DOCUMENTATION PAGE

Form Approved OMB No. 0704-0188

1a. REPORT SECURITY CLASSIFICATION Unclassified	1b. RESTRICTIVE MARKINGS None
2a. SECURITY CLASSIFICATION AUTHORITY	3. DISTRIBUTION/AVAILABILITY OF REPORT Approved for public release; distribution unlimited
2b. DECLASSIFICATION/DOWNGRADING SCHEDULE	
4. PERFORMING ORGANIZATION REPORT NUMBER(S) RMA TMR 0101	5. MONITORING ORGANIZATION REPORT NUMBER(S) WL-TR-91-2073
6a. NAME OF PERFORMING ORGANIZATION RMA Aerospace 6b. OFFICE SYMBOL (*If applicable*)	7a. NAME OF MONITORING ORGANIZATION Aero Propulsion and Power Directorate Wright Laboratory, AFSC
6c. ADDRESS (*City, State, and ZIP Code*) 883 North Shoreline Blvd., Suite B200 Mountain View, CA 94043	7b. ADDRESS (*City, State, and ZIP Code*) WL/POTX WPAFB, OH 45433-6563
8a. NAME OF FUNDING/SPONSORING ORGANIZATION 8b. OFFICE SYMBOL (*If applicable*)	9. PROCUREMENT INSTRUMENT IDENTIFICATION NUMBER F33615-85-C-2591
8c. ADDRESS (*City, State, and ZIP Code*)	10. SOURCE OF FUNDING NUMBERS PROGRAM ELEMENT NO. 61102F; PROJECT NO. 2307; TASK NO S1; WORK UNIT ACCESSION NO. 45

11. TITLE (*Include Security Classification*)
Preliminary Development of a Three-Dimensional Nonlinear Approximation Procedure for Turbomachinery Design Optimization Applications

12. PERSONAL AUTHOR(S)
S.S. Stahara, J.Lee, and J.R. Sprieter

13a. TYPE OF REPORT	13b. TIME COVERED	14. DATE OF REPORT (*Year, Month, Day*)	15. PAGE COUNT
Final Report	FROM 11/85 TO 2/91	1991 August 20	103

16. SUPPLEMENTARY NOTATION

17. COSATI CODES			18. SUBJECT TERMS (*Continue on reverse if necessary and identify by block number*)
FIELD	GROUP	SUB-GROUP	
01	01		Turbomachinery Design Optimization
01	03		Computational Fluid Dynamics

19. ABSTRACT (*Continue on reverse if necessary and identify by block number*)

A theoretical investigation was carried out involving the preliminary development of a novel three-dimensional nonlinear approximation method capable of rapidly determining approximate solutions for highly nonlinear flows such as typically occur in turbomachiniery applications. The ultimate goal of the study was the preliminary demonstration of the accuracy and utility of such a method in the three-dimensional turbomachinery design environment. The specific objectives of the present investigation were the theoretical development of the three-dimensional approximation procedure for highly sensitive, nonlinear flows involving multiple shock waves, combination of the approximation method with a nonlinear three-dimensional supercritical transonic flow solver, coupling of the combined approximation method and nonlinear flow solver with an optimization design procedure, and finally testing of the complete approximation/flow solver/optimization code on problems relevant to the turbomachinery design environment.

20. DISTRIBUTION/AVAILABILITY OF ABSTRACT ☒ UNCLASSIFIED/UNLIMITED ☐ SAME AS RPT ☐ DTIC USERS	21. ABSTRACT SECURITY CLASSIFICATION Unclassified
22a NAME OF RESPONSIBLE INDIVIDUAL Scott M. Richardson	22b. TELEPHONE (*Include Area Code*) (513) 255-4780 22c. OFFICE SYMBOL WL/POTX

DD Form 1473, JUN 86 *Previous editions are obsolete.* SECURITY CLASSIFICATION OF THIS PAGE

TABLE OF CONTENTS

	PAGE
SUMMARY	1
1. INTRODUCTION	2
2. ANALYSIS	4
2.1 Description of the Nonlinear Approximation Concept	4
2.2 Previous Applications of the Approximation Method	6
2.3 Theoretical Formulation: Approximation Method Prediction of Surface Properties on 3-D Turbomachinery Blades	7
3. RESULTS	14
3.1 Development of Multiple Invariant Point Characterization Procedure for Surface Shock Waves	14
3.2 Multiple Invariant Point Characterization and Invariant Point Preprocessing Procedure	18
3.3 Coupling of 3-D Approximation Method and 3-D Flow Solver With Design Optimization Procedures	20
3.3.1 Selection of Design Optimization Procedure	20
3.3.2 Definition of 3-D Turbomachinery Design Optimization Problem for Testbed Case Studies With Approximation Method	23
3.3.3 Results of Combined Approximation Method and Optimization Procedure for 3-D Design Optimization Case Studies	24
3.4 Extended Invariant Point Relocation Procedure and Postprocessing of Approximation Results	27
3.5 Alternative Formulation of Approximation Method With Flow Field Rather Than Surface Properties	34
4. CONCLUSIONS AND RECOMMENDATIONS	39
REFERENCES	43
FIGURES	46

PRELIMINARY DEVELOPMENT OF A THREE-DIMENSIONAL NONLINEAR APPROXIMATION PROCEDURE FOR TURBOMACHINERY DESIGN OPTIMIZATION APPLICATIONS

Stephen S. Stahara, Jasopin Lee,
and John R. Spreiter

SUMMARY

A theoretical investigation was carried out involving the preliminary development of a novel three-dimensional nonlinear approximation method capable of rapidly determining approximate solutions for highly nonlinear flows such as typically occur in turbomachinery applications. The ultimate goal of the study was the preliminary demonstration of the accuracy and utility of such a method in the three-dimensional turbomachinery optimization design environment. The specific objectives of the present investigation were the theoretical development of the three-dimensional approximation procedure for highly sensitive, nonlinear flows involving multiple shock waves, combination of the approximation method with a nonlinear 3-D supercritical transonic flow solver, coupling of the combined approximation method and nonlinear flow solver with an optimization design procedure, and finally testing of the complete approximation/3-D flow solver/optimization code on problems relevant to the three-dimensional turbomachinery design optimization environment.

1. INTRODUCTION

The remarkable success of advanced computational methods for determining accurate solutions to increasingly complex fluid dynamic phenomena has now been well established across a broad range of flow problems of practical interest. What has also become simultaneously apparent with this success is that a major impediment exists to the implementation of these emerging codes when employed in highly-repetitive usage applications. This is due to the excessive computational demands required by their straightforward application. Many such applications simply cannot afford the computational cost associated with the repetitive use of these high-level numerical solvers. Consequently, a need clearly exists for the development and implementation of complimentary nonlinear approximation methods that are sufficiently general and accurate to be used in conjuction with these advanced codes to reduce their computational demands. While this need exists across a spectrum of aerodynamic and fluid dynamic uses, it is particularly high in turbomachinery applications. For that application, both the basic fluid dynamic computation is highly time consuming and the number of variable flow and geometry parameters are large, resulting in any turbomachinery parametric or design study being computationally expensive under the best of circumstances, and in many instances using more advanced codes prohibitively so.

The ultimate objective beyond this initial study is to develop and demonstrate the feasibility of such approximation methods for substantially reducing the overall computational requirements necessary for general 3-D turbomachinery design or parametric optimization. It is conceived that these approximation methods would be coupled with high run-time 3-D turbomachinery computational flow solvers, and would be used in conjunction with these solvers in applications where large numbers of related solutions are needed. The computational time saving would be accomplished by employing these rapid approximation methods to decrease to a minimum the actual number of expensive 3-D flow solutions needed in any optimization or design study. The actual implementation would entail coupling the rapid approximation method with a 3-D tubomachinery flow solver and a design optimization procedure into a combined code, and then employing the approximation method in the combined code together with a certain minimum number of pre-determined 3-D flow solutions to then predict all of the flow solutions subsequently required by the optimization driver as that procedure searches through the design variable solution space to reach the final optimum design point.

That such procedures are in fact achievable has been successfully demonstrated for two-dimensional flows. In studies made by the present author and reported in Refs. 1-7, a remarkable nonlinear approximation method was developed and extensively tested on a wide range of both continuous and discontinuous nonlinear flow problems. Its ability to accurately predict nonlinear solutions of primary interest to this study was first confirmed in case studies invoiving a variety of strongly nonlinear transonic flows. The method was then coupled with an optimization procedure and tested on several two-

dimensional design problems. The results demonstrated the potential of the approximation method to reduce the computational work in such applications by an order in magnitude with no degradation in accuracy of the final optimized design result.

The theoretical basis of the approximation procedure encompasses both inviscid and viscous flows, 2-D and 3-D situations, and both steady and unsteady flows. It has been developed most extensively for the steady situation, however, and primarily focused in initial design applications toward design/optimization studies of highly-nonlinear 2-D internal and external transonic flows. A notable point regarding the development and use of the approximation method for the application described here is that the method does not depend on any particular turbomachinery flow analysis code. Consequently, obsolescence of the methodology due to future analysis code development is not a factor.

The work reported here involves the initial development and extension of these methods and concepts to the three-dimensional turbomachinery optimization design problem. The specific implementation involves development of the nonlinear approximation method in a form suitable for predicting surface properties on three-dimensional turbomachinery blades; and then integration of that form of the approximation method with a 3-D design optimization procedure. The QNMDIF optimization procedure recently developed at NASA/Ames Research Center and successfully demonstrated in a variety of aerodynamic design optimization applications (Ref. 8) was selected for implementation in this study. That procedure consists of the QNMDIF optimization driver (Ref. 9) coupled with the TWING three-dimensional full potential solver (Ref. 10) for determining supercritical transonic flows past wing or isolated 3-D blade geometries.

2. ANALYSIS

2.1 Description of the Nonlinear Approximation Concept

The classical approach of developing a perturbation or approximation analysis - that is, by establishing and solving a series of linear perturbation equations in the manner elegantly described and illustrated by Van Dyke (Ref. 11) -- appears as an obvious choice for the current application. However, results from the work reported in Ref. 1 demonstrate that for applications to sensitive flows such as occur in most turbomachinery situations, the basic linear variation assumption fundamental to such a technique is sufficiently restrictive that the permissible range of parameter variation is so small to be of little practical use. An interesting and novel alternative to the linear perturbation equation approach has recently been successfully examined in which a correction or approximation technique is used that employs two or more nonlinear base solutions. For the approximation method, the basic solution is determined simply by differencing two nonlinear flow solutions removed from one another by some nominal change of a particular flow or geometrical quantity. A unit approximation solution is then obtained by dividing that result by the change in the varied quantity. Related solutions are determined by multiplying the unit approximation solution by the desired parameter change and adding that result to the base flow solution. This simple procedure, however, only works directly for continuous flows for which the parameter change does not alter the solution domain. For those parameter changes which change the flow domain, coordinate stretching is necessary to ensure proper definition of the unit approximation solution. Similarly, for discontinuous flows, coordinate straining is necessary to account for movement of discontinuities due to the parameter change. We will discuss in detail the importance of coordinate straining to the approximation method below.

The attractiveness of such an approximation method is that it is not restricted to a linear variation range but rather replaces the nonlinear variation between two base solutions with a linear fit. This de-emphasizes the dependence and sensitivity inherent in the linear perturbation equation method on the local rate of change of the base flow solution with respect to the varied quantity. For many applications, particularly at supercritical transonic speeds, the flow is highly sensitive, and the linear range of parameter variation can be sufficiently small to be of no practical use. Furthermore, other than the approximation of a linear fit between two nonlinear base solutions, this new method is not restricted by any further approximations with respect to the governing differential equations and boundary conditions. Rather, it retains the full character of the original methods used to calculate the base flow solutions. Most importantly, no perturbation differential equations have to be posed and solved, only algebraic ones. In fact, it isn't even necessary to know the exact form of the perturbation equation, only that it can be obtained by some systematic procedure and that the perturbations thus defined will behave in some 'generally appropriate' fashion so as to permit a logical perturbation analysis. For situations involving variations of physical parameters, such as reported here, the governing perturbation equations are

usually transparent, or at least readily derivable. Finally, in applying this method it isn't necessary to work with primitive variables; rather the procedure can be applied directly to the final solution quantity desired. An important qualification of this method is that the two base solutions required for each parameter change considered must be topologically similar, i.e., discontinuities or other characteristic features must be present in both base solutions used to establish the unit approximation solution.

The concept of employing coordinate straining to remove nonuniformities from perturbation solutions of nonlinear problems is well established and was originally suggested by Lighthill (Ref. 12) four decades ago. The basic idea of the technique is that a straightforward perturbation solution may possess the appropriate form, but not quite at the appropriate location. The procedure is to strain slightly the coordinates by expanding them as well as the dependent variables in an asymptotic series. It is often unnecessary to actually solve for the straining. It generally can be established by inspection. The final uniformly valid solution is then found in implicit form, with the strained coordinate appearing as a parameter.

In the original applications of the method (Ref. 11), it was applied in the 'classical' sense; that is, series expansions of the dependent and independent variables in ascending powers in some small parameter were inserted into the full governing equation and boundary conditions, and the individual terms of the series determined. An ingenious variation in the application of the method was made by Pritulo (Ref.13) who demonstrated that if a perturbation solution in unstrained coordinates has been determined and found to be nonuniform, the coordinate straining required to render that solution uniformly valid can be found by employing straining directly in the known nonuniform solution, and then solving algebraic rather than differential equations. The idea of introducing strained coordinates a posteriori has since been applied to a variety of different problems (Ref. 11) and forms the basis of the current application.

The fundamental idea underlying coordinate straining as it relates to the application of perturbation or approximation methods to nonlinear flows as we apply them here is illustrated geometrically in Figure 1. In the upper plot on the left, two typical transonic pressure distributions are shown for a highly supercritical flow about a nonlifting symmetric profile. The distributions can be regarded as related nonlinear flow solutions separated by a nominal change in some geometric or flow parameter. The shaded area between the solutions represents the perturbation result that would be obtained by directly differencing the two solutions. We observe that the perturbation so obtained is small everywhere except in the region between the two shock waves, where it is fully as large as the base solutions themselves. This clearly invalidates the perturbation technique in that region and most probably somewhat ahead and behind it as well. The key idea of a procedure for correcting this, pointed out by Nixon (Refs. 14,15), is first to strain the coordinates of one of the two solutions in such a fashion that the shock waves align, as shown in the upper plot on the right of Figure 1, and then determine the unit perturbation. Equivalently, this can be considered as maintaining the shock wave location invariant during the

perturbation process, and assures that the unit perturbation remains small both at and in the vicinity of the shock wave. Obviously, shock points are only one of a number of characteristic high-gradient locations such as stagnation points, maximum suction pressure points, etc., in which the accuracy of the perturbation solution can degrade rapidly. The plots in the lower left part of the Figure 1 indicate such a situation and display typical supercritical transonic pressure distributions which contain multiple shocks and high-gradient regions. Simultaneously straining at all these locations so as to align all of the characteristic points associated with each shock or high-gradient maxima or minima, as indicated in the lower right plot, serves to minimize the unit perturbation over the entire domain considered, and provides the key to maximizing the range of validity of the approximation method. Finally, it is important to recognize that while the approximation method replaces the nonlinear variation between two nonlinear base solutions with a linear fit, the resultant approximation solution is nonlinear in the varied parameter because of the implicit nature of coordinate straining. This apparently is the basis of the extended range of accuracy of the method.

Because the method of strained coordinates is known to be nonapplicable to certain classes of perturbation problems, or worse, appear to be applicable while producing incorrect results (Ref. 11), the point arises as to its use in the present context. The question is not whether the method will produce a uniformly valid solution -- the expansion procedure guarantees that -- but whether the solution so produced may be incorrect inherently. Unfortunately, unlike the method of matched asymptotic expansions, there are no firm rules which guarantee the correctness of strained coordinate solutions. There are, nevertheless, some generally reliable guidelines. The method of strained coordinates appears to always succeed when the singularity predicted by the direct unstrained problem actually exists. In our applications, this is always the case, since we identify the singularity or invariant points as shock points, stagnation points, and other physically identifiable points. Furthermore, we restrict the allowable range of parametric variation such that the neighboring calibration and predicted flows retain these same points and create no new ones. Therefore, invariant points are neither lost nor generated over the solution domain of interest. These considerations effectively insure that the predicted approximation solutions will both be physically correct and, additionally, will not violate the basic straining principle (Ref. 11) regarding compounding of singularities.

2.2 Previous Applications of the Approximation Method

At this point, the approximation concept based on the ideas discussed above has both been implemented and thoroughly tested in a wide range of problems. In Ref. 1, several candidate approximation methods were studied and the most promising method was identified. Extensive development and testing of that method was then carried out in Ref. 4 on a large number of nonlinear flow problems involving single-parameter changes of a variety of flow and geometric parameters. Subcritical and supercritical flows past isolated airfoils and

compressor cascades were considered, with particular emphasis placed on supercritical transonic flows which exhibited large surface shock movements over the parametric range studied. Comparisons of the approximation predictions with the corresponding "exact" nonlinear solutions indicated a remarkable accuracy and range of validity of the approximation method. For example, Figure 2 from Ref. 4 provides a comparison of results illustrating the remarkable ability of the approximation method to predict nonlinear supercritical transonic flows. These results are for surface pressures obtained from full potential solutions and represent nonlifting flows past several NASA four-digit, thickness-only airfoils at $M_\infty = 0.820$. The results indicated by the dotted and dashed lines were obtained for thickness ratios of $\tau = 0.12$ and 0.08, respectively. Those results were used to define the unit perturbation required by the approximation method. With that unit perturbation in hand, the approximation method was then employed to predict surface pressure results for thickness ratios $\tau = (0.110, 0.105, 0.100, 0.095)$. The approximation results, indicated by the open symbols, were then compared with full nonlinear results obtained by running the full potential solver at those thickness ratios. As can be seen, the results are essentially identical, in particular, in the region of the strong shock.

The approximation method was next extended in Ref. 6 to treat simultaneous multiple-parameter perturbations. Extensive testing of the method demonstrated remarkable accuracy and range of validity of the multiple-parameter approximation procedure in direct correspondence with the previous results obtained for single-parameter changes. Additionally, initial applications of the multiple-parameter approximation method combined with an optimization procedure were also made to several two-dimensional airfoil design problems. The results demonstrated the potential of the approximation method for reducing the computational work in certain applications by an order of magnitude with no degradation in accuracy. Finally, in Ref. 7, the approximation method, configured in a form suitable for predicting an arbitrary number of simultaneous multiple parameter changes, was combined with the COPES/CONMIN optimization driver (Ref. 16) and coupled with the NASA TSONIC full potential blade-to-blade turbomachinery solver (Ref. 17). A series of calculations of the combined code, named BLDOPT, have verified the procedure, demonstrated the accuracy of the approximation-predicted results, and established benchmark guidelines of the potential for computational savings of the method under the various user options included in the code. In general, the approximation method was found to be capable of providing an order of magnitude reduction in computational work in those applications which involved essentially subcritical or weakly supercritical turbomachinery flows.

2.3 Theoretical Formulation: Approximation Method Prediction of Surface Properties on 3-D Turbomachinery Blades

The underlying reason for the remarkable accuracy of the approximation method developed in this study lies in the use of coordinate straining to define the unit perturbation. As shown in Figure 1, where the perturbation between two nonlinear solution states is displayed graphically as the shaded area

between the base and the strained and unstrained calibration solution, coordinate straining provides the ability to account accurately for the displacement of a multiple number of discontinuities and maxima of high-gradient regions due to a parameter change. This enables the perturbation method to maintain very high accuracy in regions of high gradients where most perturbation methods commonly fail, and to maintain that accuracy over large parametric ranges.

In what follows, we provide a brief account of the theoretical essentials of the strained-coordinate perturbation concept as configured and implemented in the present design application. This is to predict simultaneous multiple-parameter perturbation flow solutions for surface properties of supercritical wings for use in optimized wing design. The flow solutions thus considered can contain a total number of N discontinuities or high-gradient continuous regions.

To proceed with the theoretical basis of the approximation method as applied to simultaneous multiple-parameter perturbations of flows containing multiple shocks or high-gradient regions, consider the formulation of the procedure at the full potential equation level, since all of the results presented here are based on that level. Denote the operator L acting on the full velocity potential Φ as that which results in the three dimensional full-potential equation for Φ, i.e.,

$$L[\Phi] = 0 \tag{1}$$

If we now expand the potential in terms of zero and higher-order components in order to account for the variation of M arbitrary geometrical or flow parameters q_j from their base flow values q_{o_j}

$$\Phi = \Phi_o + \sum_{j=1}^{M} \varepsilon_j \Phi_{1_j} + \ldots$$

$$q_j = q_{o_j} + \Delta q_j \tag{2}$$

and then insert these expansions into the governing Equation (1), expand the result, order the equations into zero and first-order components, and make the obvious choice of expansion parameters $\varepsilon_j = \Delta q_j$ we obtain the following governing equations for the zero and M first-order components

$$L[\Phi_o] = 0$$

$$L_1[\Phi_{1_j}] + \frac{\partial}{\partial q_j} L[\Phi_o] = 0 \tag{3}$$

Here L_1 is a linear operator whose coefficients depend on zero-order quantities and $\partial L[\Phi_o]/\partial q_j$ represents a "forcing" term due to the q_j^{th} perturbation. Actual

forms of L_1 and the "forcing" term are provided in Ref. 1 for a variety of flow and geometry parameter perturbations of two-dimensional turbomachines, and in Ref. 18 for profile shape perturbations of an isolated airfoil. An important point regarding Equation (3) for the first-order perturbations is that these equations represent a unit perturbation independent of the actual value of the perturbation quantity ε_j.

Appropriate account of the movement of a multiple number of discontinuities and maxima of high-gradient regions due to the changes in the parameters q_j is now accomplished by the introduction of strained coordinates (s,t) in the form

$$x = s + \sum_{j=1}^{M} \varepsilon_j x_1 (s,t)$$

$$y = t + \sum_{j=1}^{M} \varepsilon_j y_1 (s,t) \tag{4}$$

where

$$x_1(s,t) = s + \sum_{i=1}^{N} \delta x_i (t)\, x_{1_i} (s,t)$$

$$y_1(s,t) = \sum_{i=1}^{N} \delta y_i\, y_{1_i} (s,t) \tag{5}$$

and $\varepsilon_j \delta x_i$, $\varepsilon_j \delta y_i$ represent individual x and y displacements due to perturbation of the q_j^{th} parameter of the N strained points, and $x_{1_i}(s,t)$, $y_{1_i}(s,t)$ are straining functions associated with each of the N strained points. For the applications considered here, we have assumed that all discontinuities such as shock waves or other high-gradient region maxima occur essentially normal to the wing planform so that only the (x,y) coordinates require straining. This simplification is not strictly necessary and could be relaxed in future applications. However, the effect of this assumption on the prediction of surface properties via the approximation method is known from extensive studies of the two-dimensional case to be of higher order for most optimized design flow situations of aerodynamic interest. Introducing the strained coordinate Equations (4) and (5) into the expansion formulation leaves the zero-order result in Equation (3) unchanged, but results in a change of the following form for the j^{th} perturbation

$$L_1 [\Phi_{1_j}] + L_{2_j} [\Phi_0] + \frac{\partial}{\partial q_j} L [\Phi_0] = 0 \tag{6}$$

Here the operators are understood to be expressed in terms of the strained (s,t) coordinates, and the additional operator L_{2_j} arises specifically from

displacement of the strained points. In Refs. 15 and 18, specific expressions for L_{2_j} are provided for selected perturbations involving transonic small-disturbance and full-potential equation formulations. The essential point, however, with regard to perturbation Equation (6) expressed in strained coordinates is that it remains valid as before for a unit perturbation and independent of ε_j.

In employing the approximation method, Equation (6) for the j^{th} unit perturbation is solved by taking the difference between two solutions obtained by the full nonlinear procedure after appropriately straining the coordinates. If we designate the solutions for some arbitrary dependent flow quantity Q as base Q_o and calibration Q_{c_j}, respectively, of the varied independent parameter q_j, we have for the predicted flow at some new parameter value q_j for all the M parameters

$$Q(x,y) = Q_o(s,t) + \sum_{j=1}^{M} \varepsilon_j Q_{1_j}(s,t) + \ldots \tag{7}$$

where

$$Q_{1_j}(s,t) = \frac{Q_{c_j}(\tilde{x}_j,\tilde{y}_j) - Q_o(s,t)}{\tilde{\varepsilon}_j} \tag{8}$$

$$\tilde{x}_j(s,t) = s + \sum_{i=1}^{N} \tilde{\varepsilon}_j \delta x_i(t)\, x_{1_i}(s,t) \tag{9}$$

$$\tilde{y}_j(t) = t + \sum_{i=1}^{N} \tilde{\varepsilon}_j \delta y_i\, y_{1_i}(t) \tag{10}$$

$$x = s + \sum_{j=1}^{M} \frac{\varepsilon_j}{\tilde{\varepsilon}_j} (\tilde{x}_j(s,t) - s) \tag{11}$$

$$y = t + \sum_{j=1}^{M} \frac{\varepsilon_j}{\tilde{\varepsilon}_j} (\tilde{y}_j(t) - t) \tag{12}$$

$$\tilde{\varepsilon}_j = q_{c_j} - q_{o_j} \tag{13}$$

$$\varepsilon_j = q_j - q_{o_j} \tag{14}$$

We note that in order to determine the first-order corrections $Q_{1_j}(s,t)$, we require one base and M calibration solutions in which the calibration solutions are determined by varying each of the M arbitrary independent parameters q_j by some nominal amount from the base flow value while keeping the other fixed at

their base values. In this way, the first-order corrections Q_{1_j} can be determined from Equation (8) where Q_{c_j} is defined as the calibration solution corresponding to changing the j^{th} parameter to a new value q_{c_j}, $\bar{x}_j$ is the strained coordinate pertaining to the Q_{c_j} calibration solution, and $\bar{\varepsilon}_j = q_{c_j} - q_{o_j}$ represents the change in the q_j parameter from its base flow value. Thus,

$$\bar{\varepsilon}_j \delta x_i(t) = (x_i^C(t) - x_i^O(t))_j \tag{15}$$

$$\varepsilon_j \delta x_i(t) = \frac{\varepsilon_j}{\bar{\varepsilon}_j} (x_i^C(t) - x_i^O(t))_j \tag{16}$$

$$\bar{\varepsilon}_j \delta y_i = (y_{T_i}^C - y_{T_i}^O)_j \tag{17}$$

$$\varepsilon_j \delta y_i = \frac{\varepsilon_j}{\bar{\varepsilon}_j} (y_{T_i}^C - y_{T_i}^O)_j \tag{18}$$

where $\varepsilon_j \delta x_i(t)$ given in Equation (15) represents the x displacement of the i^{th} invariant line at the spanwise t location in the j^{th} calibration solution from its base flow location due to the selected change $\bar{\varepsilon}_j$ in the q_j parameter given by Equation (13), $\varepsilon_j \delta x_i(t)$ given in Equation (16) represents the predicted x displacement of the i^{th} invariant line at the spanwise t from its base flow location due to the desired change ε_j in the q_j parameter given by Equation (14), $\bar{\varepsilon}_j \delta y_i$ given in Equation (17) represents the y displacement of the tip of the i^{th} invariant line in the j^{th} calibration solution from its base flow location due to the selected change $\bar{\varepsilon}_j$ in the q_j parameter given by Equation (13), and $\varepsilon_j \delta y_i$ given in Equation (18) represents the predicted y displacement of the tip of the i^{th} invariant line from its base flow location due to the desired change ε_j in the q_j parameter given by Equation (14), $x_{1_i}(s,t)$ is a unit-order straining function having the property that

$$x_{1_i}(x_k^O(t),t) = \begin{cases} 1 & k = i \\ 0 & k \neq i \end{cases} \tag{19}$$

which assures alignment of the i^{th} invariant line at the t spanwise location between the base and calibration solutions, and $y_i(t)$ is a unit-order straining function having the property that

$$y_{1_i}(y_T^O)_k = \begin{cases} 1 & k = i \\ 0 & k \neq i \end{cases} \tag{20}$$

which assures alignment of the tip of the i^{th} invariant line between the base and calibration solutions.

In addition to the single conditions given by Equation (19) and (20) on the straining functions, it may be convenient or necessary to impose additional conditions at other locations along the contour. For example, it is usually necessary to hold invariant the end points along the contour, as well as to require that the straining vanish in a particular fashion in those locations. All of these conditions, however, do not serve to determine the straining uniquely. The nonuniqueness of the straining, nevertheless, can often be turned to advantage, either by selecting particularly simple classes of straining functions or by requiring the straining to satisfy further constraints convenient for a particular application.

The fact of nonuniqueness of straining function, however, raises a further question of the dependence of the final approximation-predicted result on choice of straining function. An initial example of the effect of employing two different straining functions for a strongly supercritical two-dimensional flow was provided in Ref. 15, and in Ref. 4 a detailed examination was made of the dependence of approximation results on several classes of different straining functions. Although it can be demonstrated (Ref. 15) that the final approximation-predicted result obtained when employing strained coordinates is formally independent of the particular straining function used -- provided that the straining function moves the invariant points to the proper locations -- the results of Ref. 4 demonstrate that, under certain conditions, particular classes of straining functions can induce spurious approximation results. The underlying reason is that, while the approximation-predicted results at and in the vicinity of invariant points are independent of the choice of straining function (provided invariant point locations are preserved), some classes of straining functions have the undesirable property of producing unwanted straining in certain regions removed from the invariant points. The correction for this deficiency, which was found in Ref. 4 and has proven effective in all case studies undertaken, is to employ linear piecewise-continuous straining functions. This both preserves the accuracy of the approximation results in the vicinity of the invariant points, and introduces no excessive straining in regions removed from those locations.

For linear piecewise-continuous straining functions, the functional forms of the straining can be compactly written. For the x displacement we have

$$\tilde{x}_j(s,t) = s + \left\{ \frac{x^o_{i+1}(t) - s}{x^o_{i+1} - x^o_i} \bullet (x^c_i(t) - x^o_i(t))_j + \frac{s - x^o_i(t)}{x^o_{i+1}(t) - x^o_i(t)} \bullet (x^c_{i+1}(t) - x^o_{i+1}(t))_j \right\}$$

$$\bullet H(x^o_{i+1}(t) - s) \bullet H(s - x^o_i(t)) \qquad (21)$$

where H denotes the Heaviside step function. As discussed above, it is usually necessary to hold invariant both of the end points along the contour in addition to the points corresponding to discontinuities or high-gradient maxima. Consequently, for the results reported here, the array of x invariant points in the base and calibration solutions have been taken as

$$x_i^o(t) = \{0,\ x_1^o(t),\ x_2^o(t), \ldots,\ x_n^o(t),\ 1\}$$

$$x_{i\,j}^c(t) = \{0,\ x_{1j}^c(t),\ x_{2j}^c(t), \ldots,\ x_{nj}^c(t),\ 1\} \tag{22}$$

where the contour length at the spanwise location t has been normalized to unity and where n is the number of invariant points along the contour exclusive of the end points.

Similarly, for the y displacements of the tips of the continuity lines we have

$$\bar{y}_j(t) = t + \left\{ \frac{y_{T_{i+1}}^o - t}{y_{T_{i+1}}^o - y_{T_i}^o} \bullet (y_{T_i}^c - y_{T_i}^o)_j + \frac{t - y_{T_i}^o}{y_{T_{i+1}}^o - y_{T_i}^o} \bullet (y_{T_{i+1}}^c - y_{T_{i+1}}^o)_j \right\}$$

$$\bullet\ H(y_{T_{i+1}}^o - t) \bullet H(t - y_{T_i}^o) \tag{23}$$

where the spanwise locations of the tips of the discontinuity lines in the base and calibration solutions have been taken as

$$y_{T_i}^o = \{y_{T_1}^o,\ y_{T_2}^o,\ y_{T_3}^o, \ldots,\ y_{T_n}^o\}$$

$$y_{T_{i_j}}^c = \{y_{T_1}^c,\ y_{T_2}^c,\ y_{T_3}^c, \ldots,\ y_{T_n}^c\}_j \tag{24}$$

3. RESULTS

3.1 Development of Multiple Invariant Point Characterization Procedure for Surface Shock Waves

Development of an accurate procedure to enable the definition and subsequent tracking of the invariant points associated with high-gradient regions, in particular, shock waves is key to the accuracy of the approximation method. Both current and previous testing of the approximation method has demonstrated the advantages of employing a multiple invariant point representation of shock waves. Results for the approximation prediction of highly nonlinear solutions via the coordinate straining procedure employed in the method clearly show that the accuracy of the predicted results are most sensitive in the vicinity of shock waves or other high gradient compressive regions. This occurs since in those regions any misalignment of the base and calibration solutions employed to determine the unit perturbations from which the approximate solutions are obtained becomes highly magnified in the approximation predicted results due to the presence of the large gradients in these regions. Hence, a single invariant point representation of a shock is quite accurate for normal or near-normal shock waves. However, for shocks that are characterized by more gradual gradients so that the flow variation is that of a highly sloped but not vertical line, predictions based on the single invariant point representation can degrade rapidly for even moderate parameter extrapolation or interpolations from the base and calibration values. A method for alleviating this degradation in accuracy is to introduce additional invariant points to characterize the shock wave. This device acts to improve the predicted approximate solution in those high gradient regions by requiring the approximate method to track more than one topological feature of the shock. Shock waves that are typically generated by most of the currently existing Navier-Stokes, Euler, and full potential flow algorithms are usually characterized by some precursor compression region upstream of the shock, a high-gradient central shock region, and a post expansion region, such as illustrated in the sketch below.

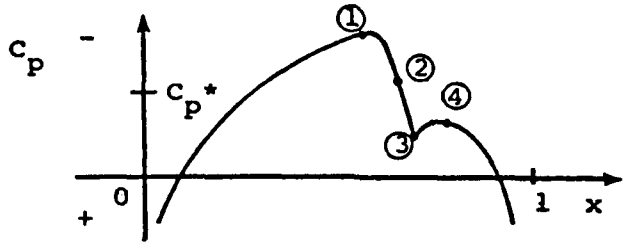

Illustration of Multiple Invariant Point Characterization for Surface Shock Wave Topology Tracking

For our purposes, a sufficiently general way to characterize such a shock would be to use four invariant points that would correspond to: (1) pre-shock minimum pressure point, (2) maximum gradient or C_p^* point, (3) post-shock maximum pressure point, and (4) post-shock minimum expansion pressure point. While such a characterization of a shock is quite general, it is not necessarily the most advantageous choice to employ in all cases. The reason is that the local topology of shock waves in many transonic flows, even over relatively small parameter ranges, can change so as to make it difficult to continuously identify all the invariant points described above. For example, in many transonic flows it is common for a change in the post-shock expansion topology to occur during a parameter variation whereby that region loses its post expansion character. The remedy for this is to use only the minimum number of invariant points needed to track a topological phenomenon over a parameter range of interest.

With regard to shock waves, we have concluded that for the class of flows of primary interest to this study that it is safe to ignore the post shock expansion region (i.e. point 4) and confine the multiple invariant point characterization to the compressive gradient portion of the shock, i.e. between points (1) and (3) illustrated above. We have done this, and have found from numerical experiments that the post expansion region remains satisfactorily predicted. Additionally, we have found that employing a third invariant point located at the maximum gradient or C_p^* location in the middle of the shock (point 2) adds no significant improvement in accuracy. Hence, for the transonic flows of concern to this study, a two invariant point characterization of shock waves is sufficient and was adopted as the standard model.

In order to track the two invariant shock points, it is necessary to establish an appropriate criteria to continuously identify them. Ideally, the criteria should be such so as to allow unambiguous identification of the invariant points throughout the anticipated range of parameter variation. In order to establish these criteria and because these shock wave invariant points play such a critical role in controlling the overall accuracy of the approximation method, it was necessary to carry out extensive numerical experimentation to identify the best criteria to set these points. As a result of this test, we have found the following strategy to identify and track the two shock wave invariant points the best of a variety of schemes.

Selection of the invariant point at the beginning of the shock was found to be best set by choosing the point where $dC_p/dx = 0$. We investigated other alternatives, such as placing the invariant point where the shock slope attains a certain value (eg. $dC_p/dx = -1$) or placement of the invariant point at a certain location upstream of the point where the pressure distribution goes through sonic ($C_p = C_p^*$). The result of these studies has shown that the choice of the point where $dC_p/dx = 0$ is the best.

Selection of the invariant point at the foot or end of the shock is more direct in the sense that the maximum pressure point behind the shock is a natural and obvious choice for termination of the shock region. However, while the choice

of the point is clear, we have found from the results of our testing that in many instances the approximation predictions in the vicinity of the shock foot degrade rapidly. Furthermore, we found that significantly improved results in that region could be achieved by modification of the location of the shock foot point. These cases occur when, due to local numerical grid spacing of the flow solver or other factors, the maximum pressure point behind a shock in the base and calibration solutions happens to lie just off the maximum gradient line of the shock, as illustrated in the sketch below on the right, rather than on the maximum gradient line as normally occurs as shown in the figure on the left.

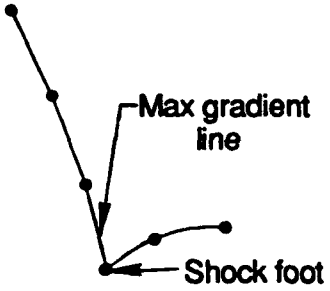

Shock Foot Point On
Max Gradient Line

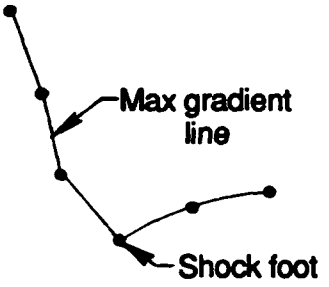

Shock Foot Point Off
Max Gradient Line

The remedy for this is to locally sharpen the shock prior to determining the unit perturbation distributions by relocating the shock foot on the maximum gradient line. We have implemented this into the approximation method, and have found that this results in significantly improved results in the predicted approximate solutions for both the location of the shock foot as well as the pressure distribution in the near vicinity of the shock foot.

Finally, even with all the careful analysis involved in the selection of the two invariant points characterizing the shock, it is inevitable in many cases involving multiple parameter perturbations that there will often occur some slight misalignment in the shock regions between the base and the various calibration solutions. This results in inaccuracies in the unit perturbations and, as a consequence, in the predicted approximation solutions. Particularly in situations involving extreme parameter extrapolation or interpolation, the predicted shock region often contains a point or points for which the results are clearly spurious. While the most direct means of eliminating this would be to employ finer grids for the computation of the base and calibration flow solutions, this is often not desirable or possible because of the increased computer storage and/or CPU costs. Consequently, what is required is a procedure for smoothing the predicted values at those points while simultaneously retaining the overall integrity of the approximation solution. We have implementated a combination of several schemes that ensure the appropriate behavior of the predicted solution in the shock region. To accomplish this, it was necessary to employ more than one smoothing procedure in order to allow for the correction of from one to a number of points in the shock region. For example, we have found it best to employ a linear smoothing correction in order to correct for one

or two points, while for three or more points it was found to be necessary to employ either quadratic or cubic least squares smoothing. The smoothing procedures developed ensure that monotonicity is maintained in both ordinate and slope throughout the predicted region.

With these procedures incorporated into the approximation method, we have performed extensive testing to verify them on difficult one, two, and three parameter perturbations involving highly nonlinear supercritical transonic flows. Figures 3 through 6 provide some examples of the remarkable predictions that the approximation method is capable of.

Figures 3a.-g. presents the results of the ability of the approximation method to predict extreme solution extrapolation results when using two very closely spaced base and calibration solutions. The base and calibration solutions shown and used to determine the unit perturbations needed for the approximation results are for highly supercritical flows past a symmetric NACA 00XX series blade profile at an oncoming Mach number of 0.82 and zero angle of attack with thickness ratios t/c = 0.115 and 0.120 for the base and calibration solutions, respectively. The predicted results indicated by open symbols are for new thickness ratios t/c = {0.110, 0.105, 0.100, 0.095, 0.090, 0.085, 0.080} and are shown in Figures 3a. to 3g. Those results are meant to be compared with the solid lines which represent the exact solutions obtained from running the flow solver at the new thickness ratios. We believe these results are remarkable in that even though the base and calibration solutions were purposely poorly selected for spanning the range of thickness ratios shown, the approximation method is able to do an excellent job of tracking the shock for extrapolations beyond 400% of the parameter difference between the base and calibration solutions. This is far beyond what any linear approximation theory is capable of achieving.

The corresponding results shown in Figures 4a.-g. are for a more reasonable choice of base and calibration solutions. For these results, the base and calibration thickness ratios were t/c ={0.900,0.110}, respectively. The predicted results are for t/c = {0.120, 0.115, 0.105, 0.100, 0.095, 0.085, 0.080}, and represent both solution interpolation and extrapolation. The approximation predictions agree extremely well with the exact results over the entire parameter range displayed.

In Figures 5a.-c. we provide results demonstrating the capability of the approximation method to simultaneously predict both upper and lower surface pressures. The results are for an angle of attack perturbation of highly supercritical flows past a NACA 0012 blade profile with oncoming Mach number M = 0.75. The base and calibration angles of attack were {1.00, 2.00} degrees, respectively, with the predicted angles at {2.50, 1.50, 0.50}. The approximation results indicated are again in good agreement with the exact solutions over the entire parameter range and on both surfaces of the blade.

Finally, in Figures 6a.-e. we provide the results of a simultaneous two-parameter perturbation of strongly nonlinear flows. The results shown are for

an oncoming Mach number and thickness ratio perturbation of a symmetric NACA 00XX blade profile at zero angle of attack. The base and calibration Mach number and thickness ratio are $M_b = 0.82$, $(t/c)_b = 0.120$, $M_c = 0.80$, $(t/c)_c = 0.110$. The predicted results are for {M, t/c} = {0.84, 0.115}, {0.83, 0.115}, {0.81, 0.115}, {0.79, 0.115}, {0.78, 0.115}. The agreement between the approximation predicted and exact nonlinear results are again excellent. We have performed many additional comparative caculations with the approximation method and have obtained similar good results as those shown above.

3.2 Multiple Invariant Point Characterization and Invariant Point Preprocessing Procedure

The first step in developing the approximation method solution is the determination of the particular invariant points to be employed to characterize the flows under consideration. For the typical nonlinear flows pertinent to this study, these invariant points can be characterized as follows: maximum pressure or stagnation point, minimum suction pressure and associated recovery points near the nose on both the upper and lower surfaces, C_p^* points denoting shock waves and their associated local minimum and maximum pressure points that characterize the initiation and termination of the shock regions. Figure 7 illustrates a 3-D pressure distribution characteristic of the ones of interest to the present study. Shown in that figure are the chordwise surface pressure distributions on both the upper and lower surfaces of a 3-D blade at 17 spanwise stations across the blade from root to tip. In locating the invariant points for this example, we begin at the trailing edge and consider the trailing edge points for both the upper and lower surface fixed. Thus, we proceed from the trailing edge point on the lower surface and move upstream searching for sonic C_p^* points and the stagnation point. If a C_p^* point is found on the lower surface, we then proceed to locate a local $dC_p/dx = 0$ point upstream of the shock and, if appropriate, search for a local maximum pressure point just downstream of the C_p^* point. After locating all the C_p^* points and their associated maximum and minimum points on the lower surface, we locate the maximum pressure or stagnation point near the nose. We then locate the minimum suction pressure point on the lower surface just downstream of the stagnation point, and the $dC_p/dx = 0$ point just downstream of the lower surface minimum suction pressure point. Next, the minimum suction pressure point on the upper surface located just downstream of the stagnation point is found, as well as the associated $dC_p/dx = 0$ points just upstream of those points and the maximum post-shock pressure points just downstream of those C_p^* points. As an example, for the sample case shown in Figure 7, nine invariant points were located according to the above criteria. These invariant points on each of the 17 chordwise pressure distributions are indicated by a (+) sign. They correspond to a C_p^* and associated $dC_p/dx = 0$ point on the lower surface near the nose, the stagnation point, the minimum suction pressure and associated

$dC_p/dx = 0$ point on the upper surface near the nose, and the maximum post-shock and associated upstream $dC_p/dx = 0$ point for the upper surface shock.

The next step in proceeding with the approximation method solution is to preprocess these numerically computed pressure distributions at each spanwise location so as to smooth them in the vicinity of the shock waves and minimum suction pressure locations. The result of this preprocessing for the example shown in Figure 7 is illustrated in Figure 8. Comparison of the results in Figure 8 with those of Figure 7 shows that as a result of the preprocessing a distinct sharpening of the shock in the vicinity of its post-shock maximum pressure has been achieved.

The final step of the preprocessing procedure is to relocate all these invariant points in each of the chordwise pressure distributions so as to ensure a globally continuous variation in the spanwise coordinate direction of the various selected points. The result of this final step of the smoothing procedure is illustrated in Figure 9. Comparison of the relocated invariant points with the original invariant points shown in Figure 7 clearly displays a smooth global variation is now present in the locations of both the $dC_p/dx = 0$ points associated with the upper surface minimum suction pressure point, and also with the upper surface post-shock maximum pressure points.

In order to demonstrate how accurately the approximation method enhanced by the new preprocessing scheme can predict strongly nonlinear 3-D flows, we have selected two different 3-D test problems. The first involves an overall thickness ratio change of an isolated 3-D blade having an ONERA M6 profile. To establish the parameter range of thickness ratios over which the approximation method would be tested, we considered changes in the overall thickness ratio of the blade from 80% to 120% in steps of 5% from its nominal value, i.e. (t/c) = {0.80, 0.85, 0.90, 0.95, 1.00, 1.05, 1.10, 1.15, 1.20} so that nine 3-D solutions were determined. These were computed at an oncoming Mach number of M = 0.86 and angle of attack of 3.06 degrees. After application of the preprocessing precedures described above, the solution for the nominal value of thickness ratio $(t/c)_{max} = 1.00$ is illustrated in Figure 10 where the chordwise upper and lower surface pressure distributions at each of the 17 spanwise locations of the 3-D grid used in the solution determination are displayed. Figures 11a.-c. provide comparisons of the approximation method at the root chord station (y/s = 0.0) when the base and calibration solutions are taken at $(t/c)_{max} = \{0.90, 1.10\}$, respectively, and the predicted results are given at $(t/c)_{max} = \{0.80, 1.00, 1.20\}$. The comparisons between the approximation method and the exact results are outstanding. Figures 12a.-c. provide similar results at the outermost spanwise station (y/s = 0.969). Again the comparisons are remarkable.

The second 3-D example problem involves a significantly more difficult test of the approximation method due to the fact that we selected it to involve an unusually large topology change in the 3-D solutions over the parameter range selected. This problem involves an oncoming Mach number parameter change

over the same 3-D blade geometry studied in the first example, but with the Mach number changing from M = 0.880 to 0.720 in steps of 0.02. Three of the nine 3-D solutions at the beginning, middle, and end of the parameter range after invariant point preprocessing are displayed in Figures 13a.-c. The large topology change is evident as we go from the strongly supercritical pressure distribution at M = 0.880 shown in Figure 13a., which has an extremely strong upper surface shock, to the subcritical distribution at M = 0.720 shown in Figure 13c., which has no upper surface shock but has an extremely pronounced and compressed upper surface minimum suction pressure region near the nose. Although such a major topology change is normally considered far beyond the assumptions under which the approximation method is valid, we have begun development of an extension of the method to allow it to at least approximate solutions through these topology changes without further recourse to yet another new set of 3-D base and calibration solutions that would cover the new topology change. This procedure involves development of a criteria to handle invariant point coalescence whereby two invariant points move toward one another and eventually meet. When that occurs, a new criteria is necessary to implement the approximation method in order to prevent the two invariant points from crossing and producing topologically spurious results. In the planned optimization applications planned for the approximation method, we believe it to be extremely advantageous if the method can continue to perform reasonably well and in an automatic fashion even under such extended circumstances. Some results of the approximation method predictions under such conditions are provided in Figures 14a.-d. These results are at the most extreme spanwise location (y/s = 0.969) along the blade, and are for a choice of base and calibration Mach numbers of M = {0.82, 0.86}, with the predictions given at M = {0.88, 0.84, 0.80, 0.72}. We clearly see the disparate differences between the base and calibration solutions in these plots. Nevertheless with regard to the comparisons, the approximation method is able to do a very reasonable job of predicting the pressure distribution change from strongly supercritical as shown in Figure 14a. to quite subcritical as shown in Figure 14d. An additional procedure to eliminate the spurious points evident behind the upper surface minimum suction pressure peak, and also to improve the approximation prediction behind the maximum suction pressure point is needed.

3.3 Coupling of 3-D Approximation Method and 3-D Flow Solver With Design Optimization Procedures

3.3.1 Selection of Design Optimization Procedure

A review was conducted of all methods and applications thereof that have been developed and applied to the general class of aerodynamic design optimization problems that are of relevance to this study. The concept of optimizing about an aerodynamic rather than structurally related design objective is relatively new (Refs. 19,20). Consequently, with one exception, comparative studies of the performance and reliability of different optimization algorithms for this class of optimization problems have not been carried out. The result has been that essentially all of the current applications involving aerodynamic optimization

studies (eg. Refs. 21-25) have involved use of the CONMIN conjugate gradient optimization method (Ref. 26), a procedure originally designed for the conceptually different problem of optimized structural design. The CONMIN method, as well as the more generalized COPES procedure (Ref. 16) which includes CONMIN as the basic optimization module but contains additional modules that provide some convenient features for carrying out certain constrained minimization problems involving side constraints and design variable bounding, have now been applied to a variety of sensitive aerodynamic design optimization problems. These have involved the optimized design of airfoils (Refs. 19,20), turbomachinery blades (Ref. 7) and wings (Refs. 23-25) at highly nonlinear supercritical transonic flow conditions. For the structural optimization problems for which the CONMIN procedure was originally developed, the method has generally performed quite satisfactorily. However, for the new class of aerodynamic optimization problems, the CONMIN procedure has demonstrated a number of deficiencies. This is not altogether surprising since structural design optimization problems typically involve large numbers (10 - 1000) of design variables and side constraints but rapid computation of the governing internal structural element solutions. In contrast, aerodynamic optimization problems typically involve relatively few design variables and side constraints but slow and expensive computations of relatively sensitive governing flow solutions.

We have reviewed all the published applications involving aerodynamic optimization problems of the general class of interest here in which the CONMIN optimization procedure has been employed. These investigations include our own substantial experiences with the CONMIN and COPES/CONMIN procedures in which we designed a pilot code for optimizing the design of blade-to-blade profiles of turbomachinery blades (Ref. 7). In assessing the performance of the CONMIN optimizer, which employs the Fletcher-Reeves conjugate gradient algorithm as the driver, all of the reported investigations appear to have encountered similar deficiencies with the method. The most significant of these is the tendency of the conjugate gradient algorithm to become focused or stuck at a local minimum, and not be able to discern that this has occurred and proceed from there toward a more global minimum. In the worst cases, the method does not move to any significant degree away from the original design. The basis of this problem lies with the manner in which the conjugate gradient method performs its optimization search. At each iteration of the technique, the gradient of the objective function with respect to each design variable is calculated and a line search is performed in the direction given by a certain linear combination of the current gradient and the last search direction. The objective function gradients are always calculated by one-sided forward differences with no provision for central differences. The step size employed can be scaled by the size of the associated variables, but is independent of the value of the objective function, its precision or its derivatives. What this ultimately means is that any variable which increases the objective function when stepped in one direction is assumed to reduce the objective function when moved in the opposite direction. This is not true when the objective is near a local minimum of one variable. It is in these regions where the method can fail disastrously. What can occur near these local minima is that as the

gradient alternates in sign about that point, the stepsize is reduced by the optimizer in hopes of resolving the problem. With the reduced stepsize, the solution process becomes unable to move away from that location. This result is exactly what has been observed with the CONMIN conjugate gradient method.

One way to try to alleviate this problem would be to employ central differencing in the gradient determinations. While this would be substantially more expensive than employing one-sided differences, it would not have to be implemented at all times, but only when the optimization search is in the vicinity of a local minimum. We have investigated implementing this possibility by examining the combined CONMIN/TSONIC blade optimization code that we previously developed (Ref. 7) to determine whether central differencing could be easily introduced into the CONMIN optimization procedure. It appears that implementing a central difference procedure into the method cannot be easily done, but would require a significant rewrite of the optimization code. This would be an effort beyond the scope of the present investigation.

The one tested alternative to the COPES/CONMIN conjugate gradient procedure for aerodynamic optimization applications is the quasi-Newtonian procedure. That procedure has now been implemented into an optimization driver called QNMDIF (Ref. 9), and configured so as to avoid several of the more serious deficiencies inherent in the CONMIN driver. The QNMDIF driver is based on the quasi-Newtonian minimization algorithm as orginally developed by Gill, et. al. (Refs. 27, 28). A number of improvements have been implemented to maintain stable convergence in the presence of roundoff errors, ill-conditioning, or occasional small discontinuities in the objective function. For example, the method will switch from forward to central differences if the search procedure fails to produce a significantly better point, and then back to forward differences if an improved rate of progress occurs later. A comparative series of systematic test cases employing both the CONMIN and QNMDIF solvers have been carried out for a number of difficult optimization problems (Ref. 9). The results have demonstrated the significantly better performance of the quasi-Newton algorithm. The QNMDIF procedure, originally developed for 2-D applications, has now been combined with the 3-D TWING full potential flow solver into an efficient optimization solver for supercritical 3-D wing design (Ref. 8).

On the basis of the demonstrated superiority of this method over the CONMIN conjugate gradient procedure, we have opted to employ the QNMDIF quasi-Newton procedure as the optimization driver of choice for the present investigation. The integration of the 3-D approximation method, as currently developed, with the combined 3-D flow field solver (TWING) and quasi-Newton optimization driver (QNMDIF) was carried out. As could be anticipated, the resulting combined code is quite large, i.e. approximately 17,000 lines of Fortran source. Consequently, we have decided that in order to expedite the initial testing of the approximation method in this combined procedure that the segment of the code containing the approximation method together with all the geometry and other routines that are required to enable prediction of the

approximation-predicted objective function be separately modularized. This was done in such a fashion as to allow separate testing of the approximation methods' performance in the solution space typical of the optimization design environment, and then to later allow direct coupling with the QNMDIF/TWING optimization procedure when the approximation method testing is complete.

3.3.2 Definition of 3-D Turbomachinery Design Optimization Problem for Testbed Case Studies With Approximation Method

After reviewing the various classes of optimization problems that can be directly implemented with the QNMDIF/TWING optimization procedure as it is presently constituted, a particular class of aerodynamic optimization design problems was selected that is sufficiently general in its overall design aspects to be representative of practical design problems relevant to turbomachinery applications. The selected problem class relates to the optimized design at highly supercritical flow conditions of a 3-D wing or isolated blade geometry so as to minimize its total drag-to-lift ratio. This choice provides a challenging design problem to the optimization method as well as the approximation method because of both the overall sensitivity of the 3-D flow to small changes in geometry, as well as the particular choice of objective function. Several investigators have found (Refs. 23-25) that although the selection of drag or drag/lift ratio as the objective function is the most relevant choice to the design process, drag was too sensitive a quantity for the optimization and inviscid flow solver codes employed at that time to produce acceptable results. In order to achieve some measure of optimization, the less satisfactory choice of employing a target pressure distribution as the objective had to be made. From a physical standpoint, this is not nearly as desirable as using overall drag as an objective since apriori knowledge of an appropriate target pressure distribution is not conveniently available for most problems. However, it has been found (Ref. 8) that by using the new quasi-Newton optimization driver together with an accurate full potential flow solver and a higher 3-D flow solution convergence tolerance the employment of inviscid drag as the objective function is practical, and that good optimization results can be achieved on that basis.

Consequently, based upon these demonstrated results the initial testbed optimization case study for the 3-D approximation method was selected to be the optimized design of a 3-D wing or isolated blade operating at highly supercritical flow conditions using the drag/lift ratio as the objective function with approximately 10 design variables related to wing surface geometry. This is a challenging design environment for the approximation method since the 3-D flow solutions required here are extremely nonlinear, and the simultaneous multiple design variable parameter changes required by the optimizer as it proceeds through the design variable solution space usually exhibit a strong nonlinear coupling between the solution states. However, the overall design problem represented by this selection is so fundamental and directly relatable to practical aerodynamic design that its accurate solution by the approximation method would be a major contribution to achieving the general transition of turbomachinery analysis codes to design mode utilization.

The specific design strategy selected is based on that employed in Ref. 8 since it appears to be one of the most efficient optimization strategies reported to date. The design problem involves the geometric optimization of the surface of a 3-D wing or isolated turbomachinery blade using a relatively small number of design variables to modify the surface geometry. The overall problem is outlined in Figure 15. In contrast to previous optimization studies which have employed various analytic shape functions distributed along the chord of the profile (Refs. 20-22) to alter the baseline profile, the technique suggested in Ref. 8 is to simply assign as design variables the vertical displacement of several pre-assigned points on the wing surface. Then, as shown in Figure 15, by holding invariant the surface geometry along that portion of the profile surface we do not wish to change, the surface geometry along the remainder of the profile is altered by employing a spline-fitting routine to redefine that portion of the surface as the pre-assigned movable points displace vertically from their baseline locations in response to the optimization process. The advantage of this strategy is that a small number of movable points is sufficient to redesign a relatively large segment of a 3-D geometric surface. For instance, for the example shown in Figure 15, at each of 3 spanwise locations on the wing three chordwise points located at approximately x/c = {0.2,0.4,0.6} were found to be sufficient to recontour the upper surface segment of the wing along the chordwise band from x/c = {0.08 to 0.75} and to enable quite satisfactory optimization results to be obtained. We will discuss these results shortly. In contrast, employing analytic shape functions distributed at various locations along the profile chord would typically require at least double the number of design variables.

The initial three-dimensional optimization case study chosen for the approximation method is then summarized as follows: using drag/lift as the objective, the planform geometry as illustrated in Figure 15, and a constant profile geometry across the span given by the NACA 64 A212 airfoil, the upper surface of the wing was modified along the chordwise band from approximately x/c = {0.08 to 0.75} using a total of 9 design variables associated with the movable spline-supported points as indicated Figure 15 and located at the 3 spanwise locations y/s = {0.25,0.50,.075} and chordwise locations x/c = {0.2,0.4,0.6}.

3.3.3 Results of Combined Approximation Method and Optimization Procedure for 3-D Design Optimization Case Studies

In order to establish the benchmark for evaluating the approximation methods performance, we have run the QNMDIF/TWING optimization procedure without employing the approximation method. This particular optimization problem was previously studied in Ref. 8 so that a direct comparative result is available. Figure 16 provides the original spanwise pressure distributions of the baseline configuration, and provides in the lower left of the figure the nominal values of the nine design variables for the baseline configuration multiplied by 100, i.e. values of the normalized Z coordinate of the movable spline-fitted points $100\cdot\{(Z/c)_1, (Z/c)_2, \ldots\}$. Figures 17, 18, 19, and 20 display the optimized wing

spanwise pressure distributions after the 7th, 8th, 9th, and 10th optimization cycles, respectively. The 10 cycles required approximately 12,000 secs. of CRAY XMP CPU time. In our calculations we have employed a finer grid (149,31,26) than that (89,25,18) previously used since we wished to resolve the upper surface shock more accurately. Figure 21 provides an interesting synopsis of the behavior of the quasi-Newton optimization procedure for this design problem. That figure provides the behavior history of the objective function each time it is evaluated from the 3-D flow solution as called by the optimization driver. As can be seen, essentially the first 30 evaluations and corresponding 3-D flow solutions are needed to set up the Hessian matrix of mixed second derivatives of the objective function with respect to the 9 design variables. Once that is completed, there is a large drop in objective function as the method proceeds to its first design point. After that, only gradient evaluations are needed, i.e. essentially one 3-D solution for each design variable, to take the method through the succesive optimization cycles. The rapid and continuing convergence of the procedure is evident, in contrast to the slow and often halting convergence behavior of the conjugate gradient method.

As the first test of the 3-D approximation method's ability to predict 3-D surface pressure distributions in the multiple design variable solution space associated with the above optimization problem we have employed the approximation method to predict the surface pressure distributions for the design variable values associated with the design point at the end of each of the last 4 optimization cycles run on the above design problem. These are the pressure distributions previously shown in Figures 17-20. Figures 22, 23, 24, and 25, respectively, provide comparisons of the approximation predicted surface pressures at the wing root chord with the exact 3-D TWING flow solutions at those same 4 design points illustrated in Figures 17-20. With the exception of several points in the near vicinity of the upper surface shock wave, the comparisons are quite reasonable. In the numerical determination of the 3-D flow solution by TWING, the computational grid used employs 25 spanwise locations on the wing. At all of these 25 spanwise stations, an approximation prediction of surface pressure is required in order to accurately calculate the approximation-predicted drag for comparison with the exact result. For this test case, however, at approximately the sixth spanwise location we found the initial approximation method predictions to break down due to shock wave invariant point crossings. This is not entirely surprising considering the topologically complex pressure distribution presented by the current optimization problem. Note that the approximation method is trying to track both the chordwise and spanwise movement of the shock wave due to the simultaneous change of 9 design variables, all occurring in a highly nonlinear, coupled flow environment. What is needed to remedy this occurrence in the approximation method is a more generalized and robust determination of the 3-D invariant point locations that are required by the approximation method. We discuss its development below.

Another issue of note is the strategy for selecting the calibration solution matrix required as input to the approximation method. For our first choice, we simply selected a subset of the 3-D solutions determined by the QNMDIF optimization

method for the Hessian matrix calculation. This strategy has the appeal that no additional 3-D flow solutions are needed to be calculated. What we found, however, was that the design variable stepsizes initially selected by the optimizer are too small and do not cover a sufficient volume of the design variable solution space that will ultimately be searched by the optimizer as it proceeds to the optimum design point. Consequently, for the approximation predicted results presented in Figures 22 to 25 the calibration solution matrix was hand picked so as to provide a reasonable coverage of the flow solution space from the baseline solution shown in Figure 16 to the final design point solution shown in Figure 20. Of course, apriori knowledge of the appropriate range for design variable movement is generally not available. Consequently, the most effective strategy for determining the calibration solution matrix, and perhaps even more generally, the best way to employ the approximation method, i.e. from the very start of the optimization problem so that even the Hessian matrix is determined using approximation-predicted 3-D solutions, or immediately after the Hessian matrix is determined, or at the end of the first optimization cycle, or some combination or variation of these different strategies, requires investigation.

In working with the combined QNMDIF/TWING/APPROX pilot code, it was immediately found to be necessary to separate and modularize the 3-D geometry and grid generator routines from the combined pilot code so as to allow direct interaction with either full 3-D TWING solutions or with approximation-predicted solutions. The reason for separating and modularizing the 3-D wing geometry and finite difference grid generator from the combined QNMDIF/TWING/APPROX pilot code was to permit the extensive testing of the approximation method to be carried out without continually being burdened by the overhead of the entire QNMDIF/TWING/APPROX program combination. Carrying this overhead is not necessary for testing the approximation method, and modularization of these routines adds considerably to the computational efficiency. Note that just as with the full 3-D TWING solutions, in order to compute the approximation-predicted lift and drag, it is necessary to redetermine the wing geometry for each variation in design variables so that pressure integrations can be carried out over the newly-designed wing surface. In determining full 3-D TWING solutions, the TWING grid generator redetermines the chordwise distributions of wing surface points that are initially determined by the wing geometry generator and then input to it. We also elected to employ the TWING grid generator to determine the points at which the approximation-predicted pressures were to be determined. This insures that for the approximation-predicted results a smooth distribution of chordwise points will be achieved at each spanwise location. Additionally, it further guarantees that unnecessary inaccuracies associated with solution interpolations are avoided when comparing approximation-predicted and exact TWING results.

After the separation and modularization of those geometry and grid generator routines, verification calculations of the lift and drag using the approximation method were performed in order to verify the modularization. This testing was accomplished by employing the modularized geometry and grid generator

routines together with the approximation method to reproduce the results associated with the 3-D TWING base and calibration solutions. That was carried out by setting the design variable values to be those of the base and calibration solutions. Hence, the approximation method then simply repredicts the base and calibration pressure distributions. If the geometry and grid generator routines then correctly determine the wing geometry information required to calculate the lift and drag at each spanwise location, the results so calculated should compare identically with those determined from the exact 3-D TWING calculations. It was verified that the predicted sectional lift and drag predicted by the modularized code exactly reproduces that determined by the full TWING code.

Examples of the output of the predicted sectional lift, drag, and drag/lift ratio as determined from the modularized code are provided in Figures 26-29. For example, illustrated in Figure 26a. are the spanwise distributions at each of the 25 spanwise locations along the wing of the sectional lift, drag, and drag/lift ratio for the optimized wing surface pressure distribution shown in Figure 26b. Note that this pressure distribution is the result that was obtained after the 7th optimization cycle for the benchmark case study.

Additional successfully-predicted results from the modularized code for the sectional lift and drag are provided in Figures 27a.-b. to 29a.-b. Those results are for the optimized pressure distributions after the 8th, 9th, and 10th optimization cycles, respectively, for the benchmark case study. Consequently, the results illustrated in Figures 26-29 represent both the target pressure distributions and the sectional lift and drag results that the approximation method will attempt to predict for the testbed optimization study.

3.4 Extended Invariant Point Relocation Procedure and Postprocessing of Approximation Results

An improved methodology for redefining the 3-D chordwise and spanwise invariant point locations associated with shock waves that occur in the base and calibration solutions was developed. This was found to be necessary as a result of testing carried out on the benchmark optimization case study. This involved determination of a procedure for relocating the shock wave invariant points in the spanwise direction that provides a continuous and smooth variation of both the invariant point locations as well as the associated values of the pressure at those points. An illustration of the typical improvement provided by the relocation procedure is provided in Figures 30a.-b. to 32a.-b. In Figure 30a., results are given for the unmodified base TWING solution employed in the benchmark case study. The plot on the left of that figure displays the spanwise locations of the invariant points associated with the upper surface shock, while the plot on the right shows the associated Cp values of those same points. In both of the plots, the triangular symbols represent the invariant point locations associated with the beginning of the shock wave, while the square and circular symbols represent, respectively, the correponding sonic point and shock termination locations. Note the nonsmoothness evidenced by several of the

points, particularly as shown in the Cp values. Figure 30b. illustrates the same plots after the relocation procedure has been applied. The smooth variation in both location and Cp values is evident. More remarkable results of the procedure are provided in Figure 31a.-b. That figure illustrates analogous results for one of the calibration solutions in which the original invariant point location procedure could not locate a distinguishable invariant point marking the beginning of the shock wave at several spanwise locations near the root chord, as can seen in Figure 31a. However, as shown in Figure 31b., the relocation procedure successfully provides smoothly-varying invariant points marking the beginning of the shock wave at those locations for this calibration solution. The final result provided in Figures 32a.-b. illustrates how irregular the locations of the invariant locations associated with certain shock topologies can become. The plot shown in Figure 32a. exhibits a gap occurring at approximately mid-span in the identification of the invariant points associated with the pre-shock and sonic locations in the pressure distribution for this calibration solution. This phenomena has apparently occurred since this particular pressure distribution does not recover through sonic velocity over that spanwise location. Although while this phenomena may occur physically, such a topology change will prevent a prediction by the approximation method if not corrected. The relocation procedure corrects this problem by locating a smooth distribution of invariant points across that spanwise gap as shown in Figure 32b.

Finally, as a result of all the above development of the 3-D approximation method, Figures 33a.-y. display a complete prediction of a 3-D pressure distribution by the approximation method as it is presently constituted. Illustrated in these figures are comparisons of the approximation method and the exact TWING results for the chordwise pressure distributions at all of the 25 spanwise stations across the wing at which the grid generator has located the computational grid for the 3-D pressure distribution associated with the 7th optimization cycle of the benchmark case study (see Figure 26b.). Also shown on each of those figures for comparative purposes are the base and 9 calibration pressure distributions which are employed by the approximation method to predict the pressure distribution results shown. The corresponding prediction of the spanwise sectional lift, drag, and drag/lift ratio are given in Figure 34a. and compared with the exact result in Figure 34b. taken from Figure 26. As can be seen in Figure 34, with the exception of spanwise locations 15, 19, and 25, quite reasonable predictions of these integrated spanwise quantities are obtained from the approximation-predicted pressures. However, in order to insure a consistent and smooth spanwise variation of all the integrated quantities, development of a post-processing procedure to correct and relocate the final approximation-predicted invariant point locations in the spanwise direction is still necessary and is discussed below.

Considering Figure 34 and setting aside for the moment the fact that the total integrated lift, drag, and drag/lift ratio of the approximation-predicted results indicated in Figure 34a. are somewhat in error compared with the exact result provided in Figure 34b., the overall approximation prediction for the spanwise variation of sectional quantities appears quite reasonable. In our initial

investigation of this problem, it appeared that the major source of error preventing accurate prediction by the approximation method of the total integrated forces lie with the several spanwise locations, such as locations 15, 19, and 25 shown in Figure 34a., in which clearly inconsistent behavior is observed in the approximation prediction of the sectional quantities. Implementation of an additional post-processing invariant-point smoothing procedure for correcting the final approximation-predicted invariant point locations in the spanwise direction appeared straightforward and was carried out. Comparison of the post-processed invariant point spanwise pressure distributions, which are not shown here, with those in Figure 34a. exhibited some variation from the nonpost-processed distributions but resulted in no dramatic changes. Figure 35 provides the new approximation results based on post-processed spanwise surface pressure distributions to be compared with the previous approximation and exact results shown in Figures 34a. and 34b., respectively. This new approximation result exhibits somewhat stronger discontinuous behavior at several spanwise locations than other results that we have obtained when applying slightly different spanwise smoothing criteria in the invariant point location procedure, and it illustrates the basic sensitivity problem that we've encountered with these multi-parameter 3-D solution predictions. That is, that while the invariant point relocation procedures developed and employed here with the 3-D approximation method can and do insure continuous variations of invariant point locations in the spanwise direction, a continuous variation in the sectional integrated quantities obtained from those pressure distributions, such as lift and drag, is not similarly insured. The reason for this is due to the strong tendency for extremely rapid local topology change in the basic surface pressure distribution for these strongly-nonlinear flows. These rapid topology changes in surface pressure can have the result that a small error in the spanwise invariant point location distribution can cause the strength and location of the shock at one or more spanwise locations to be sufficiently in error to cause a significant discontinuous variation in the spanwise variation of the integrated quantities.

The most direct way of correcting for this problem is to further enhance the current invariant point relocation procedure both for redefining the invariant point locations in the base and calibration solutions as well as post-processing the final approximation-predicted invariant point distributions. An alternative would be the possibility of working with another basic flow property rather than such a strongly sensitive quantity as surface pressure. An interesting idea which comes to mind is that instead of employing the pressure as our fundamental dependent quantity which is discontinuous through a shock, we employ instead the mass flux or some similar quantity that remains continuous through a shock, and then subsequently determine the flow properties that are of interest from these quantities.

Recall that the primary function of the invariant point location procedure is to provide a continuous spanwise variation of both the invariant point locations as well as the associated values of the pressure at those points. The relocation procedure corrects descrepancies due to numerical 'jitter' in the vicinity of high-gradient regions such as shock waves in the base and calibration solutions.

This jitter if uncorrected results in significant degradation of the unit perturbation distributions which are determined by differencing in strained coordinates the various calibration solution distributions and the base solution distribution. In addition to employing the invariant point relocation procedure on the base and calibration solutions, which can be thought of as preprocessing those solutions in preparation for use by the approximation solution procedure, as a result of additional numerical experimentation with the approximation method we have also found it necessary to again apply an invariant point relocation procedure to the approximation-predicted invariant points. This in effect postprocesses the approximation solution. We have found this to be necessary due to the fact that the approximation-predicted location of the invariant points often contains numerical jitter as well, particularly for multi-parameter perturbations involving four or more simultaneous perturbations. This jitter often results in nonuniformities in the spanwise distribution of the invariant points. Although the spanwise continuity of the predicted pressure distributions can appear reasonable, integration of these distributions across the span direction often displays nonuniform variation in the integrated sectional quantities such as lift and drag.

In order to investigate the underlying cause and determine the appropriate method to correct the observation of the descrepancies in the spanwise variation of the approximation-predicted sectional lift and drag, we have performed a detailed evaluation of the performance of the approximation method involving one, two, three, and nine design parameters when employing combined preprocessing of the invariant points in the base and calibration solutions plus postprocessing of the invariant points in the 3-D approximation-predicted solution. As a result of this numerical testing, we have made the following observations. Application of the invariant point relocation procedure to smooth out the numerical jitter in the invariant point locations in the original base and calibration solutions is very effective and results in accurate approximation predictions of the new invariant point locations for situations involving a small number of simultaneous multiple parameter perturbations. We have found that for the cases we have considered, a two or three-parameter perturbation problem can usually be accurately modeled by the approximation procedure. The tested problems involved strongly supercritical flows with a strong, single shock wave across the upper wing surface. However, when the number of multiple parameters to be simultaneously altered increases beyond three then what seems inevitably to occur in the approximation prediction is that some small numerical jitter in the invariant point locations, steming from either imperfections in the original base and calibration solution locations or from the preprocessing procedure that may slightly misalign one or more invariant points, results in a large discrepancy in the predicted results at one or more of the spanwise locations. In order to treat this problem, we have proceeded to develop and test a procedure to relocate the invariant points in the predicted solution prior to using the approximation-predicted surface pressure distributions to determine integrated sectional quantities. As a result of this, we have been able to demonstrate that the employment of a post-processing procedure to relocate and realign the various invariant point distributions in the approximation-predicted results can resolve essentially all of the discrepancies

in the predicted results again when the number of varied parameters is small. However, when the number of multiple parameters increases to a larger number typically required in a realistic design problem, a number which would usually be 10 or more, the current smoothing procedures cannot guarantee consistent results. The basic requirement on the methods being developed in this study is to track and accurately replicate the motion of invariant points characterizing high-gradient, discontinuous regions of the flow field. The prediction capability of these methods is critically dependent upon the goodness of the basic numerical solutions for the base and calibration flow fields that are input to them. For classes of highly sensitive flows as we have been studying, which are inevitably the ones of most interest for practical design applications since they usually represent situations that can benefit the greatest from design refinements, small discrepancies in the basic numerical flow solutions that are input to the approximation procedure can lead to large discrepancies in the predicted pressure distributions in these high-gradient regions. Since some numerical jitter in these regions in the base and calibration numerical solutions is unavoidable, the resultant accuracy and range of validity of the approximation method predictions will be significantly reduced in these applications when the basic input to the approximation method consists of highly-sensitive surface pressure distributions.

An alternative method to alleviate this basic restriction on the accuracy of the approximation method, as mentioned briefly above, is to employ as input to the approximation method flow properties other than those on the wing or blade surface where the gradients are naturally the highest. Since most practical design/optimization problems in both aerodynamics and turbomachinery are focused on seeking an improvement of an integrated flow quantity, such as drag or loss coefficient, working with surface properties is not always necessary. For example, in order to determine the forces acting upon an aerodynamic configuration one can employ control surfaces removed from the actual aerodynamic surface and located at any convenient location in the flow field where information is available. Because numerical flow field solution methods provide information everywhere in the flow field, that information is already available. In the present study, as well as in all of the previous work involving the approximation method, we have employed surface pressure as the basic dependent variable since surface pressure is both a fundamental aerodynamic quantity and surface pressure distributions were found to be very convenient to use in the comparative testing involved in the preliminary development of the approximation method. However, there is no fundamental need or restriction to employing surface quantities with the approximation method. Any convenient distributions will serve equally as well. For our purposes, it appears just as suitable to employ distributions of flow properties at the outer edge of the computational grid where the flow contains significantly less high-gradient features and is more of a small-disturbance flow. A strict small disturbance flow is not necessary for accurate use with the approximation method. The far-field flow can contain one or several shocks passing through the outer boundary and the approximation method will work accurately without restriction. The essential point is that the features of the flow field at points removed from the actual blade surface will be less severe and subsequently less susceptable to numerical

jitter than for example at the foot of a strong shock wave on the surface. In fact, employment of outer flow field information to predict integrated quantities has been recognized in the past and previously employed. Henne and Hicks (Ref. 29) have developed and employed a contour integration procedure applied to the outer computational grid boundary of the 3-D transonic flow code FLO22NM to evaluate the lift and drag of wings and wing/bodies at transonic speeds. This was done in order to avoid working with surface pressures to determine the drag which was found to be in error due to small numerical inaccuracies in the predicted surface pressures. The result was a consistent and more accurate prediction of drag throughout the transonic regime. We suggest that the alternative of employing flow field rather than surface properties as the basic input to the approximation method be examined.

Before making the final decision on whether to alter the mode of operation of the approximation method from employing surface pressure distributions as the basic input information to using flow field properties, we have carefully reviewed all of our previous approximation method results involving single and multiple-parameter simultaneous changes to determine the precise sources that cause the discrepancies currently observed in the predicted results and to insure that no simple mechanism for easily correcting these discrepancies has been overlooked. We have reviewed the following four major steps in the approximation procedure: (1) the preprocessing procedure for identifying and relocating the invariant point locations in the base and calibration solutions in order to provide a smooth variation of these invariant points in the spanwise direction, (2) the procedure for determining the approximation-predicted solution based upon the preprocessed base/calibration solutions, in particular the prediction of the new invariant point locations, (3) the post-processing procedure for relocating the predicted invariant point locations in the spanwise direction, (4) the integration of the post-processed approximation-predicted solutions to determine integrated sectional quantities in the spanwise direction.

For the class of flow solutions characterizing the benchmark case study, it appears that, even after careful post-processing, integrated sectional results of the approximation-predicted solutions tend to exhibit noncontinuous spanwise behavior due to invariant point misalignment. Although the benchmark test case study involves topologically complex flows in the sense that strongly supercritical flows are involved, we believe it to be a good test of the approximation method if the method is to achieve a reasonably general applicability to turbomachinery flows where flow topologies are at least as complex as those considered here.

As a result of our review, we believe we have now identified the multiple sources causing the limitation in the application of the approximation method in three-dimensional studies. The primary factors are a combination of numerical inaccuracies in the base/calibration solutions near the invariant point locations associated with the foot of the shock together with a geometrical compounding of these errors when the approximation-predicted invariant point locations are dependent upon the simultaneous variation of a large number of multiple parameters. The fundamental action of the approximation method is to move

the invariant points linearly in multiply-strained coordinate space with respect to each perturbation parameter. The predicted results from such a formulation have been found to be extremely accurate in 2-D situations where the shock structure was relatively simple and well-resolved by the numerical solution procedure so that the associated invariant points were also well defined. For three-dimensional situations, however, the shock structure on or near the surface of the 3-D configuration is not so well defined by the flow solvers. Consequently, the definition of the invariant point locations in the base/calibration solutions is correspondingly lacking. Attempting to correct these locations by employing general smoothing criteria can improve the situation at some locations but inevitably increases the error at other locations. Finally, when the approximation-predicted invariant point locations are determined as a sum of all the individual contributions from each varied parameter, the possibility of a significant spurious result occurring at even one location is high. For example, in a problem involving 10 design variables, if the approximation prediction accurately accounts for the invariant point motions and resultant flow topology changes of 9 of the design variables, but misses the prediction for the 10th at one spanwise location, the resultant error in the integrated sectional quantities at that one location will usually destroy the overall accuracy of the total force prediction. Trying to correct these errors by some automatic smoothing process becomes increasingly complex as the number of multiple variables increases and the various combinations of invariant point motions permutes.

The basic conclusion is that as both the sensitivity and number of the base/calibration flow solutions that are input to the approximation method increase, the accuracy and range of validity of the prediction from the method will rapidly reduce. The strategy of trying to maintain a constant range of validity by developing increasingly more complex pre-and post-processing procedures to try to consistently remove these inaccuracies appears to be impractical since it requires major verification and testing and possibly even redevelopment of the processing procedures as both the number of design variables increases and the complexity of the surface flow topology increases. An alternative strategy of simply increasing the numerical accuracy of the base/calibration solutions by refining the computational grids and increasing the flow field resolution is also not satisfactory since in many situations it may not be feasible to do this due to computer limitations. Furthermore, it has the negative feature of requiring the determination of higher accuracy flow solutions when using the approximation method than when not using it.

In order to try to maintain as wide a range of validity of the approximation method as possible as both the complexity of the surface flow topology and number of design variables increases, it appears that the most logical way to proceed is to choose an alternative input to the method that is not so strongly sensitive as surface pressures. Flow field properties, in particular those distributions in the far field, are a natural choice. As pointed out previously, since many practical design/optimization problems in both external and internal flows seek improvement of a figure of merit represented by an integrated quantity such as drag or loss coefficient, the information to determine that

integrated quantity is contained as well in the far field flow properties, and can be calculated by employing control volume integrations.

3.5 Alternative Formulation of Approximation Method With Flow Field Rather Than Surface Properties

We have posed the problem of applying the approximation method when employing flow field information rather than surface pressure distributions as the basic input, and have carried out some preliminary work for the three-dimensional problem. At the full potential level of solution, the following far field flow quantities are required: (U,V,W) distributions. Since the flow is assumed isentropic, pressure and density distributions can be determined directly from the velocity distributions. At the Euler and Navier-Stokes level of solution, the following far field quantities are required: (U,V,W,RHO,ENERGY) distributions. In order to evaluate the contour integrals involved in determining the integrated forces and moments acting upon the configuration inside the control volume, the first step in the process is to determine the pressure and momentum fluxes around the entire outer boundary. For this purpose, it is convenient to use a contour associated with the computational grid at one or two mesh points inside the outermost mesh boundary location. In employing the TWING full potential code, the first step in this process is to determine the physical velocity components from the velocity potential. In the TWING code, as in essentially all current CFD flow solvers, during the solution convergence procedure all computations are carried out in a transformed computational domain. An illustration of the overall relationship between the physical and computational domains embodied in the present TWING solver is provided in Figure 36. Physical flow properties are not required nor determined during the convergence process. After solution convergence, physical results are then calculated as a final output step. Although grid and potential information are available as output from the TWING code, directly differencing the potential in physical coordinates will not retain the 2nd order accuracy maintained in the original solution algorithm. In order to maintain the 2nd order accuracy for the physical flow field distributions, which are needed for accurately determining the total forces, it is necessary to difference the potential in a fashion consistent with the original solution process. This is accomplished by employing the same grid metrics and computational molecule surface flux formulations employed in the solution algorithm. Although this information is embedded in the flow solver, extracting the information directly from the solver is not easily done since selected metric arrays are overwritten during the solution convergence process in order to reduce computer memory requirements. Consequently, we found it to be more expedient to write a separate code to redetermine the grid metrics and then calculate the needed physical flow field quantities. We have now completed that code. The computational grid employed in the TWING solver is comprised of a combination of two-dimensional O-type grids located in (X,Z) planes placed at successive spanwise stations along the wing from the wing root to beyond the tip, as illustrated in Figures 37 to 39 from Ref. 10. The outer boundary of the grid, illustrated in perspective in Figure 40, tapers inward at span locations along the wing, and then becomes cylindrical beyond the wing

tip out to the outer lateral sidewall boundary. Typical results for physical flow field quantities at one grid point location inside the grid outermost boundary are provided in Figures 41 to 43 where distributions of the velocity components (U,V,W) are provided at each of the 30 separate spanwise stations. The distributions of the U velocity component are quite smooth, while not surprisingly both the V an W components exhibit the influence of the wing tip trailing vortex passing through the grid directly downstream of the wing. The influence of the wing tip vortex is shown even more graphically in Figure 44 which displays density contours on the same grid surface.

With the physical flow properties in the region of the outer grid boundary determined, we have now proceeded to write the procedure for evaluating the pressure and momentum fluxes through each of the surfaces defining the control volume of interest, i.e. the quasi-cylindrical grid surface enclosing the wing, the circular surface boundary at the symmetry plane, and the corresponding circular surface boundary at the freestream sidewall boundary as shown in Figure 36.

With the code complete for providing second-order accurate physical flow field properties from the TWING solver at any arbitrary location on the computational grid, we have proceeded to complete the procedure for evaluating the pressure and momentum flux integrals on a control surface formed by the quasi-cylindrical grid surface enclosing the wing, i.e. a K = constant grid shell and the the bounding circular end planes at the symmetry plane and the freestream sidewall boundary, as illustrated in Figure 36. The forces acting on the wing contained within the control volume can be evaluated by determining the following two surface integrals:

$$F = -\int_S (p - p_\infty) dS - \int_S \rho(V - V_\infty)\cdot(V \cdot dS) \qquad (25)$$

where S represents the three surfaces referred to above and illustrated in Figure 36. The procedure is realized numerically by determining the cell surface areas and normal vectors on the outward-facing surfaces on each side of the grid cells contained on the control surface. Implemetation is done by carrying out the integration over a selected K = Constant radial computational grid shell (i.e. over all I's,J's) as well as the two lateral boundary surfaces located at the symmetry plane (J=1) and the sidewall boundary (J=JMAX). Appropriate control volume surfaces can range from the K = 2 grid shell planned for use here down to the K = KMAX shell which conforms to the wing and ficticious wing extension surface (See Fig. 36). A check calculation at the K = KMAX surface should identically reduce to the previous determination of the forces by surface pressure integrations since contributions from the momentum flux integral in Equation (25) should be zero along both the wing and ficticious wing extension surfaces.

We have carried out test calculations for control volumes ranging from the K = 2 to K = KMAX grid shells. Results for the total lift and drag for the K = KMAX control volume from our evaluation of Equation (25) produced identical results to those previously obtained from TWING using surface pressure integrations. The momentum flux terms at the wing surface were of the order (10), and the net momentum flux on the ficticious wing extension was identically zero. However, the results for the total forces for the control volumes from K = 2 to K = KMAX-1 did not check either with each other or with the results obtained previously from surface pressure integrations. A careful check of the code for obvious errors did not reveal the source of the discrepancy. As an additional check, we next examined the conservation of mass using the same control volume approach. Since the full potential equation employed here is identically the continuity equation, conservation of mass should be satisfied for any arbitrary control volume chosen, i.e. from individual computational grid cells to the far-field control volumes used above for the total force computations. The results from the mass flux integrations over the same K = Constant grid shells plus two bounding end planes used in the momentum computations produced erroneous non-zero mass fluxes. We then proceeded to try to isolate the source of the error. We decomposed the far-field control surface into the sum of component spanwise rings formed by chordwise strips (all I's) between adjacent spanwise J nodes. We then examined the total mass flux entering and leaving a ring control volume defined by these individual rings that were one radial K cell thick. We found that the net mass flux was also not zero for these rings. We next performed a check on the cell surface area and cell surface normal determinations by imposing a freestream velocity everywhere and then computing the mass flux. A non-zero result for mass flux for this case would indicate an error in either or both of the determinations of the cell surface areas and cell surface normals. The results of this computation was that zero mass flux (within 10) was found for: (1) individual cells, (2) spanwise rings one K cell thick, and (3) the far-field control volumes used in the momentum computations. This result verified the computation of the cell surface areas and normals. We next verified the accuracy of the physical (U,V,W) velocity distributions being determined and employed in our current procedure. Since the TWING potential flow is isentropic, the velocity distributions can be used to determine all the subsequent flow properties.. We used our caculated physical (U,V,W) velocity distributions to determine the corresponding density distributions. We then compared that result with that determined by the TWING solution procedure in the computational domain and which uses contravariant velocity components. The density results from each of these separate computations compared exactly. Finally we met with and discussed these results with the NASA/Ames Research Center scientists Dr. T.L. Holst and Mr. S.D. Thomas who are the authors of the TWING code. They were not aware of this discrepancy in the code, nor of anyone else who has tried to use far-field distributions from the code to determine total forces. During development of the solver, they had checked the predictions of TWING with a number of other 3-D solvers and had made successful verifications of pressure distributions and forces obtained from the code. As a final result of the control volume formulation, we found that if we sum the individual pressure and momentum flux surface integrations over all individual cells throughout the total control volume, we then obtain the same

result for the lift and drag previously determined from surface pressure integrations. This result implies that the summing procedure we are using is correct and that all internal fluxes cancel correctly.

With the resources remaining to the investigation, it was decided at this point that, rather than continue to try to resolve the discrepancies encountered with the 3-D TWING flow code in determining the lift and drag forces acting on the configuration vis-a-vis employing contour integration of momentum fluxes on an outer boundary removed from the actual geometrical surface, a preliminary investigation employing flow field rather than surface properties with the approximation method would be carried out at the axisymmetric level. The flow solver selected for use in this preliminary study was one developed by the present author and successfully tested in an extensive series of applications (Refs. 30-32) involving highly-supercritical nonlinear flows throughout the transonic regime. The solver employs a SLOR procedure to solve the transonic small-disturbance equations in fully-conservative form, and has demonstrated its ability to be accurate and robust in determining accurate flow solutions not only throughout the transonic regime but at subsonic and low supersonic speeds as well. The method has been configured to treat free-air as well as a variety of wind-tunnel outer boundary conditions (Ref. 31). Hence, it can be directly applied to the present problem of predicting the aerodynamic forces acting on a configuration by using contour integration of momentum fluxes over an outer control surface. With this flow solver we formulated an initial test case for the approximation method based on using flow field rather than surface properties by considering the axisymmetric transonic flow past a body of revolution enclosed by a solid sidewall boundary, as illustrated in Figure 45. The control surface employed for the contour integration of the momentum flux coincided with the circular inflow and outflow surfaces at the upstream and downstream boundaries, together with the cylindrical sidewall surface. The body geometry selected was chosen to be a particular parabolic-arc geometry for which accurate wind tunnel data are available from Ref. 33. The particular parabolic-arc body has a thickness ratio of 1/12 together with a cylindrical sting attached to the rear of the body at the 85% length location. For the calculations, the sidewall boundary was located laterally at 6 body lengths from the body longitudinal axis, and the upstream and downstream boundary locations were set at 3 body lengths, respectively, from the nose and tail of the body. Drag calculations were then carried out, both by integration of body surface pressures and by contour integration of momentum fluxes over the control surface discussed above, for oncoming Mach numbers ranging from M = 0.90 to 1.20 in steps of 0.025. The agreement between the two calculations was very satisfactorily, as indicated in Figure 45. Next, the approximation method determination was reformulated in terms of the distributions of the two velocity components on the various control surfaces. For this simple problem, this was only necessary at the downstream boundary since at the upstream boundary, constant oncoming conditions prevail, while at the lateral solid sidewall boundary the momentum flux is identically zero. Comparative calculations with the approximation method were then carried out employing various base and calibration solutions to try to reproduce the drag curve determined by the exact methods. The particular approximation results displayed in Figure 45 employed

base and calibration solutions for M = {0.95, 1.025} respectively, but are typical of approximation results obtained for other choices of base and calibration solutions. As can be seen from the figure, the approximation predictions, while close to the exact results, exhibit a spurious character. We were unable to determine the precise cause of this inconsistent behavior, but suspect that the sensitivity that was previously encountered with the approximation method in the vicinity of shock waves when using surface pressure distributions has now been transferred to a corresponding sensitivity in the flow field velocity distributions in the near vicinity of the body surface. A corresponding analog for the three-dimensional problem previously considered above with the TWING code would be the sensitivity in the flow field velocity distributions in the vicinity of the wing trailing vortices that was noted and displayed in Figures 41 to 44. Successful treatment of these regions of high-gradient sensitive flow vis-a-vis the approximation method requires a reformulation of the method in terms of appropriate invariant points for whatever flow quantities or distributions are selected for use. This corresponds in a direct fashion to the methodology developed in this present study for the problem of characterizing various shock wave invariant points when employing surface pressure distributions as the basic input to the approximation method.

4. CONCLUSIONS AND RECOMMENDATIONS

An investigation was conducted involving the preliminary development of a three-dimensional nonlinear approximation procedure for determining rapid and accurate approximations to highly nonlinear flows such as typically occur in turbomachinery applications. The overall objective was to develop and demonstrate the feasibility of such approximation methods to successfully work in a general 3-D turbomachinery design or parametric optimization environment to substantially reduce the overall computational requirements necessary for optimum design. The approximation procedures employ unit perturbations, determined from two or more nonlinear "base" solutions which differ from one another by a nominal change in some geometry or flow parameter, to predict a family of related nonlinear solutions. The solutions can be either continuous or highly discontinuous. It is conceived that these methods would be coupled with high run-time three-dimensional computational flow solvers, and would be used in conjunction with these solvers in applications where large numbers of related solutions are needed. The computational time saving would be accomplished by employing these rapid approximation methods to decrease the actual number of expensive 3-D flow solutions needed in any optimization or design study to a minimum.

The work undertaken here relates to the initial development and extension of these methods and concepts to problems characteristic of three-dimensional turbomachinery optimization design. The specific objectives of this study were: theoretical development of the three-dimensional approximation procedure in a form suitable for predicting surface properties on three-dimensional turbomachinery blades for highly sensitive supercritical transonic flows involving multiple shock waves, combination of the approximation method with a nonlinear three-dimensional transonic flow solver, coupling of the combined approximation method and nonlinear flow solver with an optimization design procedure, and finally testing of the complete approximation method/3-D flow solver/optimization code on problems relevant to the three-dimensional turbomachinery design optimization environment.

Application of the approximation method to three-dimensional transonic flows with multiple shock waves required the development of a multiple invariant point characterization procedure for identifying and tracking through parameter solution space the characteristic topology features associated with shock waves appearing in the surface pressure distributions used as input to the approximation method. It was found from numerical experimentation that a two-point characterization of shock topology in surface pressure distributions was adequate for the transonic flows of interest in this study. The characterization procedure was extended to include additional invariant points required for topology tracking of other high-gradient features characteristic of the general class of three-dimensional transonic surface pressure distributions being considered. These include stagnation point and minimum suction pressure and associated recovery points near the nose on both upper and lower surfaces. Finally, a global invariant point preprocessing procedure was developed to ensure a continuous variation in the spanwise coordinate direction of all the

selected invariant points. The approximation method was then tested on a number of three-dimensional example problems involving strongly supercritical transonic flows. The three-dimensional transonic full potential flow solver TWING was employed to provide the flow solutions. Comparative results of the approximation method predictions with the exact nonlinear solutions indicated that the approximation method is able to provide good nonlinear predictions over relatively large parametric ranges for three-dimensional problems involving one to three simultaneous parameter variations.

Existing aerodynamic design optimization methods and applications thereof were reviewed and, as a result, the quasi-Newton optimization driver QNMDIF was selected as superior for optimization studies of the general class of interest to this study. That optimization method was then coupled with the three-dimensional approximation method and the three-dimensional TWING flow field solver. Using past studies with the QNMDIF optimization driver as a guide, a 3-D design optimization problem was then defined for testbed case studies involving the combined code. The testbed optimization problem selected employed as design variables the vertical displacement of a number of pre-assigned points located in a certain region on the geometric surface of a 3-D isolated blade which was to be modified, and incorporated a spline-fitting procedure to redefine the surface geometry as the pre-assigned points displace vertically from their baseline locations in response to the optimization process. The drag/lift ratio was selected for the objective function. The testbed problem was first solved using only full nonlinear 3-D TWING flow solutions in order to obtain the exact optimum design point toward which the approximation method could be tested. Application of the approximation method was then made to the testbed problem to examine the capability of the method to produce accurate results in a typical design environment, and also to evalutate its potential for computational savings. Sensitivity studies were performed to examine the accuracy dependence of the approximation method on the choice of the initial calibration solution matrix.

Comparisons of the three-dimensional approximation method, configured with a multiple invariant point characterization for surface shock waves, stagnation point, and upper and lower surface suction pressure and recovery points, with the corresponding exact nonlinear solutions for surface pressure distributions indicated good accuracy and range of validity of the approximation method for those situations where the basic flow topology did not significantly change over the parameter range studied. For the sensitive transonic flows considered in the testbed optimization case study, however, it was found necessary to develop an additional postprocessing procedure to relocate all the invariant points in order to provide a globally continuous variation in both the spanwise invariant point locations as well as their associated surface pressure values. With this enhancement of the approximation method, the method was applied to predict both surface pressure distributions and spanwise sectional lift and drag distributions within the 9 design variable solution space encompassed by the testbed problem. The comparative results for the surface pressure distributions provided reasonable overall agreement with the exact results, but exhibited discrepancies related to the rapid topology changes occurring in the spanwise

direction in these flows. However, the spanwise sectional lift and drag distribution comparisons revealed a major shortcoming in the approximation method. That is, while the sophisticated invariant point relocation procedures developed here insure continuous variations of invariant point locations and surface pressure values at those locations, this by itself does not insure a continuous variation in the sectional integrated quantities obtained from those pressure distributions. The reason for this is again due to the tendency for extremely rapid local topology changes to occur in the basic surface pressure distribution for these strongly nonlinear flows. These rapid topology changes in surface pressure resulted in a small displacement error in the spanwise invariant point location distribution causing the strength and location of the shock at one or more spanwise locations to be sufficiently in error that a significant error in the spanwise variation of the integrated sectional quantities resulted. To investigate this problem further, a detailed evaluation of the performance of the approximation method was carried out involving problems having one to nine parametric variables. The following four major steps in the approximation procedure were carefully reviewed: (1) the preprocessing procedure for identifying and relocating the invariant point locations in the base and calibration solutions, (2) the procedure for determining the approximation-predicted solution based upon the preprocessed base/calibration solutions, (3) the post-processing procedure for relocating the predicted invariant point locations in the spanwise direction, (4) the integration of the post-processed approximation predicted solutions to determine integrated spanwise sectional quantities. As a result of the review, the multiple sources causing the observed limitation of the approximation method in three-dimensional studies were identified. The primary factors involve a combination of inherent numerical inaccuracies in the three-dimensional base/calibration solutions near the invariant point locations associated with the foot of the shock, together with a geometrical compounding of these errors when the approximation predicted invariant point locations are dependent upon the simultaneous variation of a large number of multiple parameters. The fundamental action of the approximation method is to move the invariant points linearly in multiply-strained coordinate space with respect to each perturbation parameter. The results predicted from such a formulation have been found to be extremely accurate in two-dimensional situations where the shock structure is both relatively simple and well resolved by the numerical solution procedure so that the associated invariant points are also well defined. For three-dimensional situations, however, the shock structure on or near the surface of a 3-D configuration is not so clearly defined by the flow solvers. Consequently, the definition of the invariant point locations in the base/calibration solutions is correspondingly lacking. Attempting to correct these locations by employing global smoothing criteria does improve the situation at most locations but inevitably increases the error at other locations. The basic conclusion is that as both the sensitivity and number of the base/calibration flow solutions that are input to the approximation method increase, the accuracy and range of validity of the prediction from the method will rapidly reduce. The strategy of trying to maintain a constant range of validity by developing increasingly more complex pre-and post-processing procedures to try to consistently remove these inherent inaccuracies appears to be impractical since it requires major verification and

testing and possibly even redevelopment of the processing procedures as both the number of design variables increases and the complexity of the surface flow topology increases.

It appears that the most logical way to proceed is to employ an alternative input to the approximation method that is not so strongly sensitive and subject to rapid toplogy changes as surface pressures. In order to test this hypothesis, the approximation method was reformulated in terms of using flow field velocity distributions at or near the outer grid boundary, and an initial preliminary investigation was carried out employing the TWING flow field solver. Discrepancies encountered in the mass and momentum flux determinations over a control surface located near the outer boundary of the TWING computational mesh prevented a definitive conclusion regarding the accuracy of the three-dimensional approximation method based on input flow field properties. Initial results from a corresponding axisymmetric flow case study provided promising results for wave drag prediction, and pointed to the need for the appropriate characteristic invariant point development associated with the particular flow field properties employed.

Finally, the results of the present investigation provide an important guideline for future development. We believe that the demonstrated potential of the approximation method from both the present investigation and past studies, in particular for design optimization studies involving highly nonlinear two-dimensional transonic internal and external flows where its ability to reduce the computational work by an order of magnitude with no degradation in accuracy was clearly shown, warrants further development of the method for the three-dimensional turbomachinery design problem. Furthermore, since the approximation method does not depend upon any particular flow analysis code, obsolescence of the methodology developed due to future analysis code improvement will not occur. Flow field property formulations of the approximation method should be pursued as being most suitable for complex multiple parameter design problems.

REFERENCES

1. Stahara, S. S., Chaussee, D. S. and Spreiter, J. R.: Perturbation Solutions for Transonic Flow on a Blade-to-Blade Surface of Compressor Blade Rows. NASA CR-2941, January 1978.

2. Stahara, S. S., Crisalli, A. J., and Spreiter, J. R.: Evaluation of a Strained Coordinate Perturbation Procedure: Nonlinear Subsonic and Transonic Flows. AIAA Paper No. 80-0339, January 1980.

3. Stahara, S. S., Elliott, J. P., and Spreiter, J. R.: A Rapid Method for the Approximate Determination of Nonlinear Solutions: Application to Aerodynamic Flows. ICAS Paper No. 80-7.5, October 1980.

4. Stahara, S. S., Elliott, J. P., and Spreiter, J. R.: A Rapid Perturbation Procedure for Determining Nonlinear Flow Solutions: Application to Transonic Turbomachinery Flows. NASA CR-3425, May 1981.

5. Stahara, S. S.: The Rapid Approximate Determination of Nonlinear Solutions: Application to Aerodynamic Flows and Design/Optimization Problems. Transonic Aerodynamics. (Ed. D. Nixon) Vol. 81, Progress in Astronautics and Aeronautics. AIAA, N.Y., 1982, pp. 637-659.

6. Stahara S S., Elliott, J. P., and Spreiter, J. R.: Development of a Multiple-Parameter Nonlinear Perturbation Procedure for Transonic Turbomachinery Flows: Preliminary Application to Design/Optimization Problems. NASA CR-3657, January 1983.

7. Stahara, S. S.: Development of a Turbomachinery Design Optimization Procedure Using a Multiple-Parameter Nonlinear Perturbation Method. NASA CR-3831, September 1984.

8. Cosentino, G. B. and T. L. Holst: Numerical Optimization Design of Advanced Transonic Wing Configurations. NASA Tech. Memo. 85950, May 1984.

9. Kennelly, R. A., Jr.: Improved Method for Transonic Airfoil Design-by-Optimization. AIAA Paper No. 83-1864, July 1983.

10. Numerical Solution of Transonic Flow Fields. T.L. Holst and S.D. Thomas, AIAA Journal, Vol. 21, No. 6, June 1983, pp. 863-870.

11. Van Dyke, M.: Perturbation Methods in Fluid Mechanics. The Parabolic Press, California, 1975.

12. Lighthill, M. J.: A Technique for Rendering Approximate Solutions to Physical Problems Uniformly Valid, Philosophical Magazine, Vol. 40, 1949, pp. 1179-1201.

13. Pritulo, M. F.,: On the Determination of Uniformly Accurate Solutions of Differential Equations by the Method of Perturbation Coordinates, Journal of Applied Mathematics and Mechanics, Vol. 26, 1962, pp. 661-667.

14. Nixon, D.: Perturbation Methods in Transonic Flow. AIAA Paper No. 80-1367, July 1980.

15. Nixon, D.: Perturbations in Two- and Three-Dimensional Transonic Flows. AIAA J., Vol. 16, July 1978, pp. 699-709.

16. Madsen, L. E. and Vanderplaats, G. N.: COPES - A Fortran Control Program for Engineering Synthesis. NPS 69-81-003, March 1982.

17. Katsanis, T. and McNally, W. D.: Fortran Program for Calculating Velocities and Streamlines on a Blade-to-Blade Stream Surface of a Tandem Blade Turbomachine. NASA TND-5044, 1969.

18. Nixon, D.: Design of Transonic Airfoil Sections Using a Similarity Theory NASA TM 78521, October 1978.

19. Hicks, R. M. and Vanderplaats, G. N.: Application of Numerical Optimization to the Design of Low-Speed Airfoils. NASA TM X-3213, 1975.

20. Hicks, R. M., Vanderplaats, G. N., E. M. Murman, and R. R. King: Airfoil Section Drag Reduction at Transonic Speeds by Numerical Optimization. SAE Paper 760477, 1976.

21. Hicks, R. M. and P. A. Henne: Wing Design by Numerical Optimization. AIAA Paper 77-1247, 1977.

22. Hicks, R. M. and Vanderplaats, G. N.: Application of Numerical Optimization to the Design of Supercritical Airfoils without Drag-Creep. SAE Paper 770440, 1977.

23. Haney, H. P., R. R. Johnson, and R. M. Hicks: Computational Optimization and Wind Tunnel Test of Transonic Wing Designs. AIAA Paper 79-0080, 1979.

24. Haney, H. P.: A-7 Transonic Wing Designs. Transonic Aerodynamics. (Ed. D. Nixon) Vol. 81, Progress in Astronautics and Aeronautics. AIAA, N.Y., 1982, pp. 431-450.

25. Hinson, M. L.: A Series of Airfoils Designed by Transonic Drag Minimization for Gates Learjet Aircraft. Transonic Aerodynamics. (Ed. D. Nixon) Vol. 81, Progress in Astronautics and Aeronautics. AIAA, N.Y., 1982, pp. 489-510.

26. Vanderplaats, G. N.: CONMIN - A Fortran Program for Constrained Function Minimization, User's Manual. NASA TMX-62, 282, August 1973.

27. Gill, P. E., E. W. Murray, and R. A Pitfield: The Implementation of Two Revised Quasi-Newton Algorithms for Unconstrained Optimization. National Physical Lab., Division of Numerical Analysis and Computing Report No. NAC 11, 1972.

28. Gill, P. E., E. W. Murray, and M. H. Wright: Practical Optimization. Academic Press, London, 1981.

29. Henne, P. A. and R. M. Hicks: Private Communication. January 1989.

30. Stahara, S. S. and J. R. Spreiter: Transonic Flows Past Nonaxisymmetric Slender Shapes: Classical Equivalence Rule Analysis, AIAA Journal, Vol 17, March 1979, pp. 245-252.

31. Stahara, S. S. and J. R. Spreiter: A Transonic Wind Tunnel Interference Assessment -- Axisymmetric Flows. AIAA Journal, Vol 18, January 1980, pp. 63-71.

32. Stahara, S. S., Elliott, J. P. and Spreiter, J. R.: Transonic Flow Past Axisymmetric and Nonaxisymmetric Boattail Projectiles. AIAA Journal, Vol 20, October 1982, pp.1329-1337.

33. Taylor, R. A.: Pressure Distributions at Transonic Speeds for Bumpy and Indented Midsections of a Basic Parabolic-Arc Body. NASA Memo 1-22-59A, 1959.

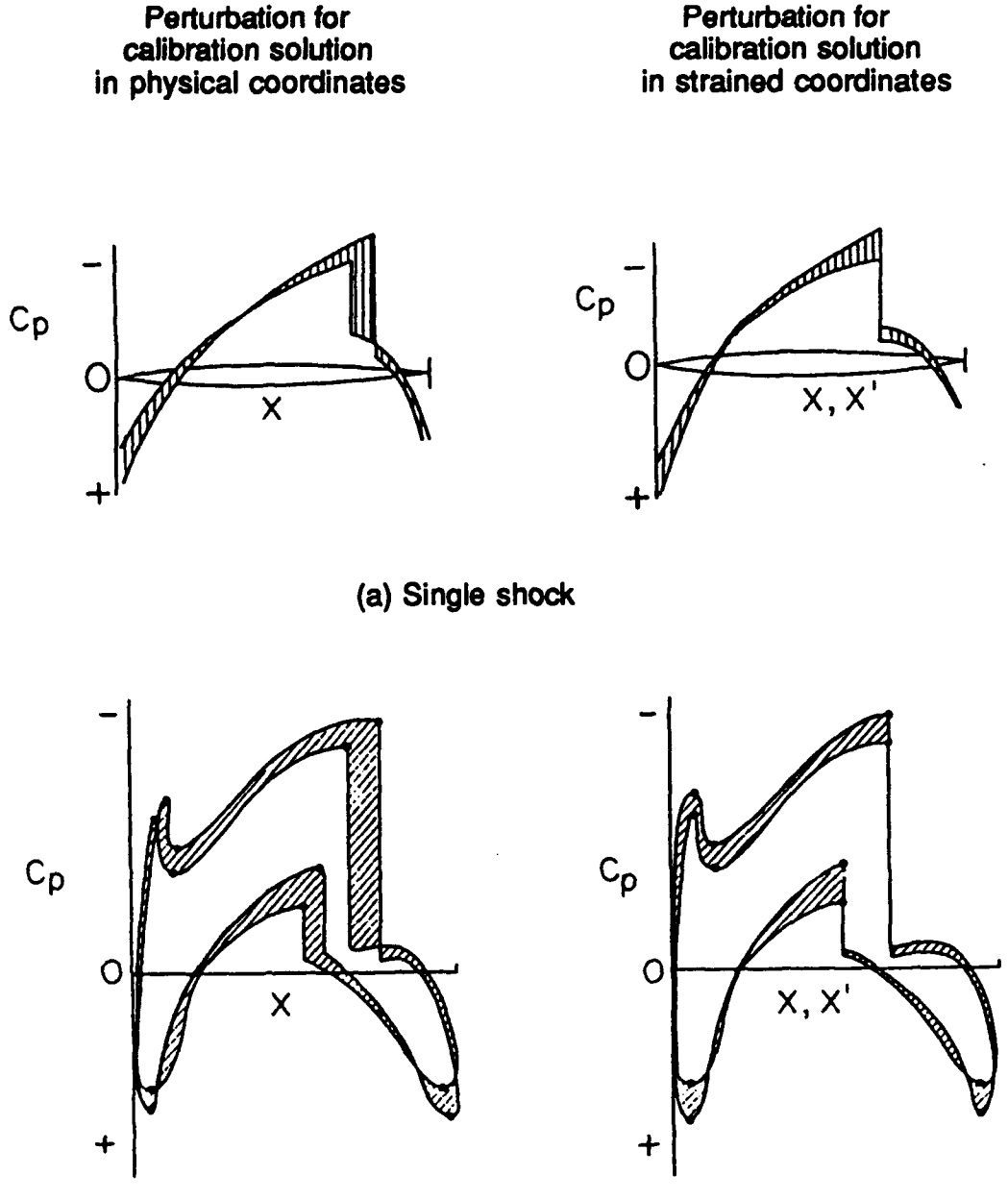

Figure 1. Illustration of perturbation solution for calibration solution in physical and strained coordinates

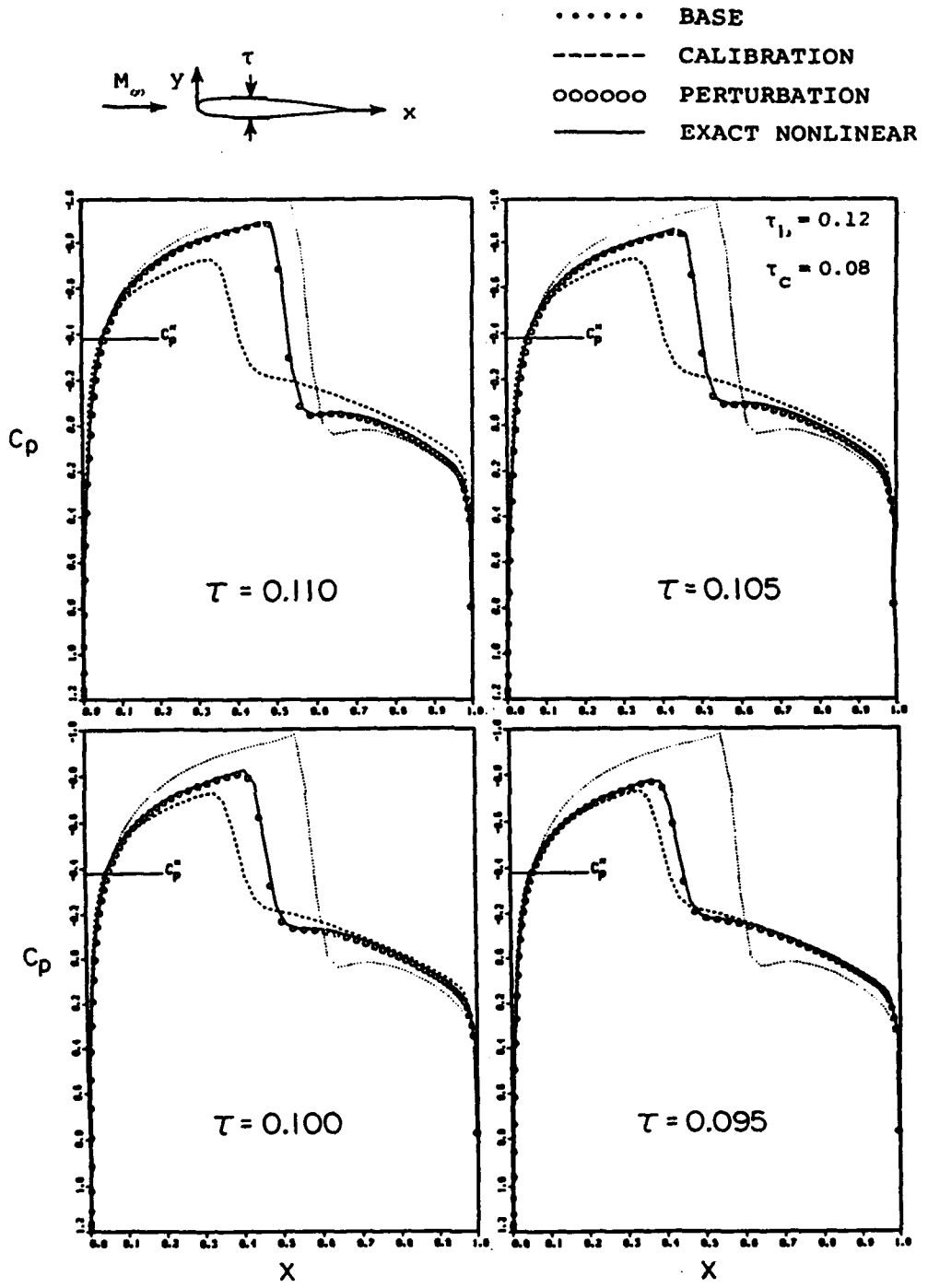

Figure 2. Comparison of perturbation and exact nonlinear surface pressure distributions for a thickness-ratio perturbation of an isolated NACA 00XX blade profile at $M_\infty = 0.820$ and $\alpha = 0°$ for solution interpolation

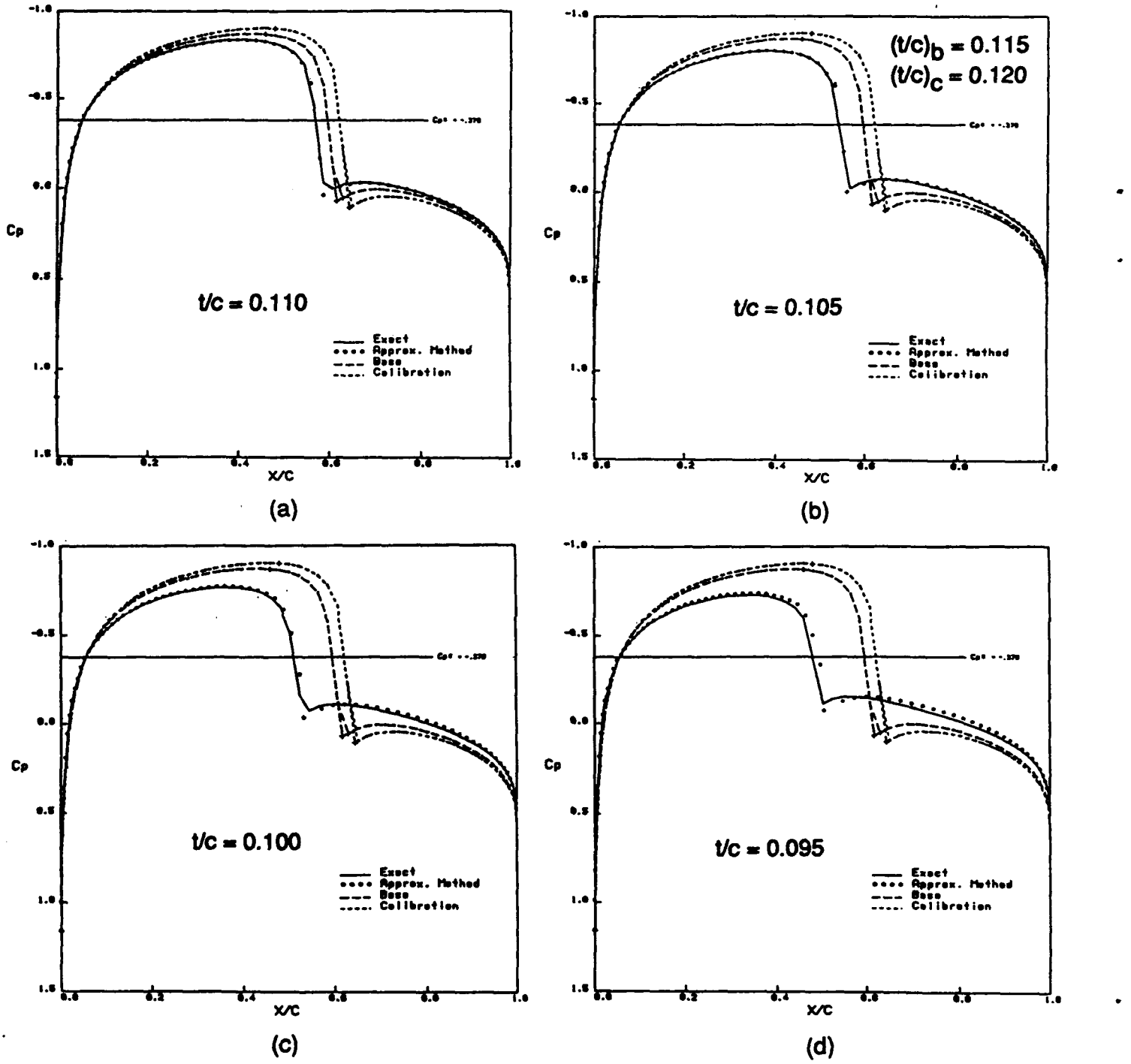

Figure 3. Comparison of approximation predicted and exact nonlinear surface pressure distributions for a thickness-ratio perturbation of a NACA 00XX blade profile at $M_\infty = 0.820$ and $\alpha = 0°$ for extreme solution extrapolation

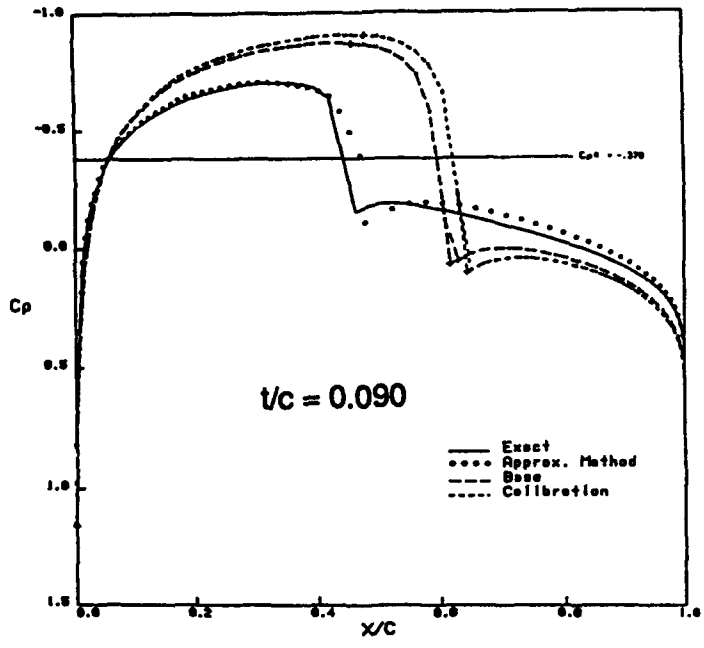

(e)

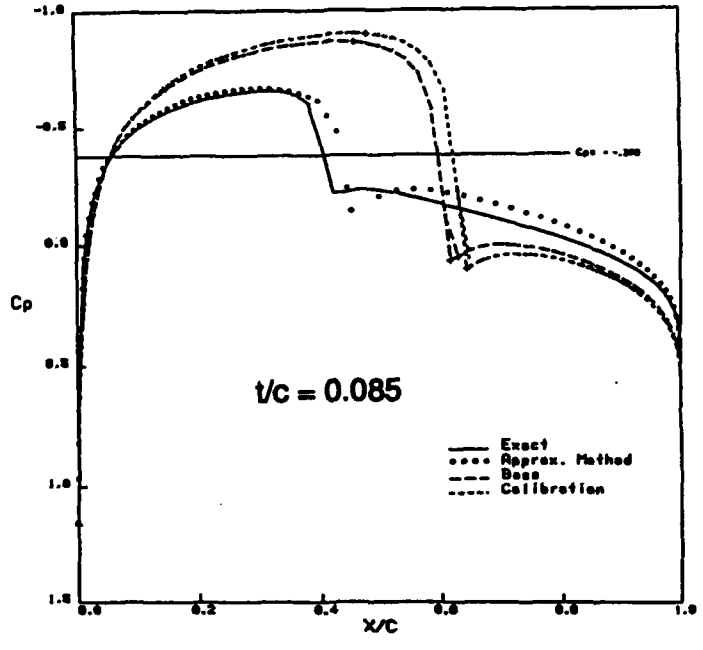

(f)

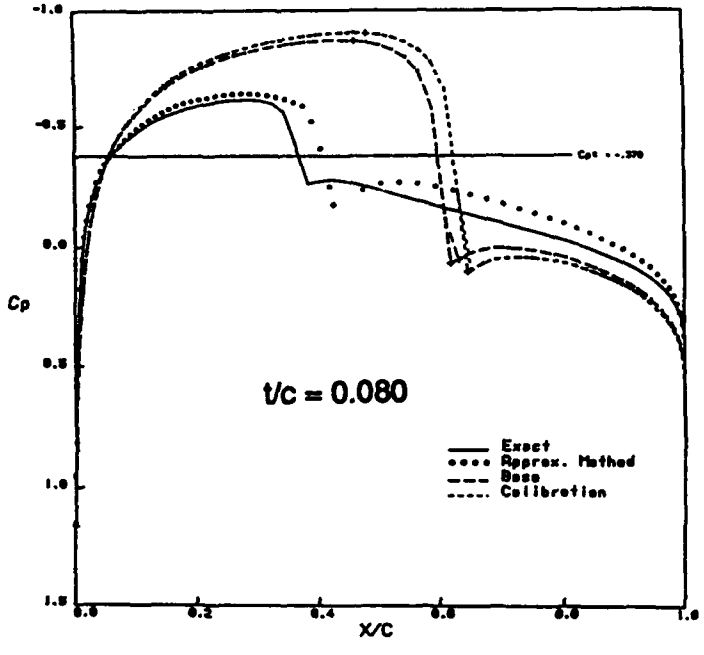

(g)

Figure 3. - Concluded

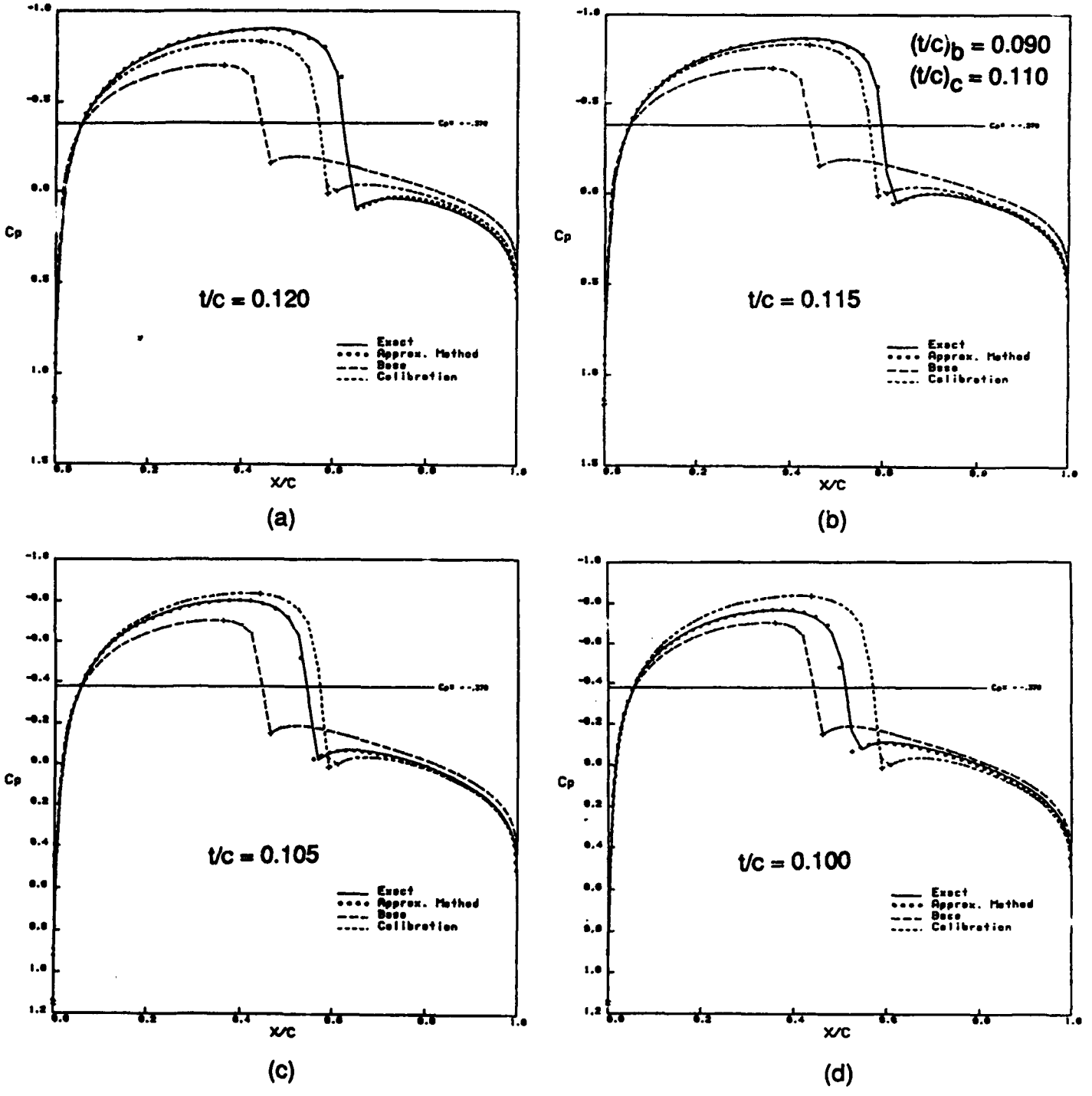

Figure 4. Comparison of approximation predicted and exact nonlinear surface pressure distributions for a thickness-ratio perturbation of a NACA 00XX blade profile at $M_\infty = 0.820$ and $\alpha = 0°$ for illustrating both solution interpolation and extrapolation

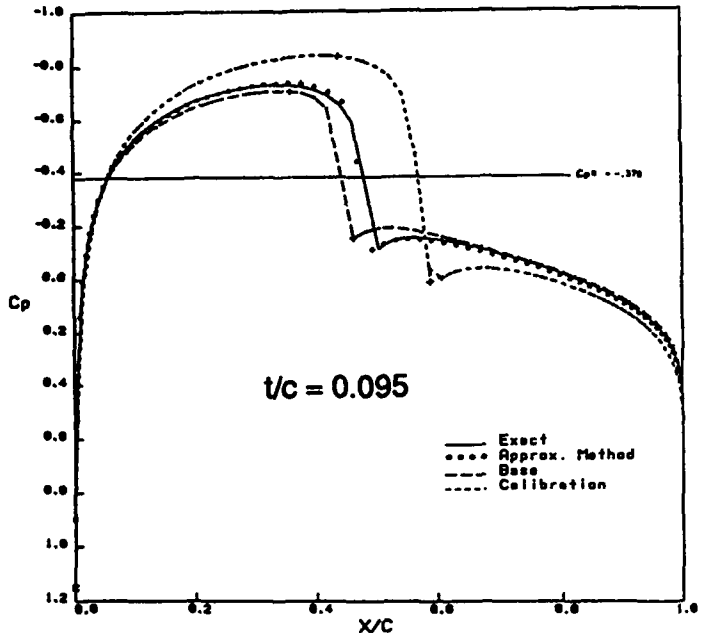

(e)

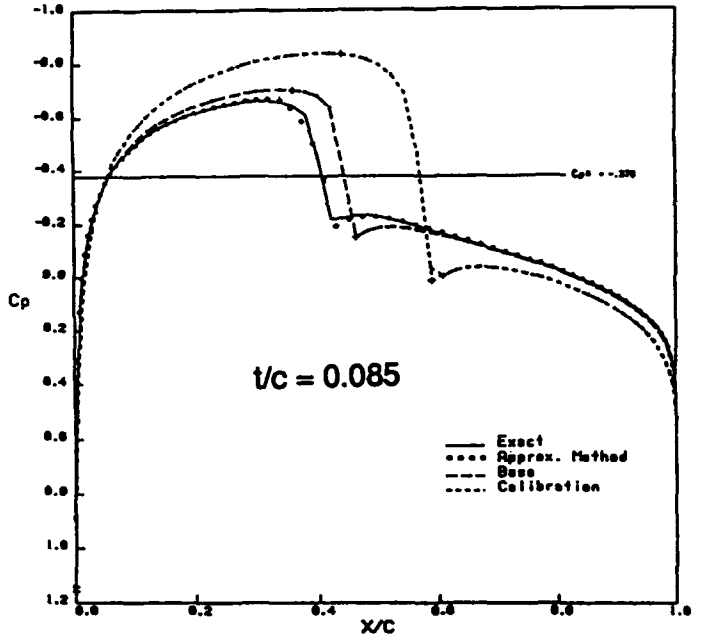

(f)

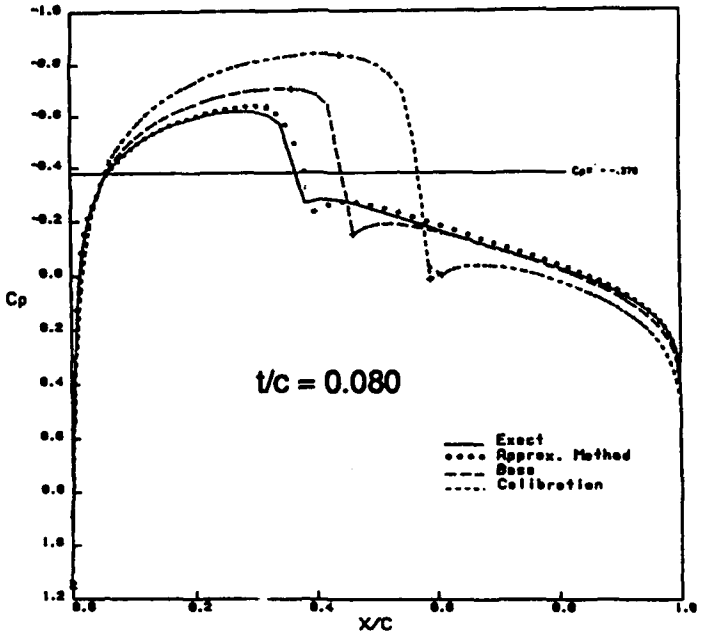

(g)

Figure 4. - Concluded

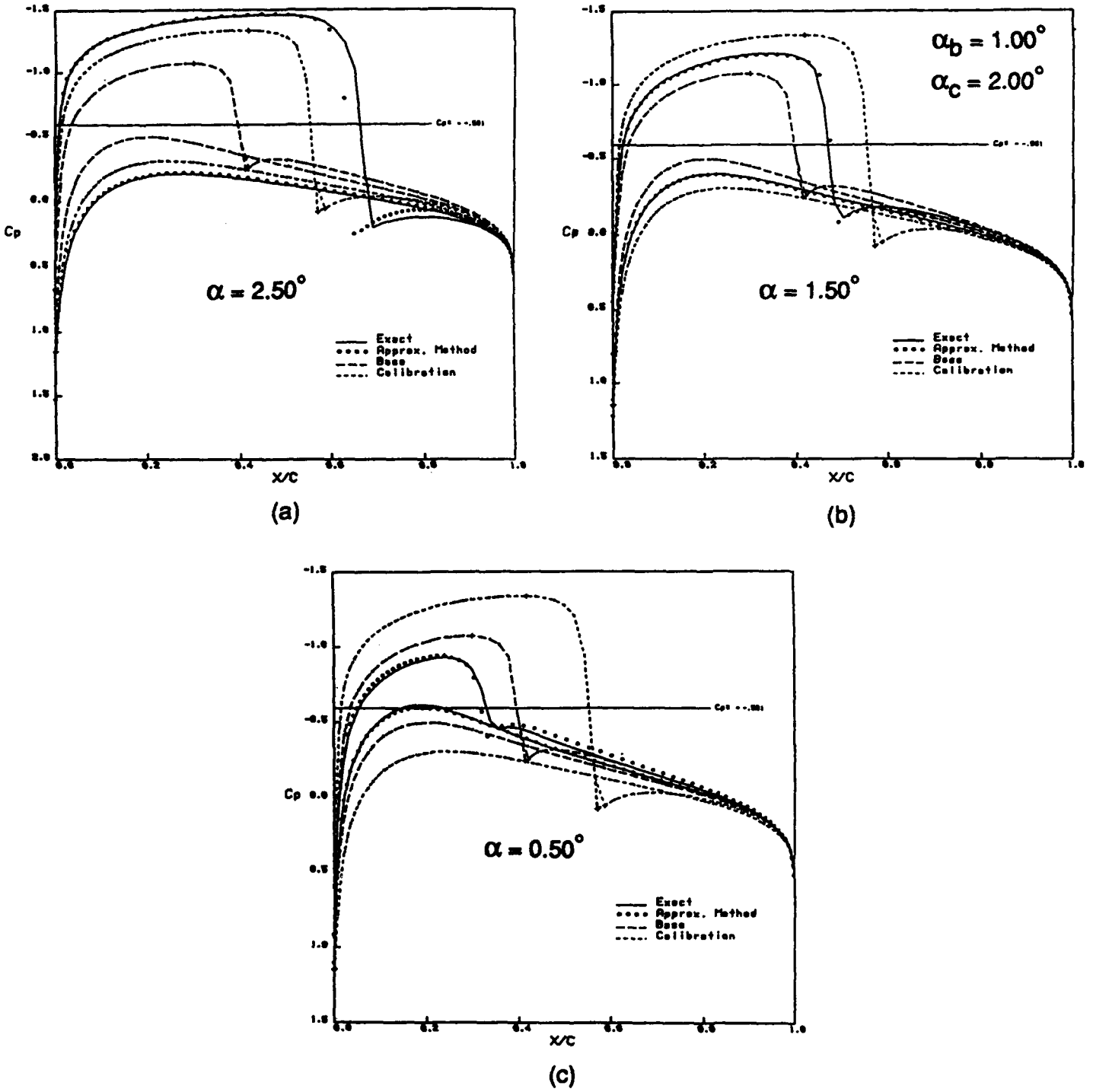

Figure 5. Comparison of approximation predicted and exact nonlinear upper and lower surface pressure distributions for an angle-of-attack perturbation of a NACA 0012 blade profile at M_∞ = 0.750 illustrating both solution interpolation and extrapolation

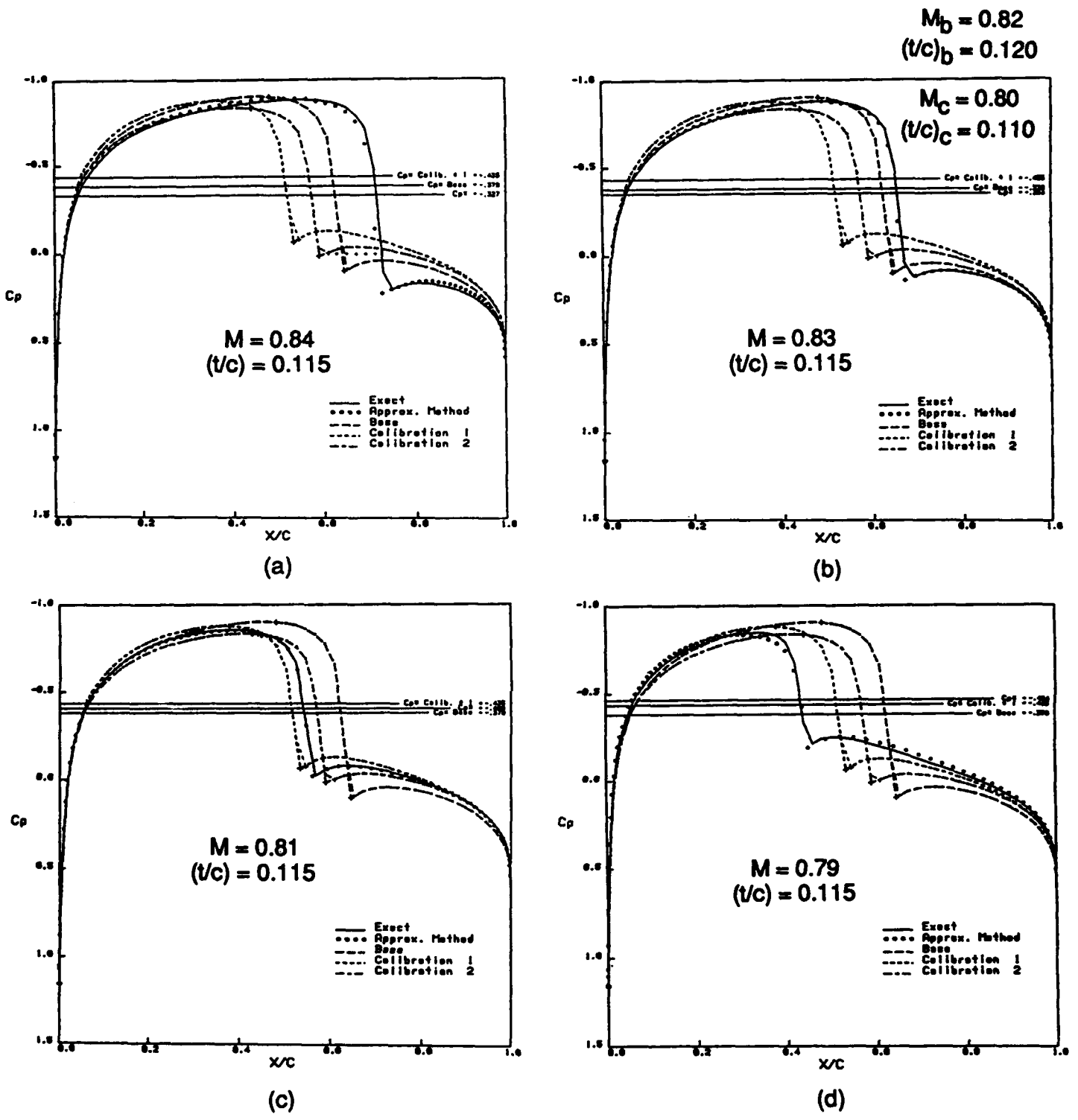

Figure 6. Comparison of approximation predicted and exact nonlinear surface pressure distributions for a simultaneous perturbation of a oncoming Mach number and thickness ratio of a symmetric NACA 00XX blade profile illustrating both solution interpolation and extrapolation

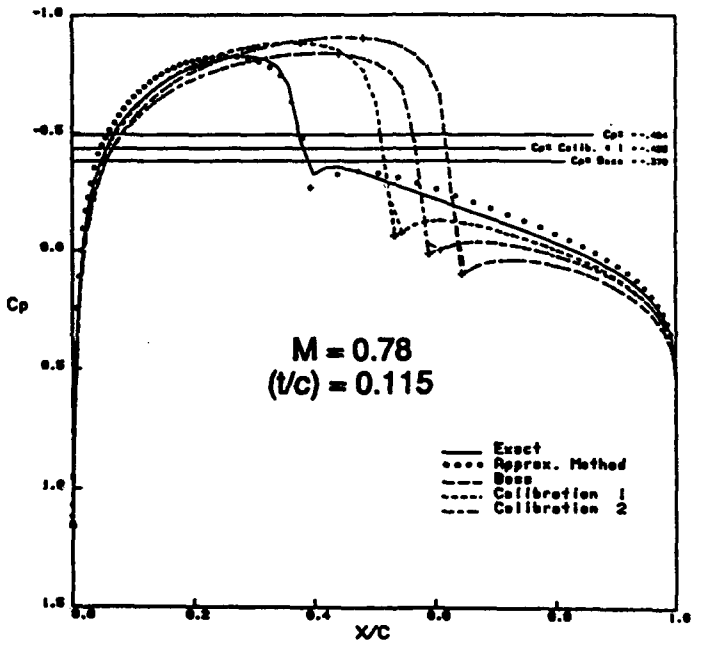

(e)

Figure 6. - Concluded

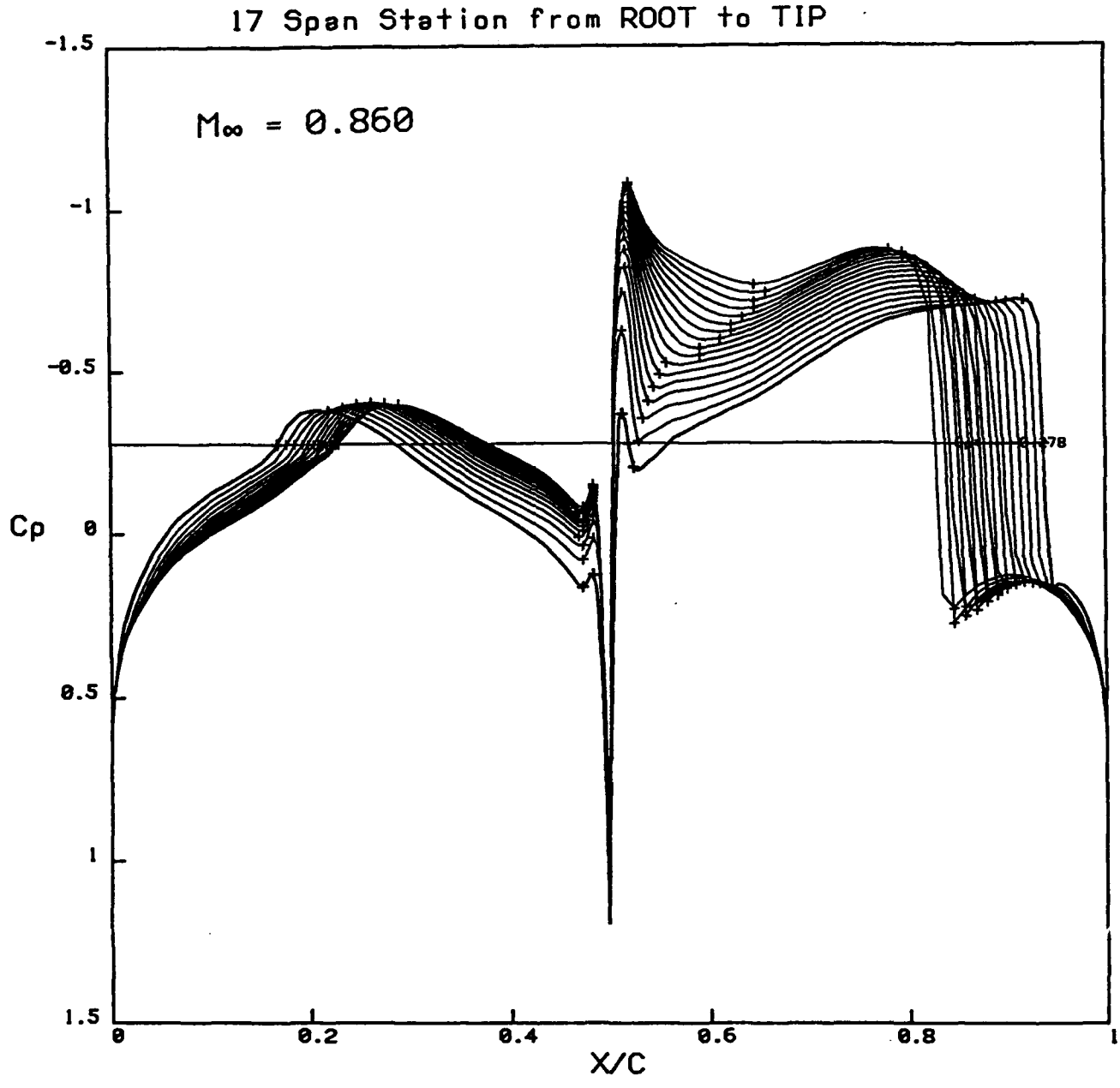

Figure 7. Illustration of a typical 3-D surface pressure distribution characteristic of the type employed in the current 3-D approximation method development and characterization of the various invariant points; chordwise upper and lower surface pressure distributions at 17 spanwise stations from root to tip along blade profile

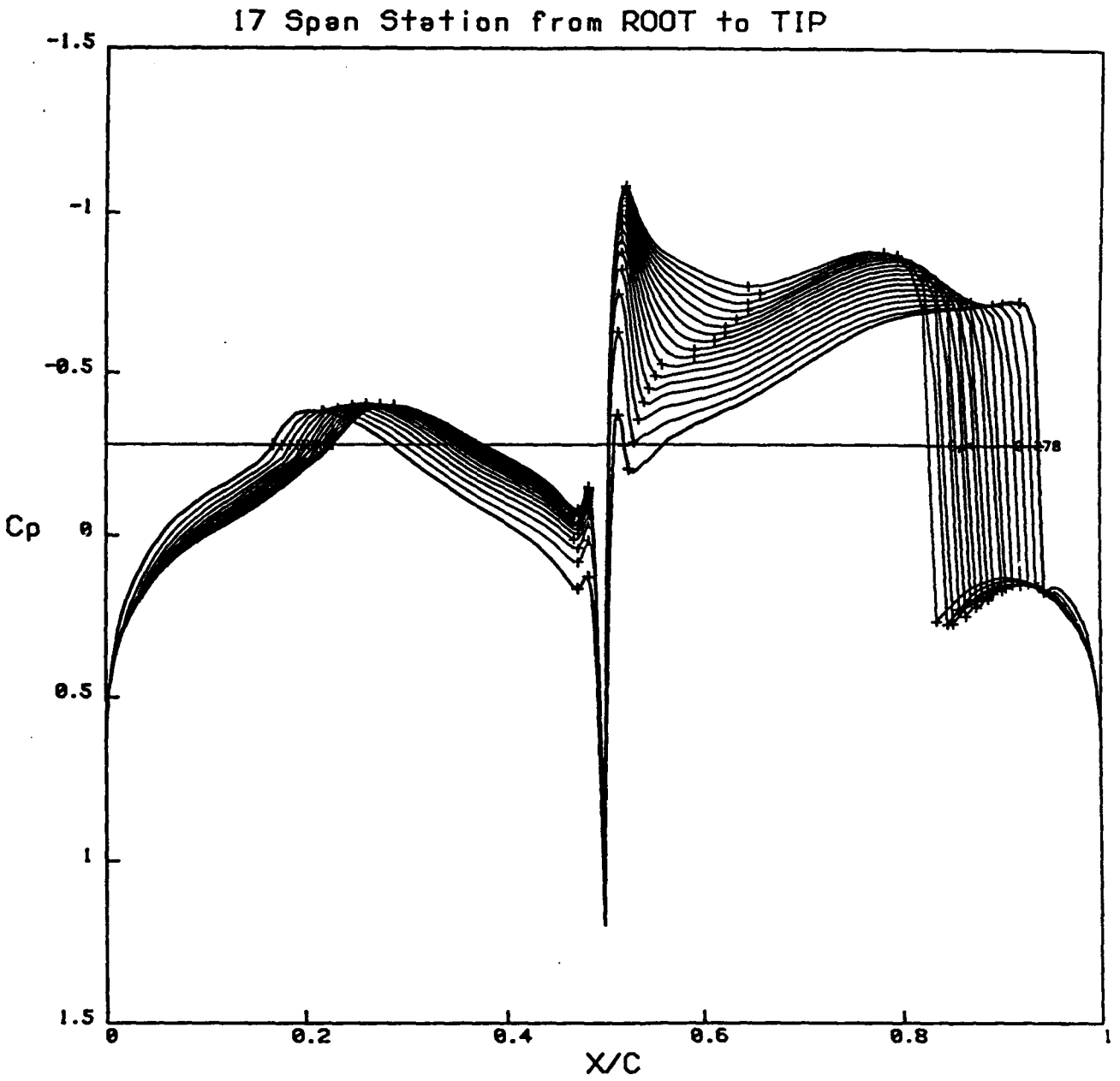

Figure 8. Illustration of the shock wave sharpening achieved by the preprocessing procedure involving the invariant points associated with the surface shock waves on the 3-D supercritical surface pressure distribution shown in Figure 7

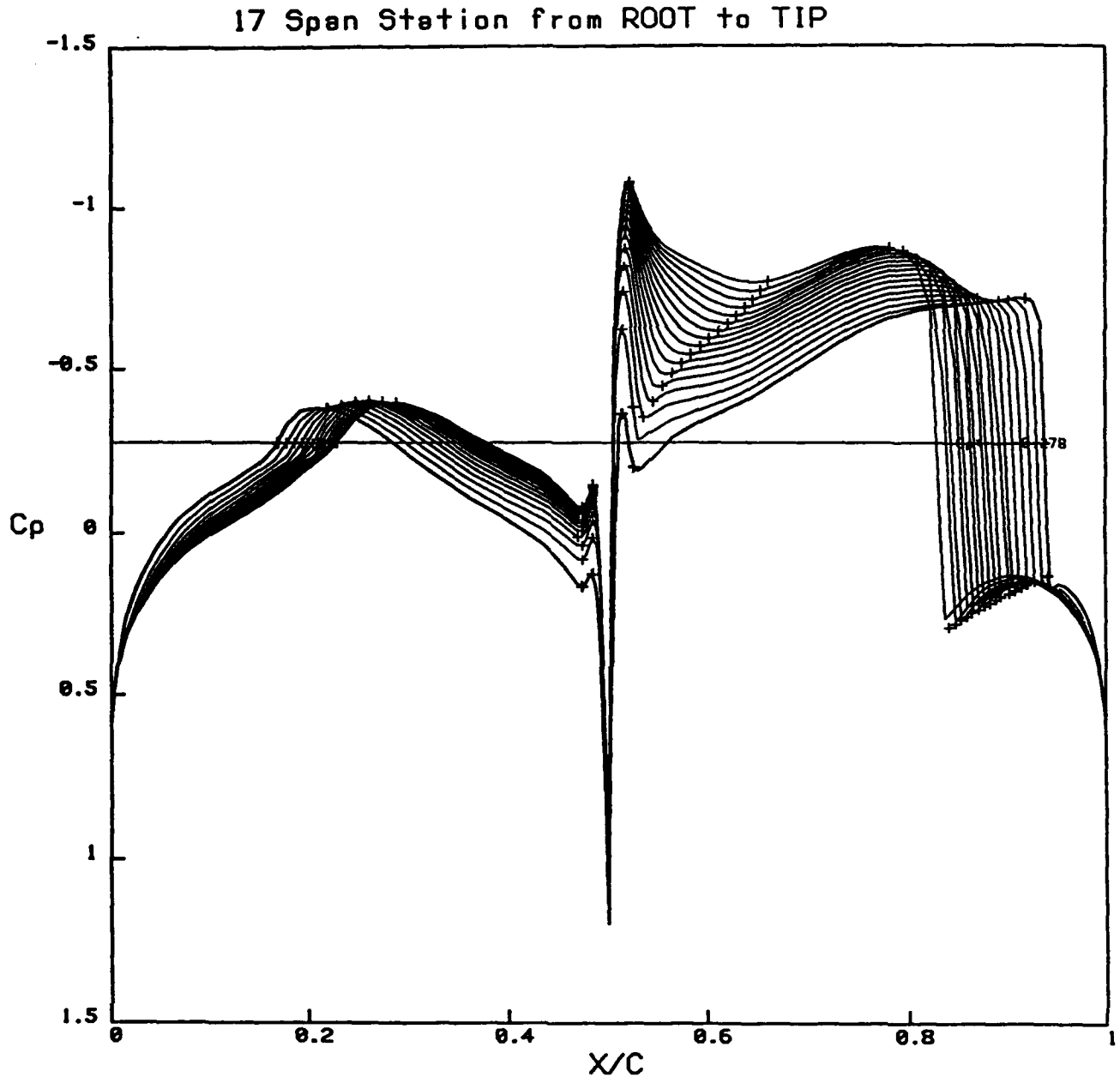

Figure 9. Illustration of the smooth global spanwise correction achieved by the preprocessing procedure acting on all of the invariant points associated with the 3-D supercritical surface pressure distribution shown in Figure 7

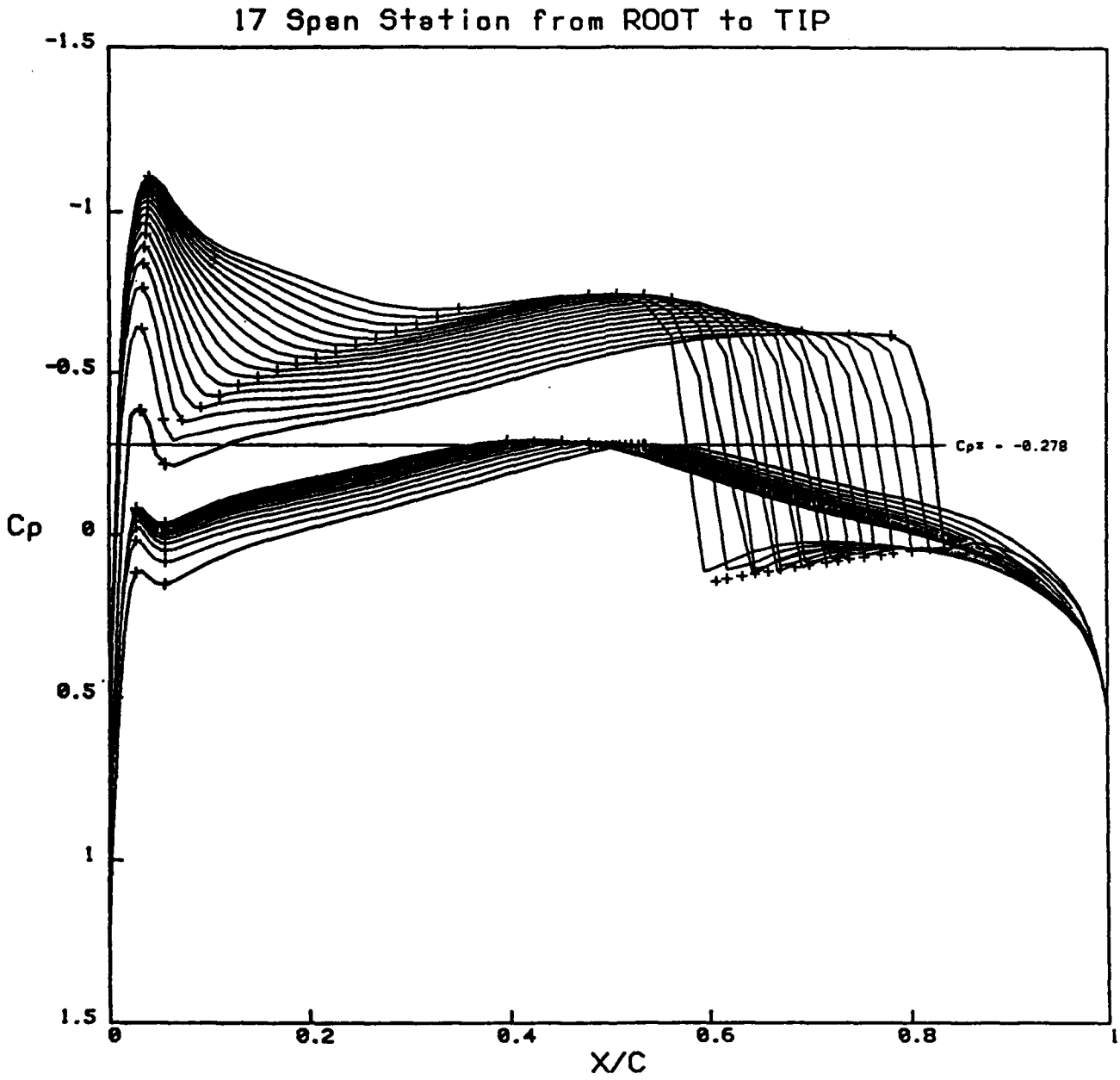

Figure 10. Chordwise surface pressure distributions at 17 spanwise stations for the baseline flow past an isolated 3-D blade having an ONERA M6 profile for $M_\infty = 0.820$ and $\alpha = 3.06°$

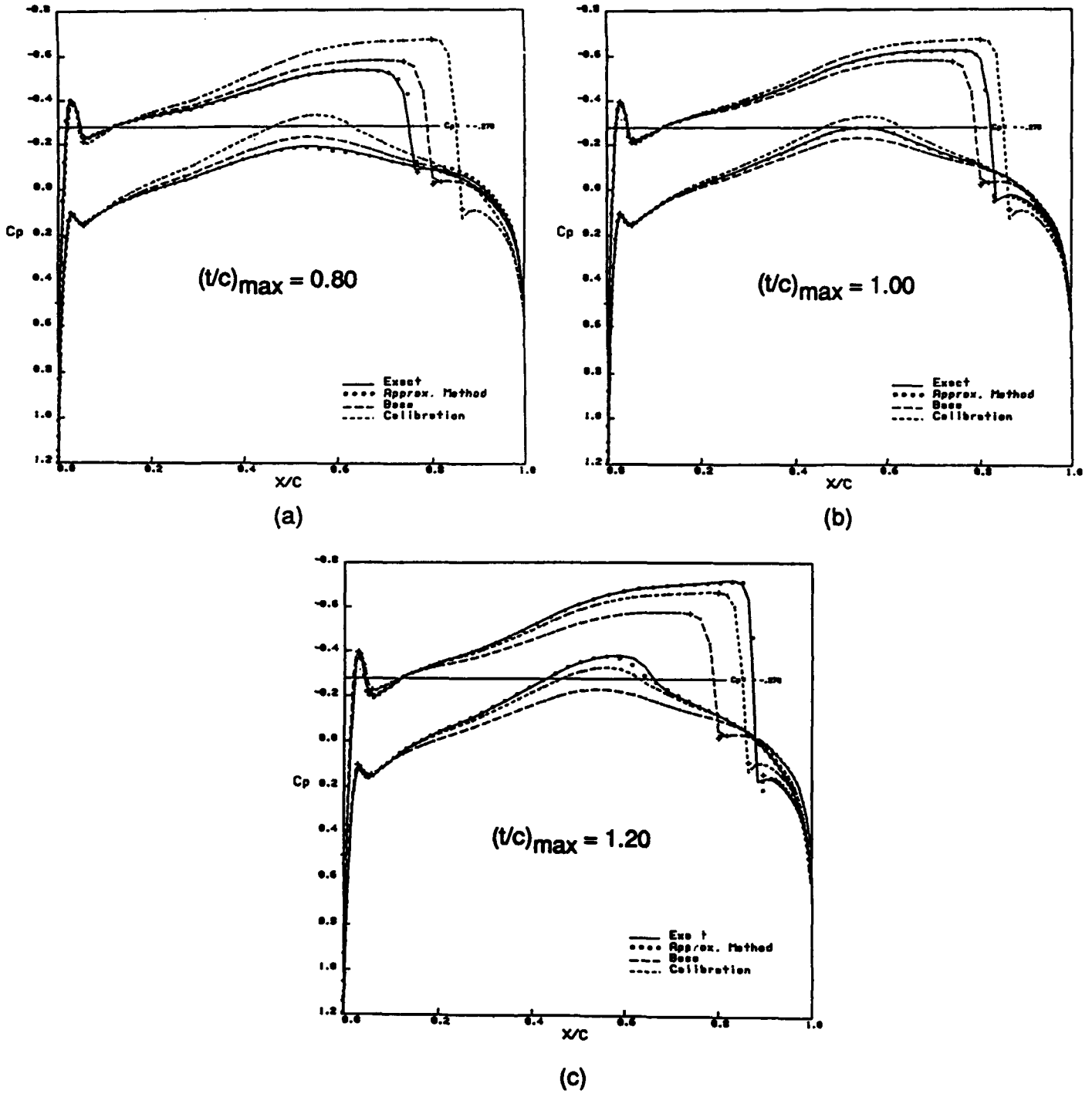

Figure 11. Comparison of 3-D approximation predicted and exact nonlinear surface pressure distributions at the root chord station (y/s = 0.0) for a thickness ratio perturbation of the ONERA M6 blade profile shown in Figure 10 illustrating both solution interpolation and extrapolation

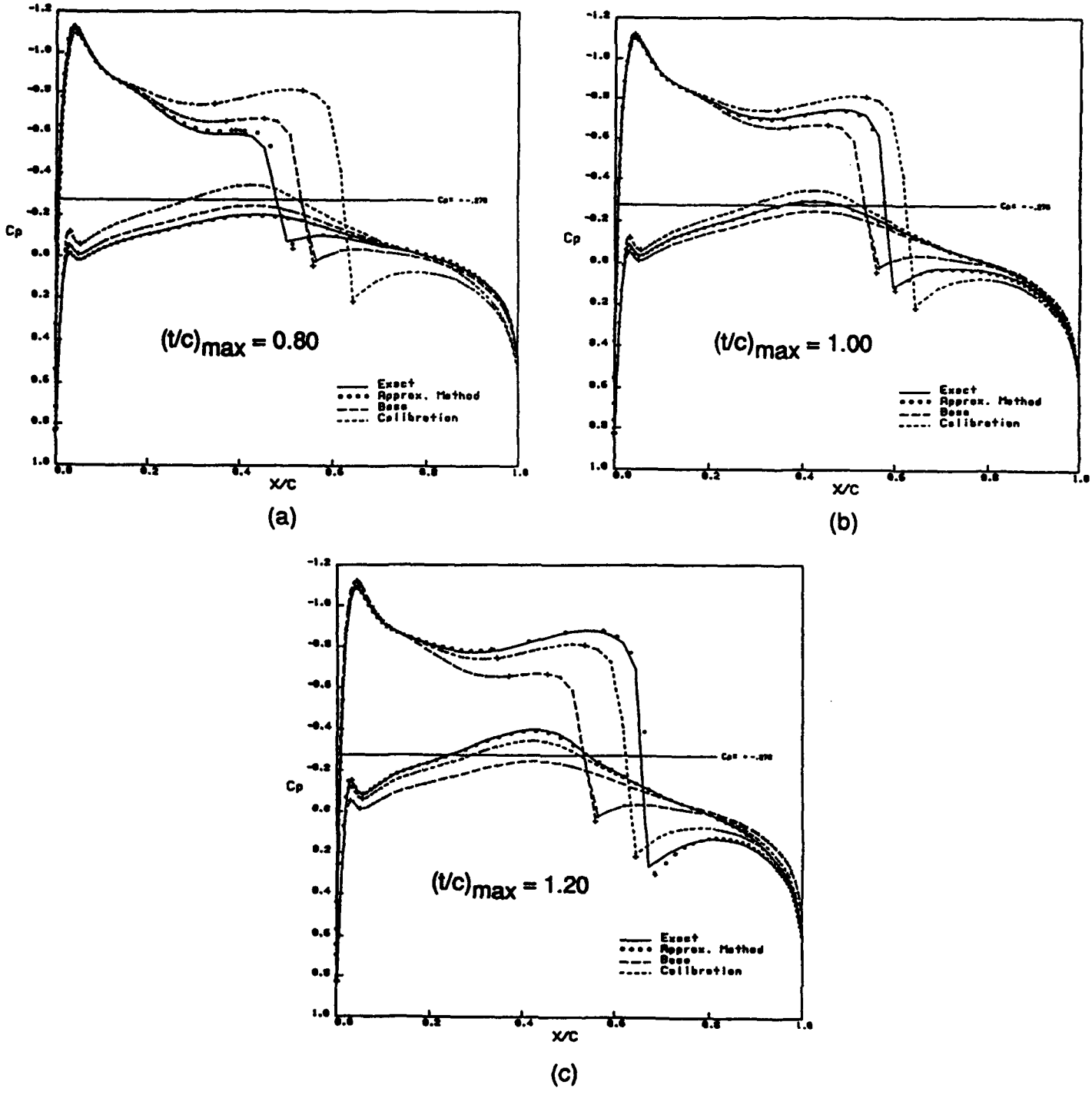

Figure 12. Comparison of 3-D approximation predicted and exact nonlinear surface pressure distributions at the outermost spanwise station (y/s = 0.969) for a thickness ratio perturbation of the ONERA M6 blade profile shown in Figure 10 illustrating both solution interpolation and extrapolation

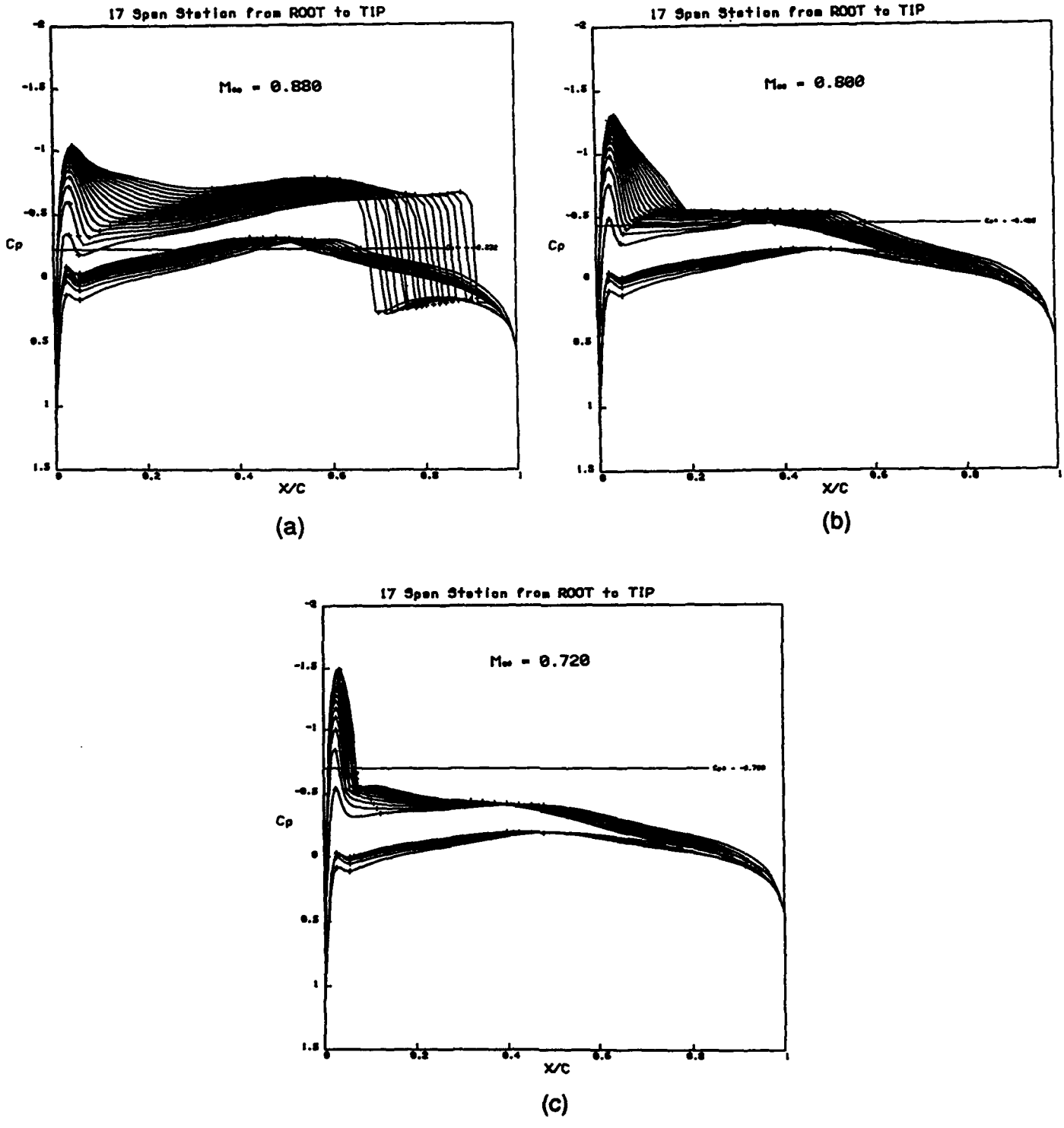

Figure 13. Illustration of the extreme surface pressure topology change involved in the oncoming Mach number perturbation test problem; surface pressure distributions at the beginning, middle, and end of the parameter range M = {0.880, 0.800, 0.720}

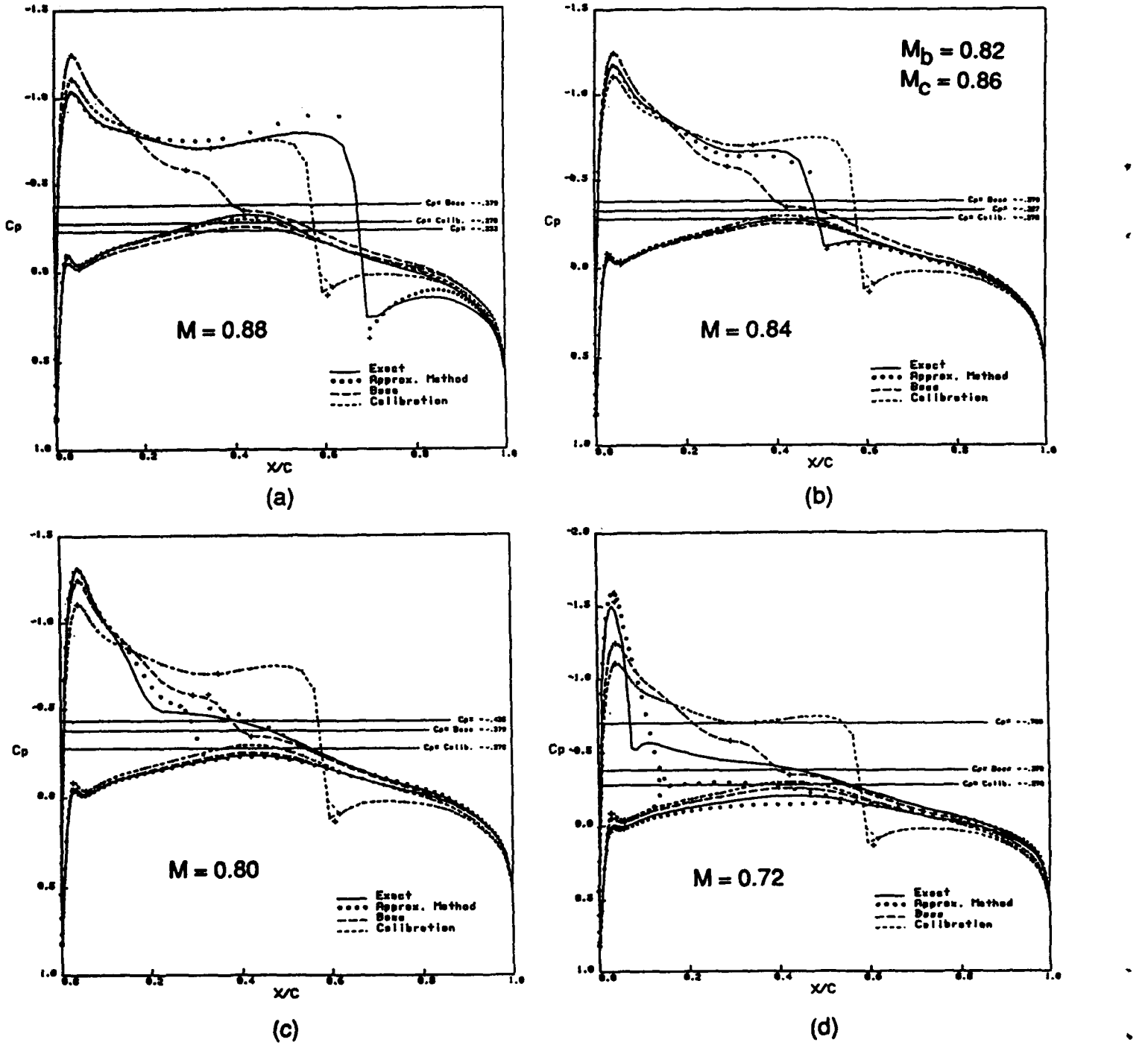

Figure 14. Comparison of 3-D approximation predicted and exact nonlinear surface pressure distributions at the outermost spanwise station (y/s = 0.969) of the ONERA M6 blade profile shown in Figure 10 for an oncoming Mach number perturbation illustrating both solution interpolation and extrapolation

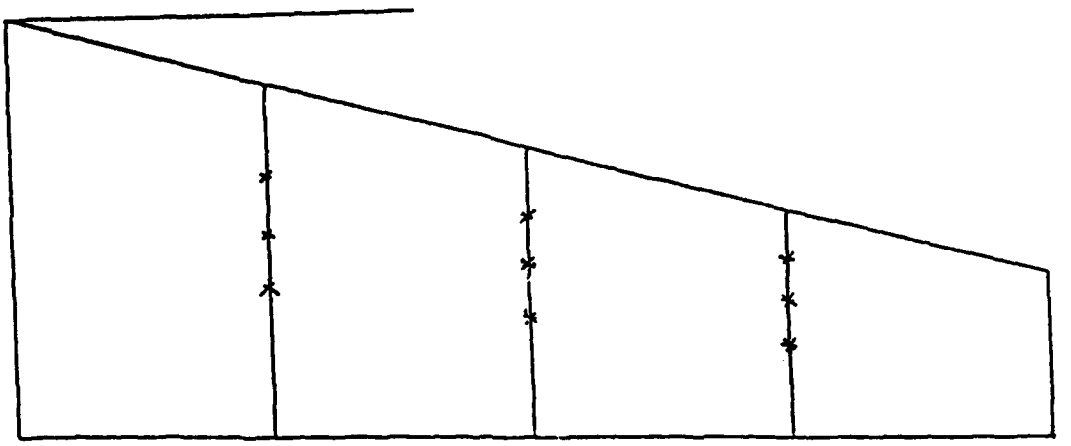

Planform

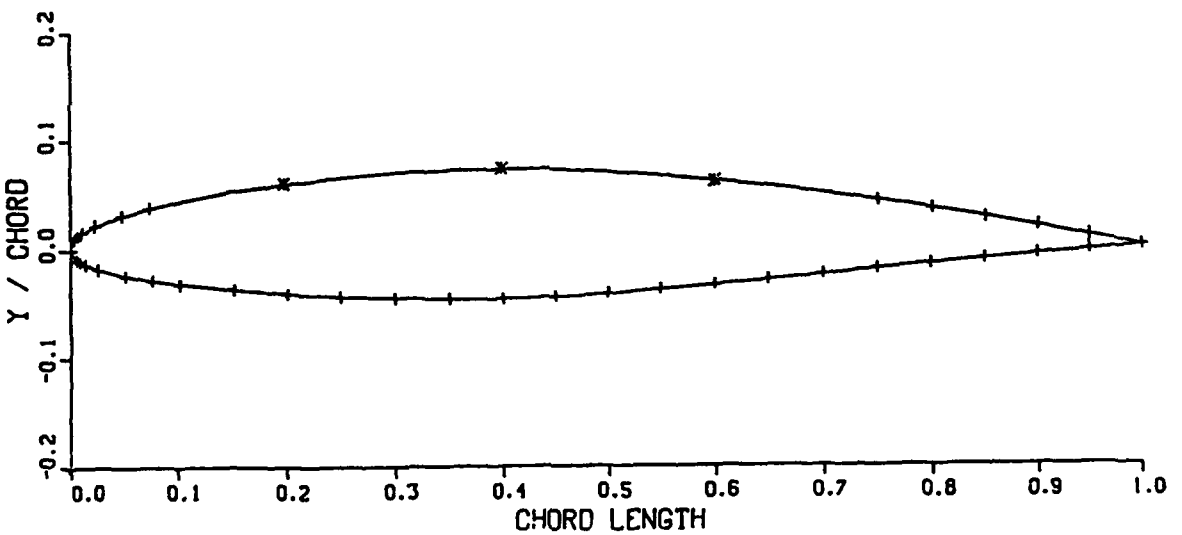

Location of the fixed (+) and movable (*) spline-support points on the NACA 64_1A212 airfoil

Figure 15. Outline of overall optimization design test problem to be employed as the benchmark case study for testing the 3-D approximation method in a design environment; illustration of the isolated blade planform geometry and location of design variable points

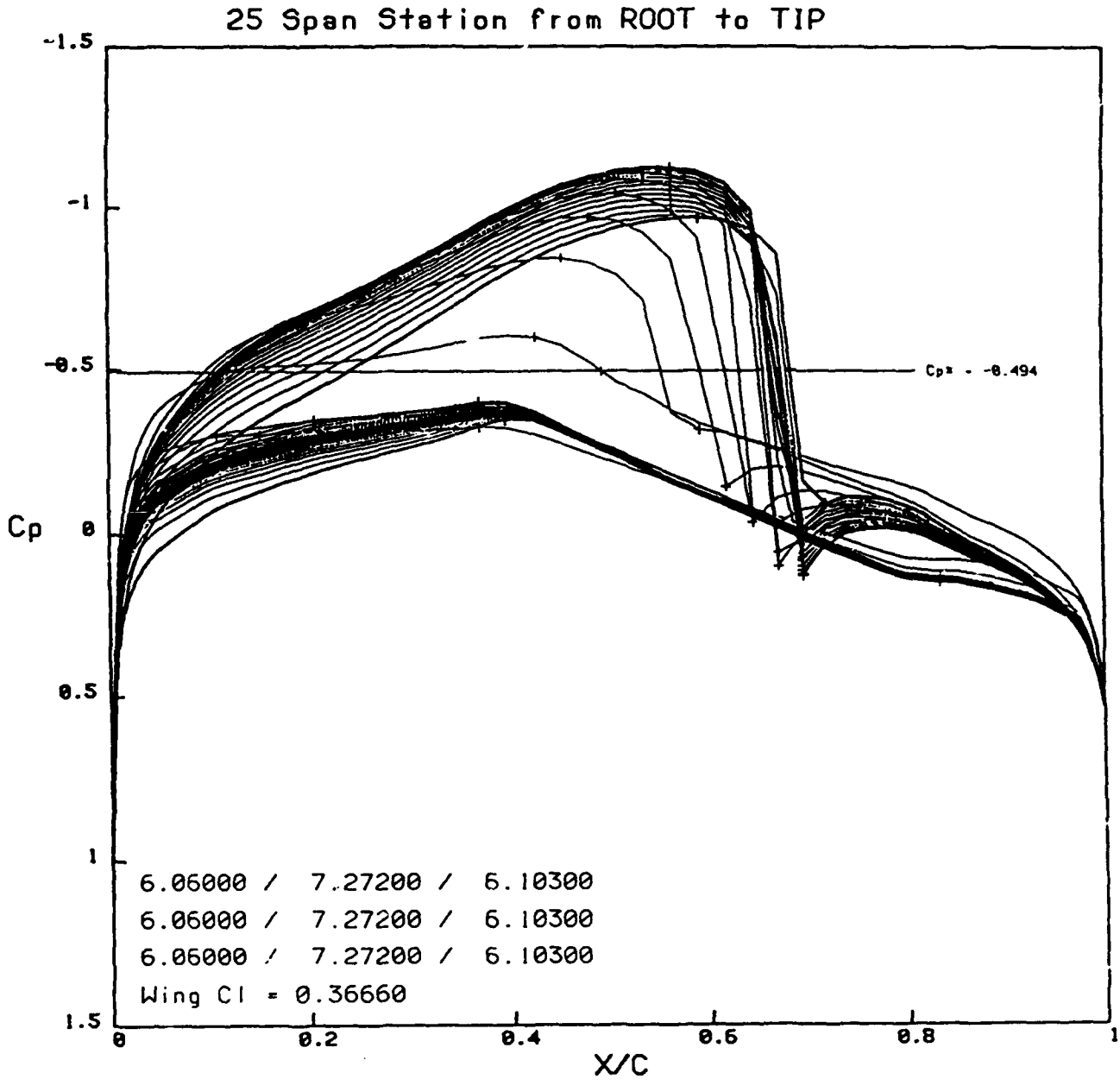

Figure 16. Illustration of the 3-D surface pressure distribution for the original (nonoptimized) configuration for the benchmark optimization case study

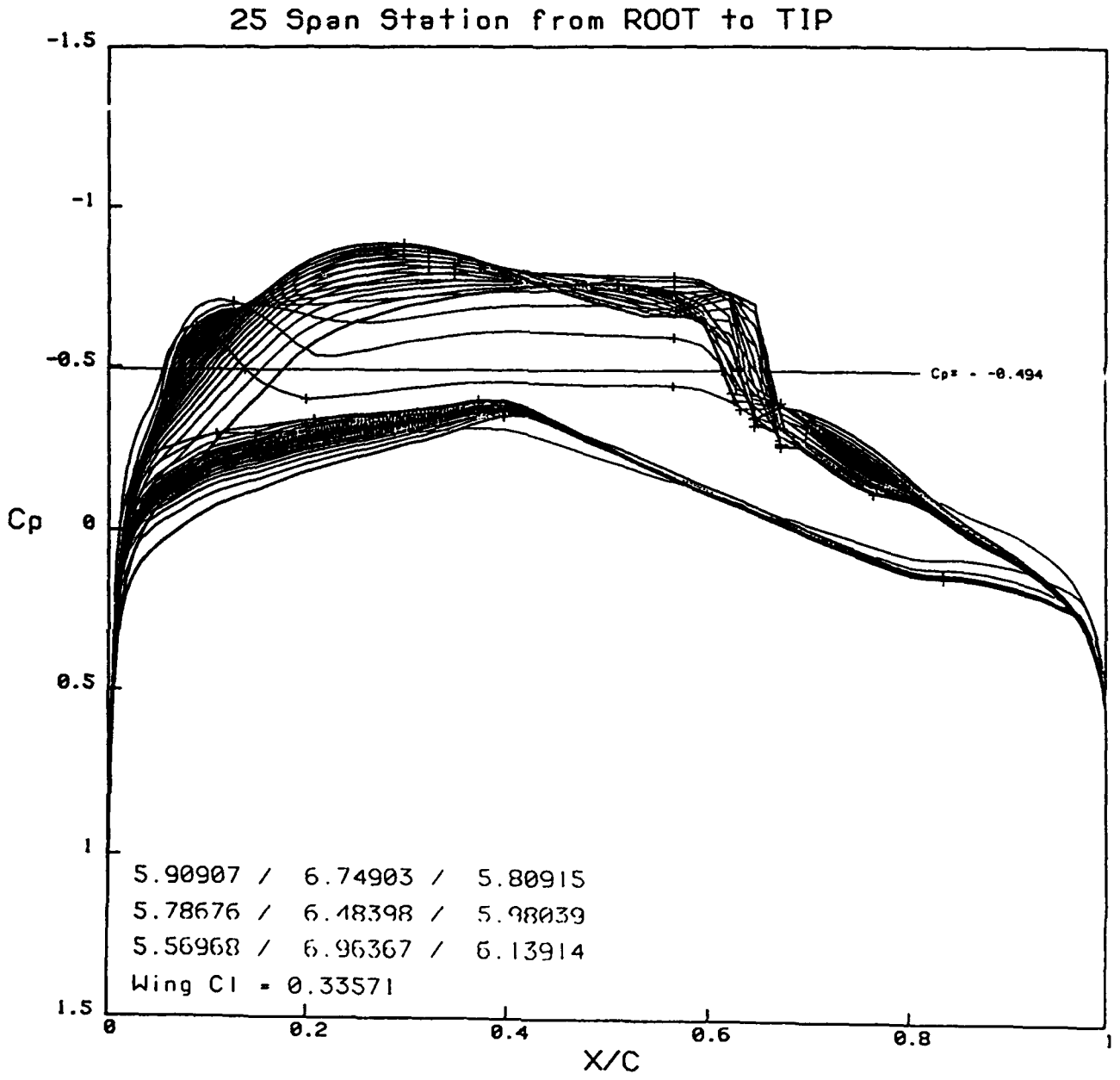

Figure 17. Illustration of the 3-D surface pressure distribution for the optimization-modified configuration after the 7th optimization cycle

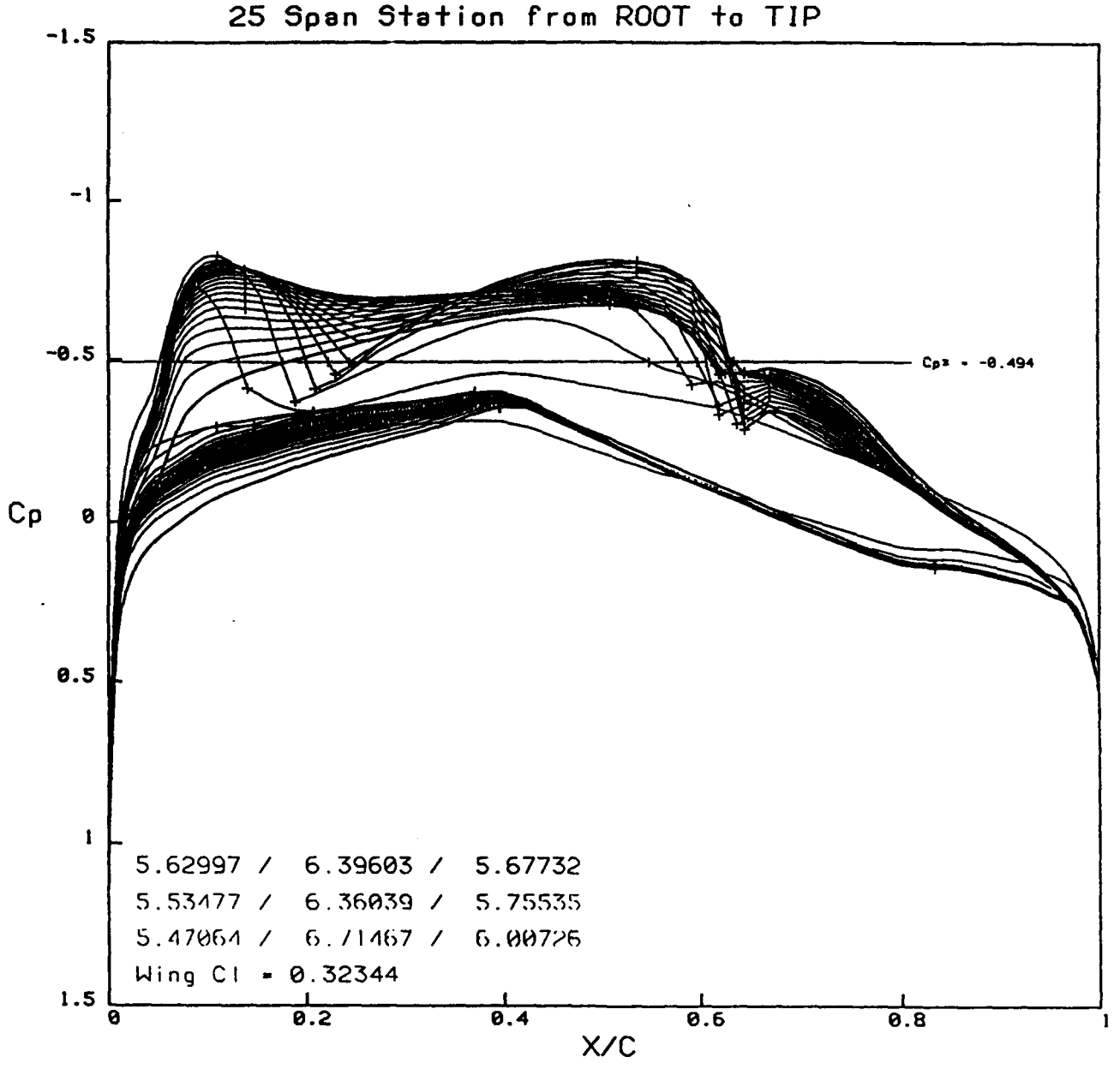

Figure 18. Illustration of the 3-D surface pressure distribution for the optimization-modified configuration after the 8th optimization cycle

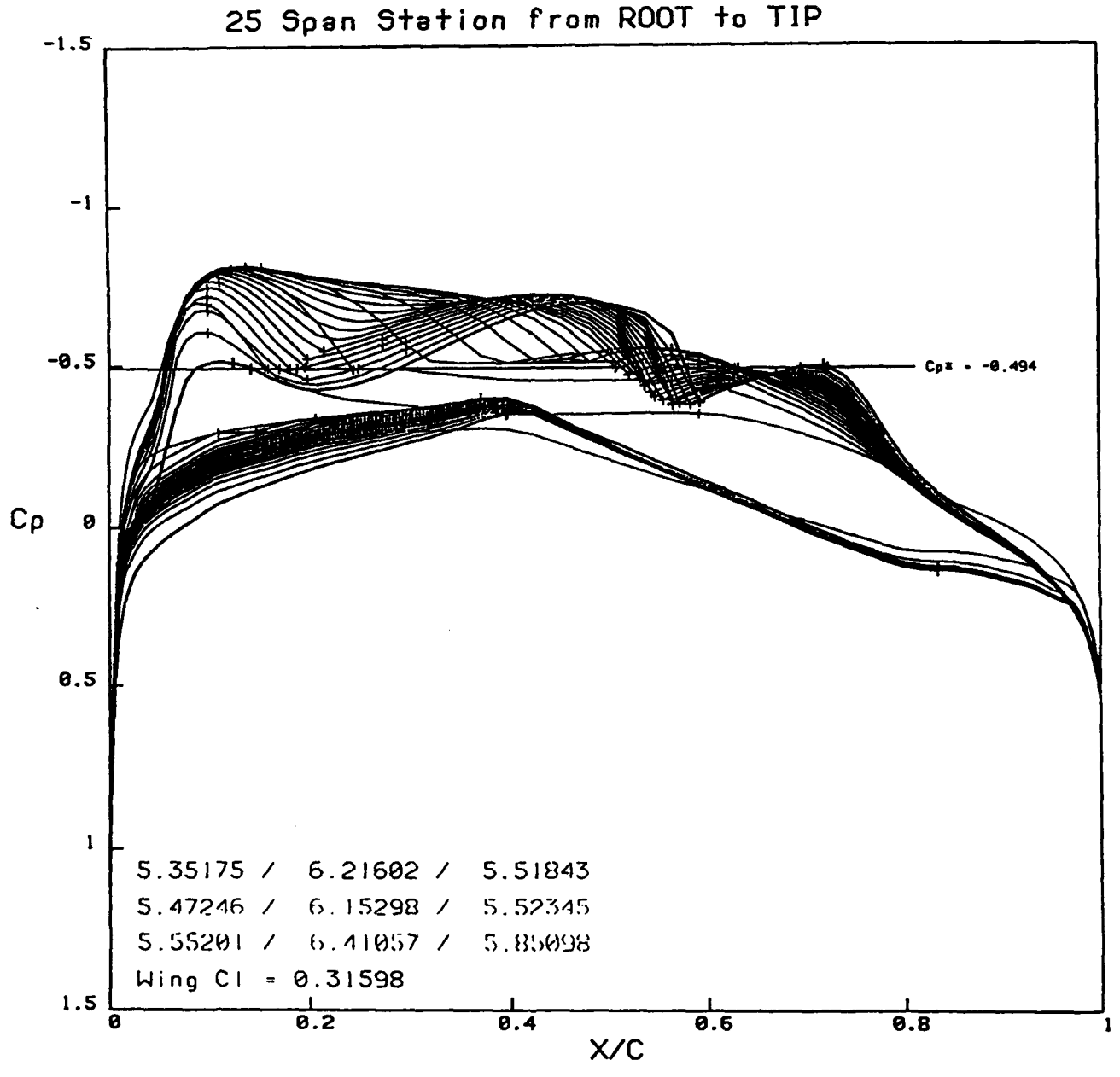

Figure 19. Illustration of the 3-D surface pressure distribution for the optimization-modified configuration after the 9th optimization cycle

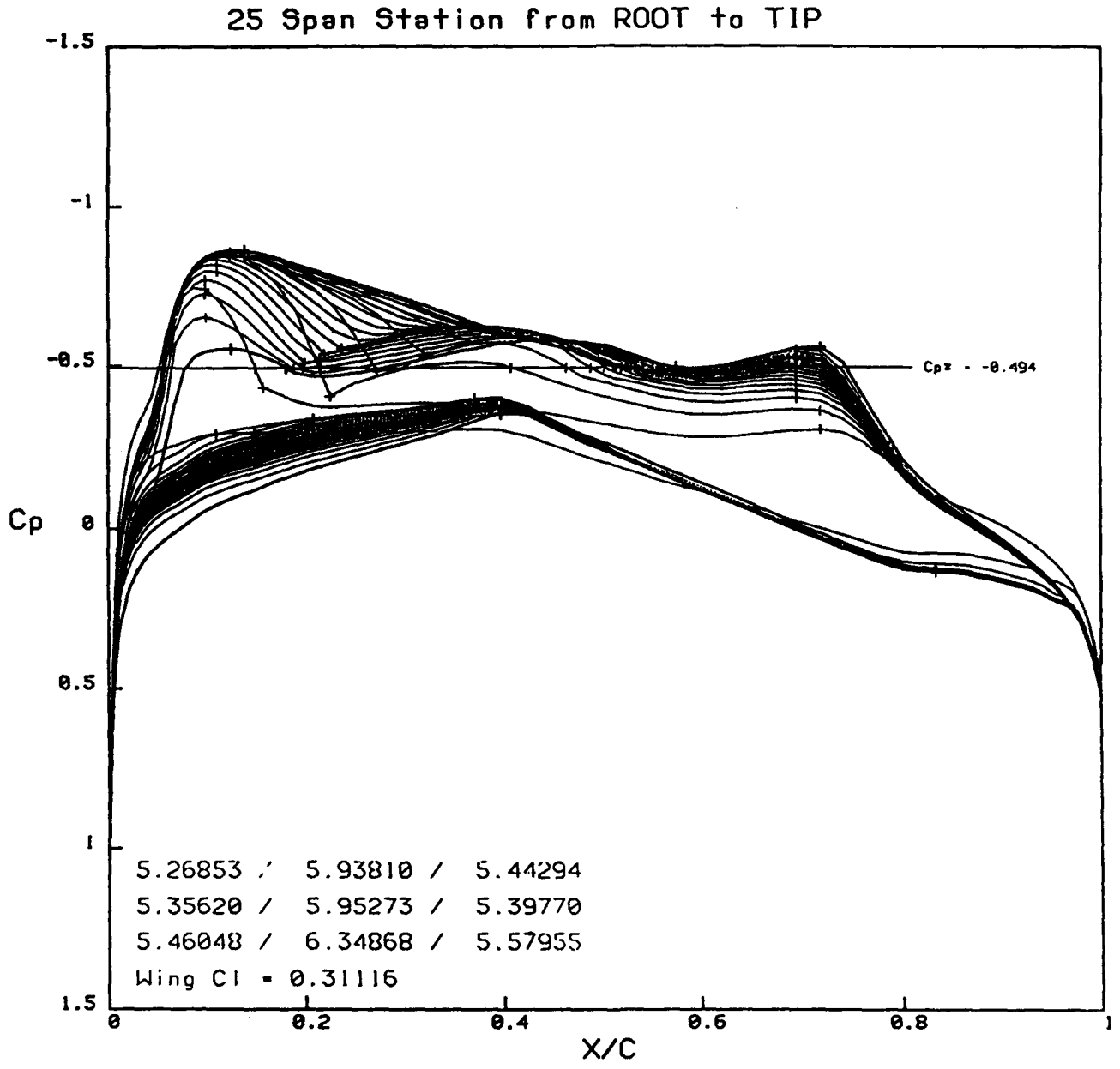

Figure 20. Illustration of the 3-D surface pressure distribution for the optimization-modified configuration after the 10th optimization cycle

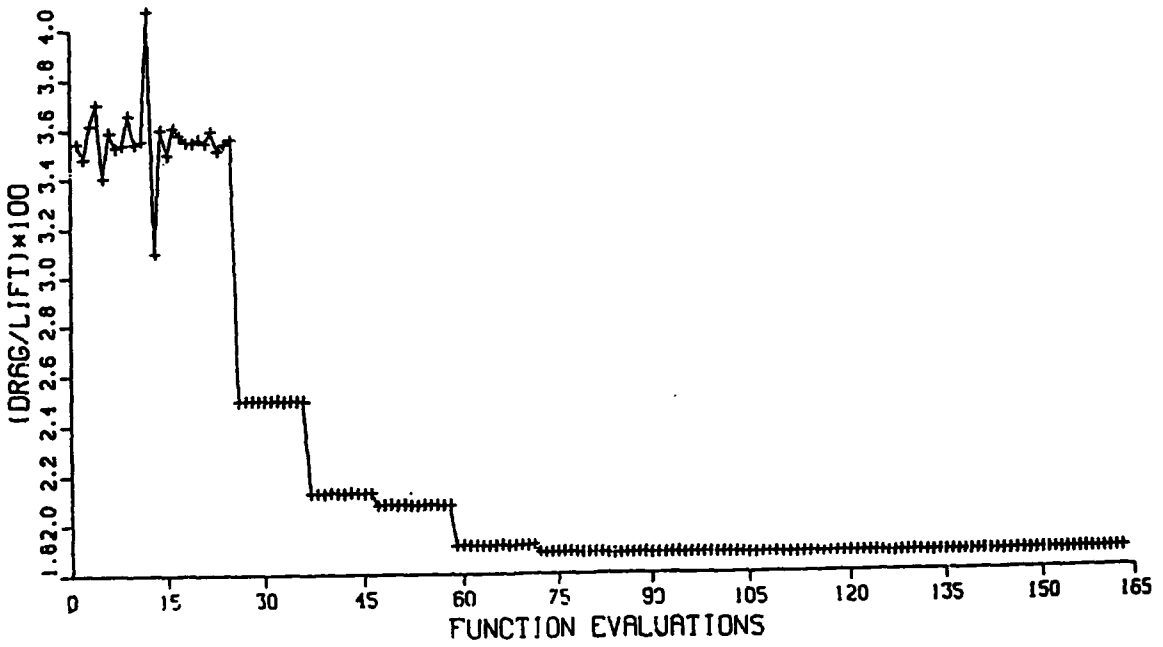

Objective function (C_D/C_L × 100) versus the number of TWING flow solutions

Figure 21. Convergence history of the optimization problem described in Figures 15 to 20; plot of objective function at each evaluation by 3-D flow solver as called by optimization driver from problem start through the 10th optimization cycle

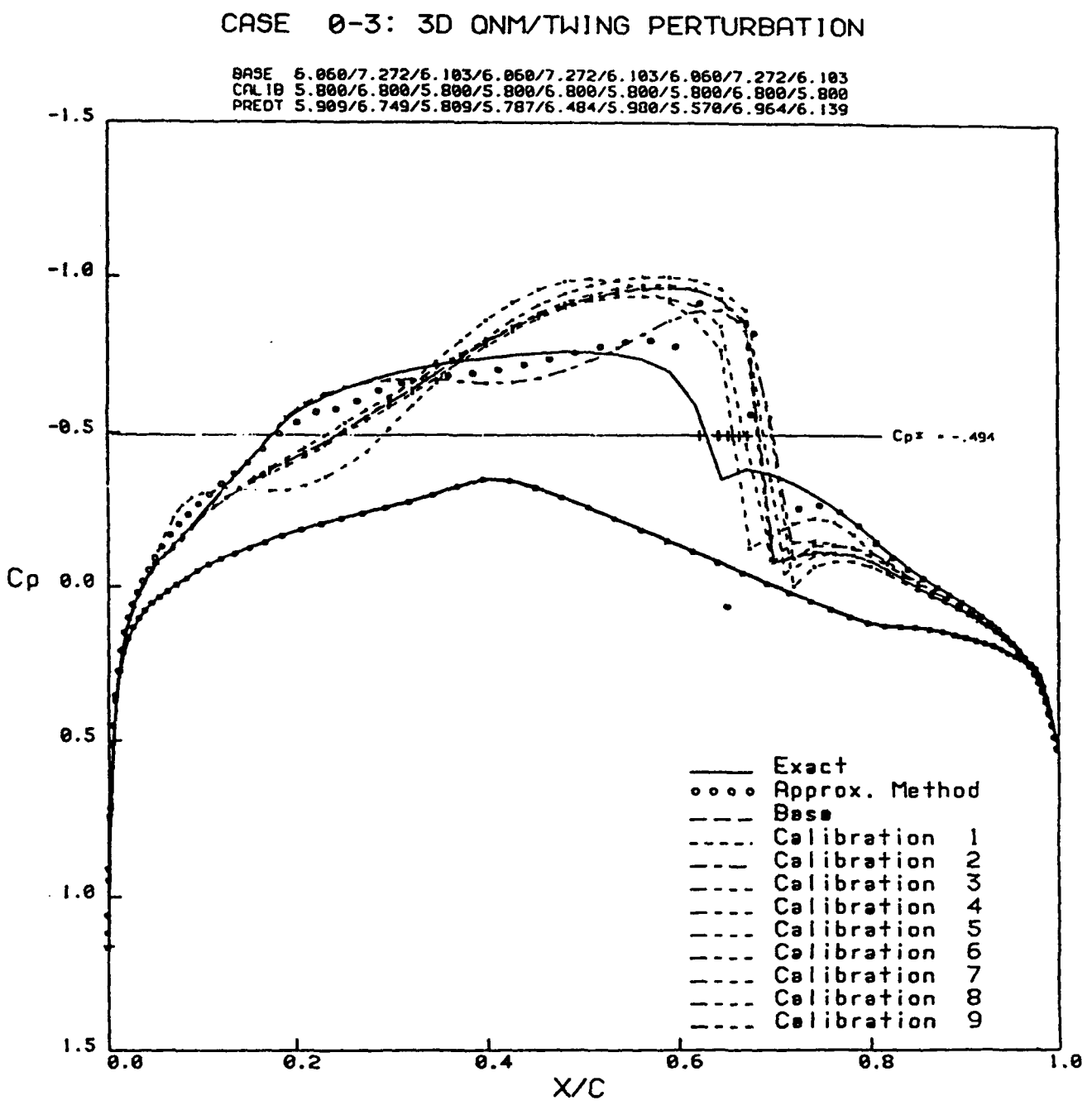

Figure 22. Comparison of 3-D approximation predicted and exact nonlinear surface pressure distributions at the root chord station (y/s = 0.0) for the particular values of the 9 design variables at the end of the 7th optimization cycle; complete exact nonlinear 3-D surface pressure distribution shown in Figure 17

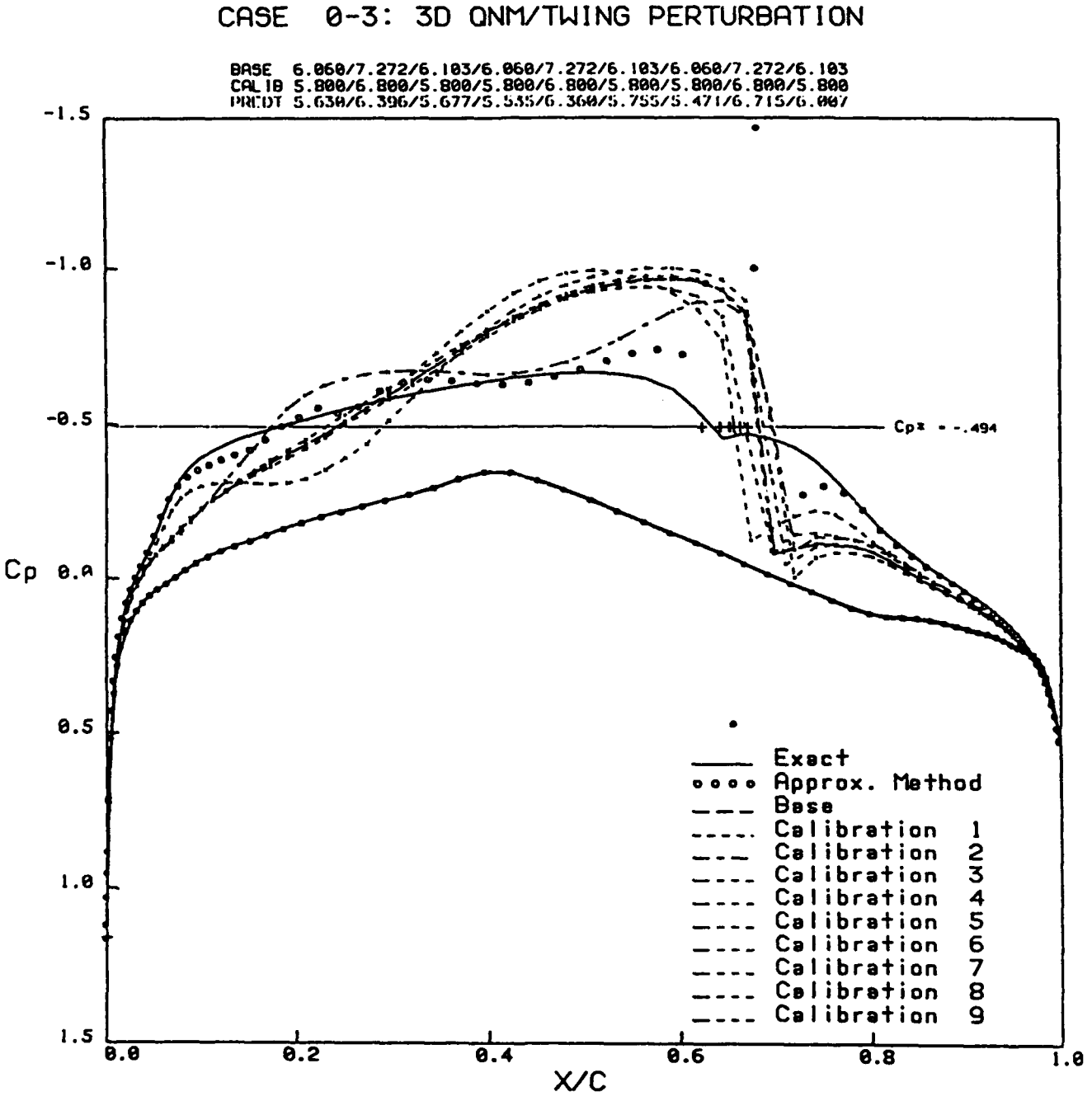

Figure 23. Comparison of 3-D approximation predicted and exact nonlinear surface pressure distributions at the root chord station (y/s = 0.0) for the particular values of the 9 design variables at the end of the 8th optimization cycle; complete exact nonlinear 3-D surface pressure distribution shown in Figure 18

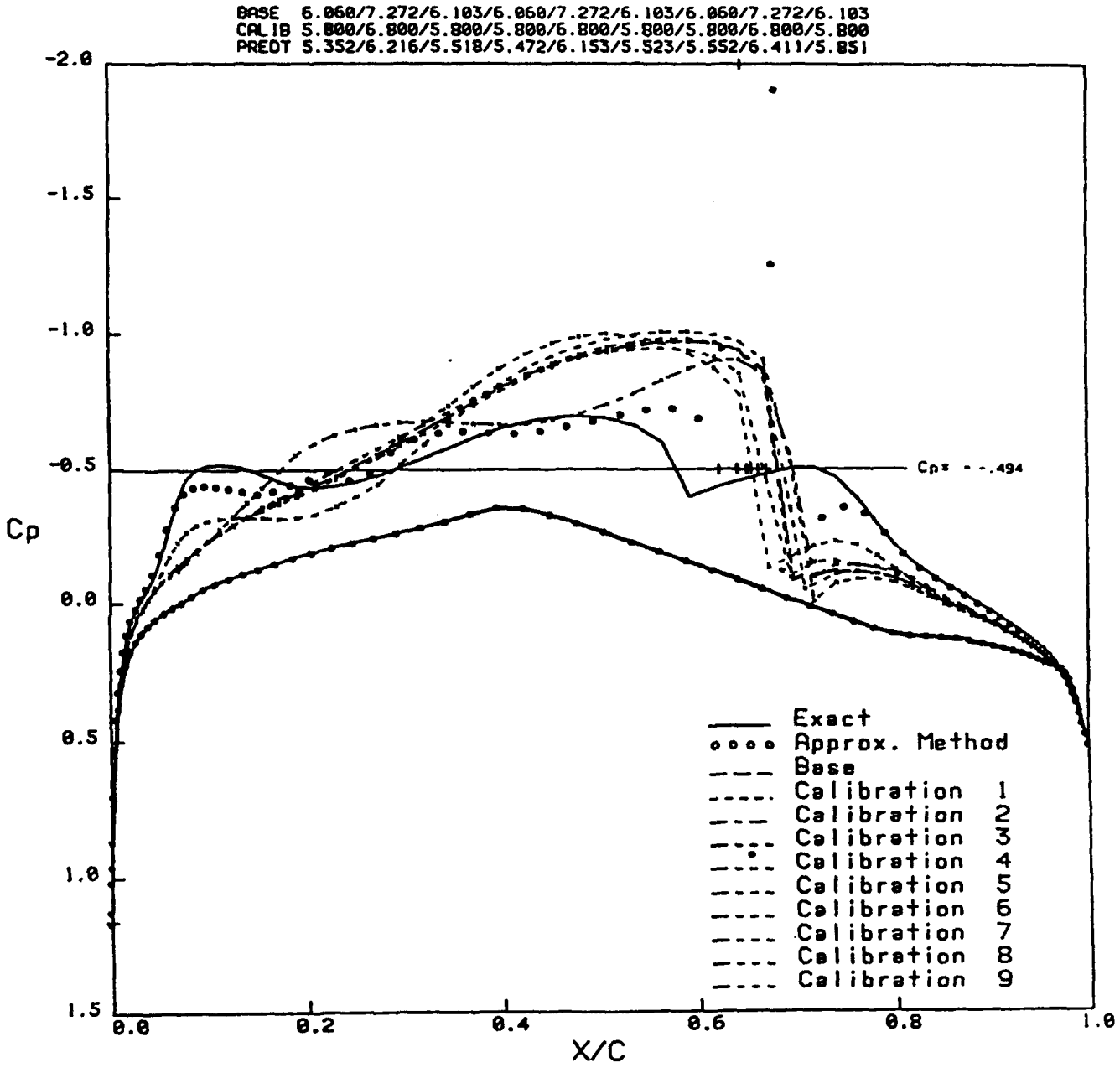

Figure 24. Comparison of 3-D approximation predicted and exact nonlinear surface pressure distributions at the root chord station (y/s = 0.0) for the particular values of the 9 design variables at the end of the 9th optimization cycle; complete exact nonlinear 3-D surface pressure distribution shown in Figure 19

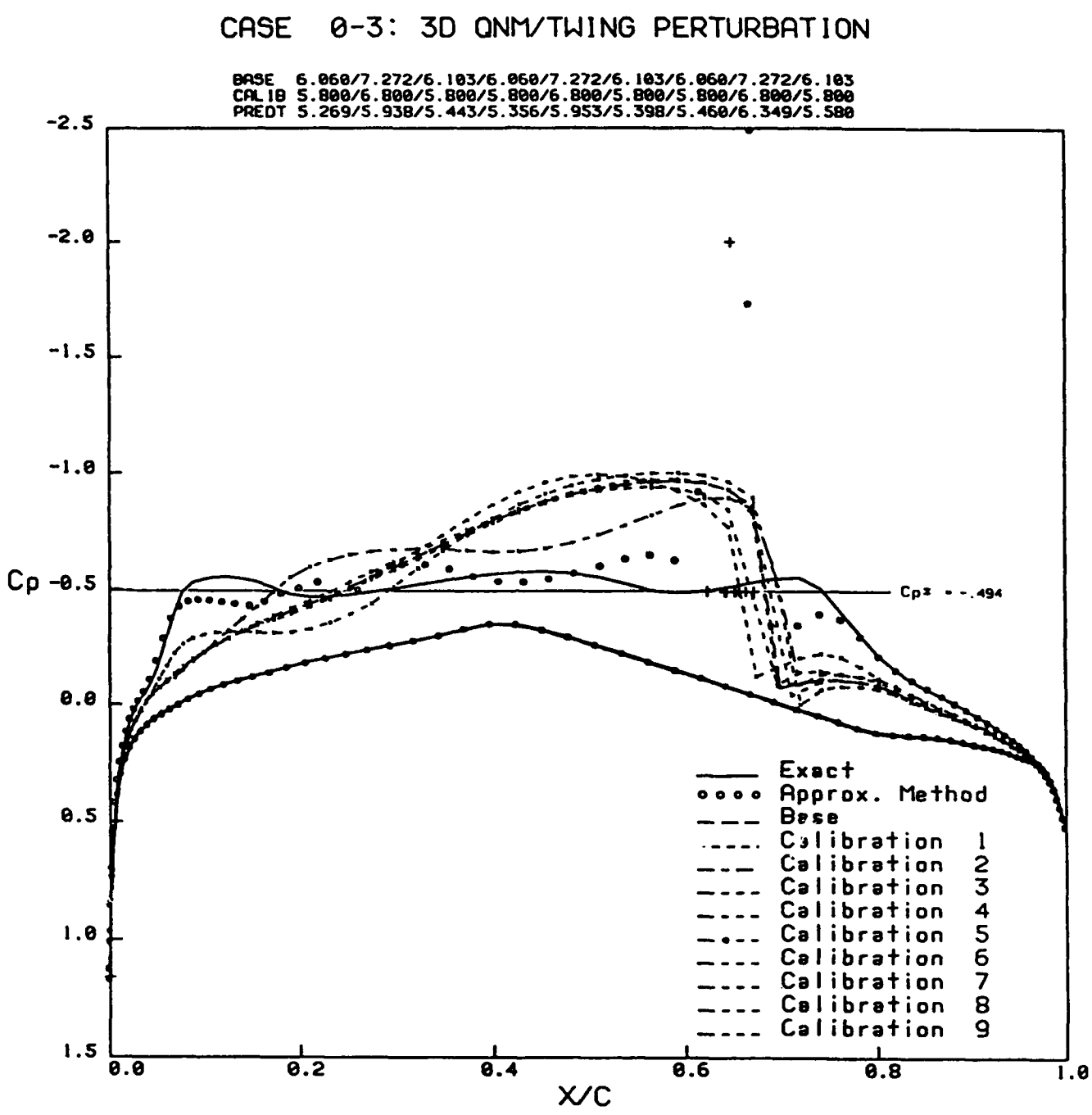

Figure 25. Comparison of 3-D approximation predicted and exact nonlinear surface pressure distributions at the root chord station (y/s = 0.0) for the particular values of the 9 design variables at the end of the 10th optimization cycle; complete exact nonlinear 3-D surface pressure distribution shown in Figure 20

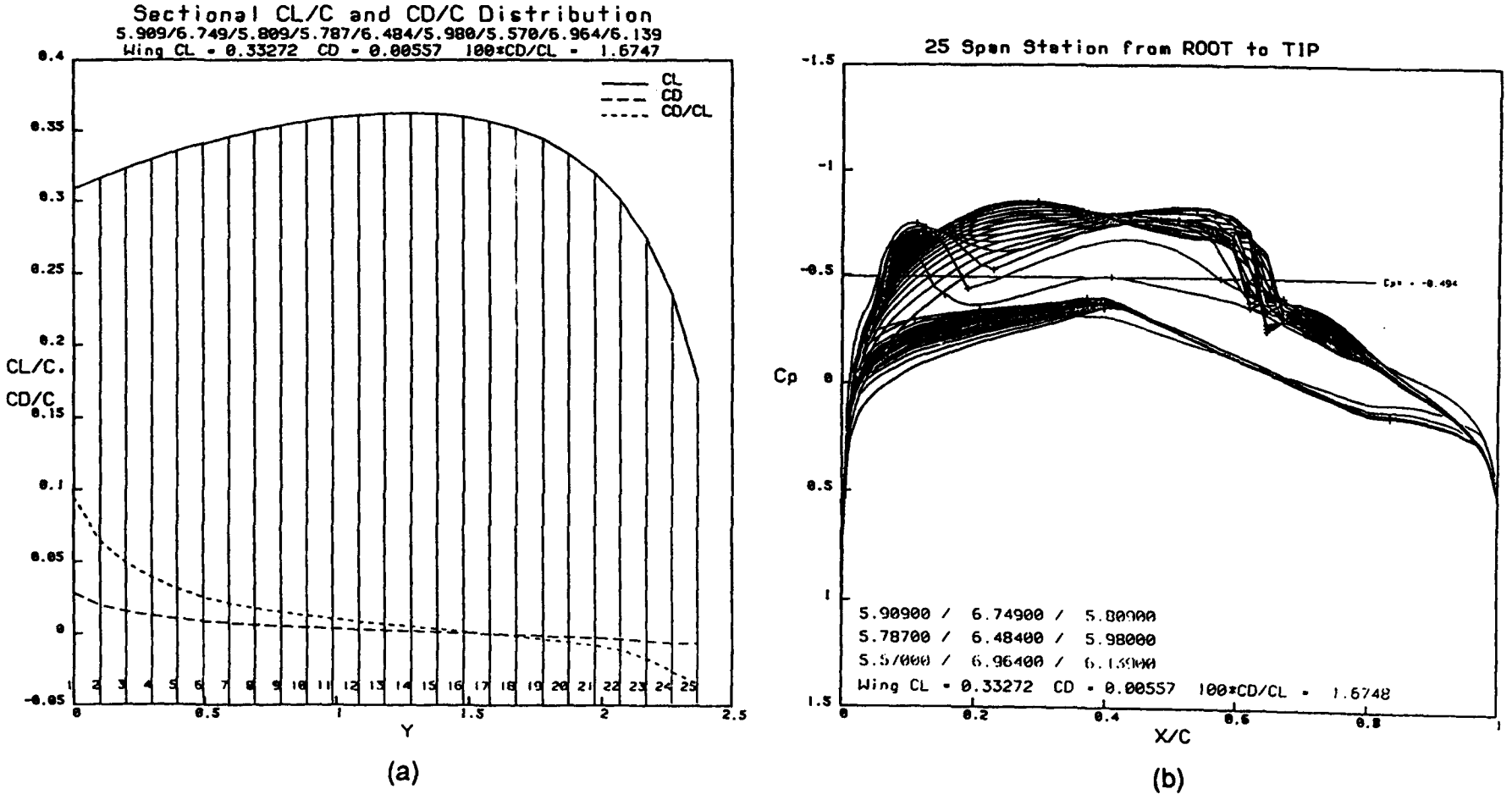

Figure 26. Illustration of the spanwise sectional lift, drag, and drag/lift ratio at each of the 25 spanwise locations along the 3-D profile for the surface pressure distribution shown as obtained at the end of the 7th optimization cycle for the benchmark case study

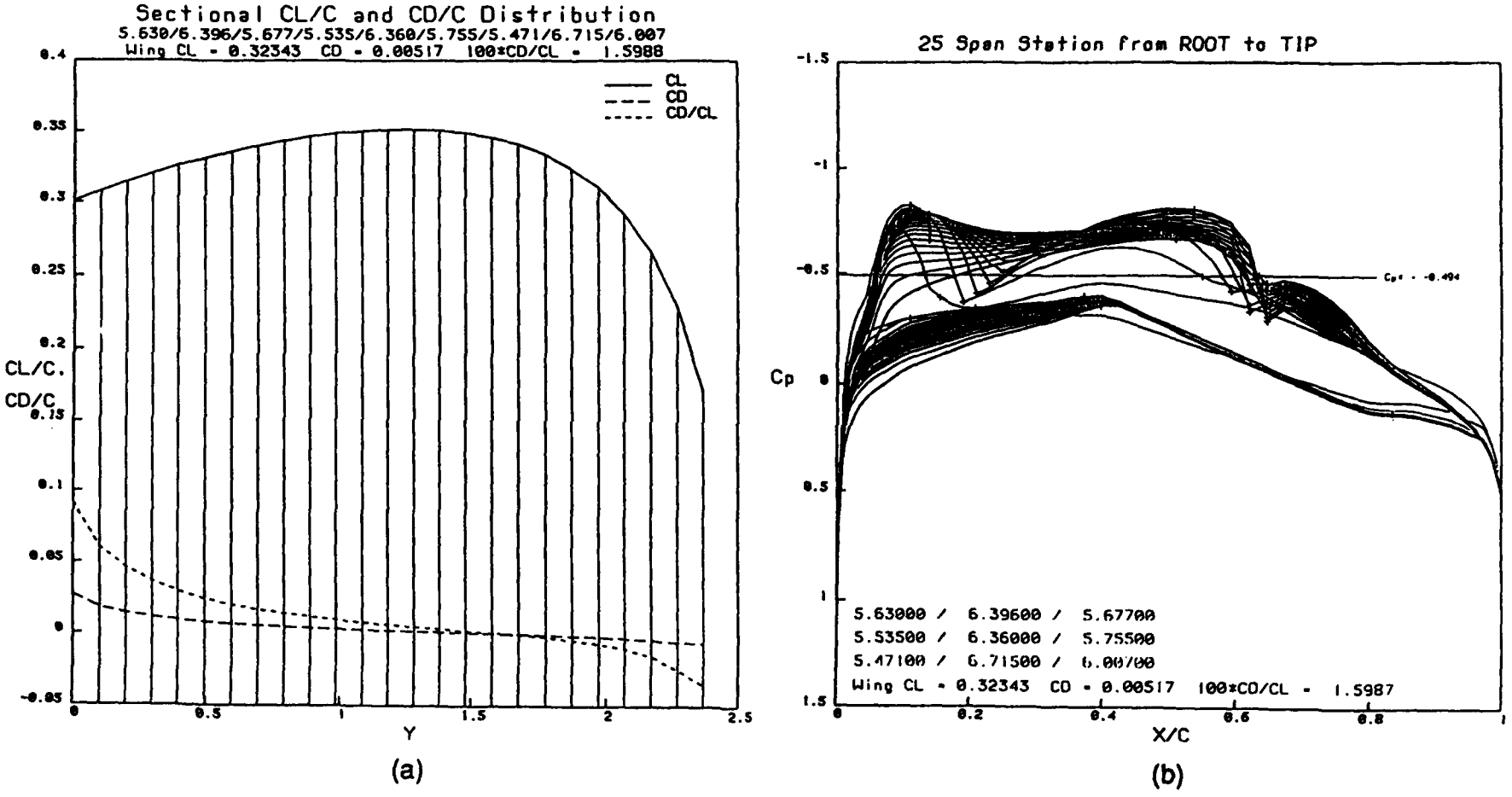

Figure 27. Illustration of the spanwise sectional lift, drag, and drag/lift ratio at each of the 25 spanwise locations along the 3-D profile for the surface pressure distribution shown as obtained at the end of the 8th optimization cycle for the benchmark case study

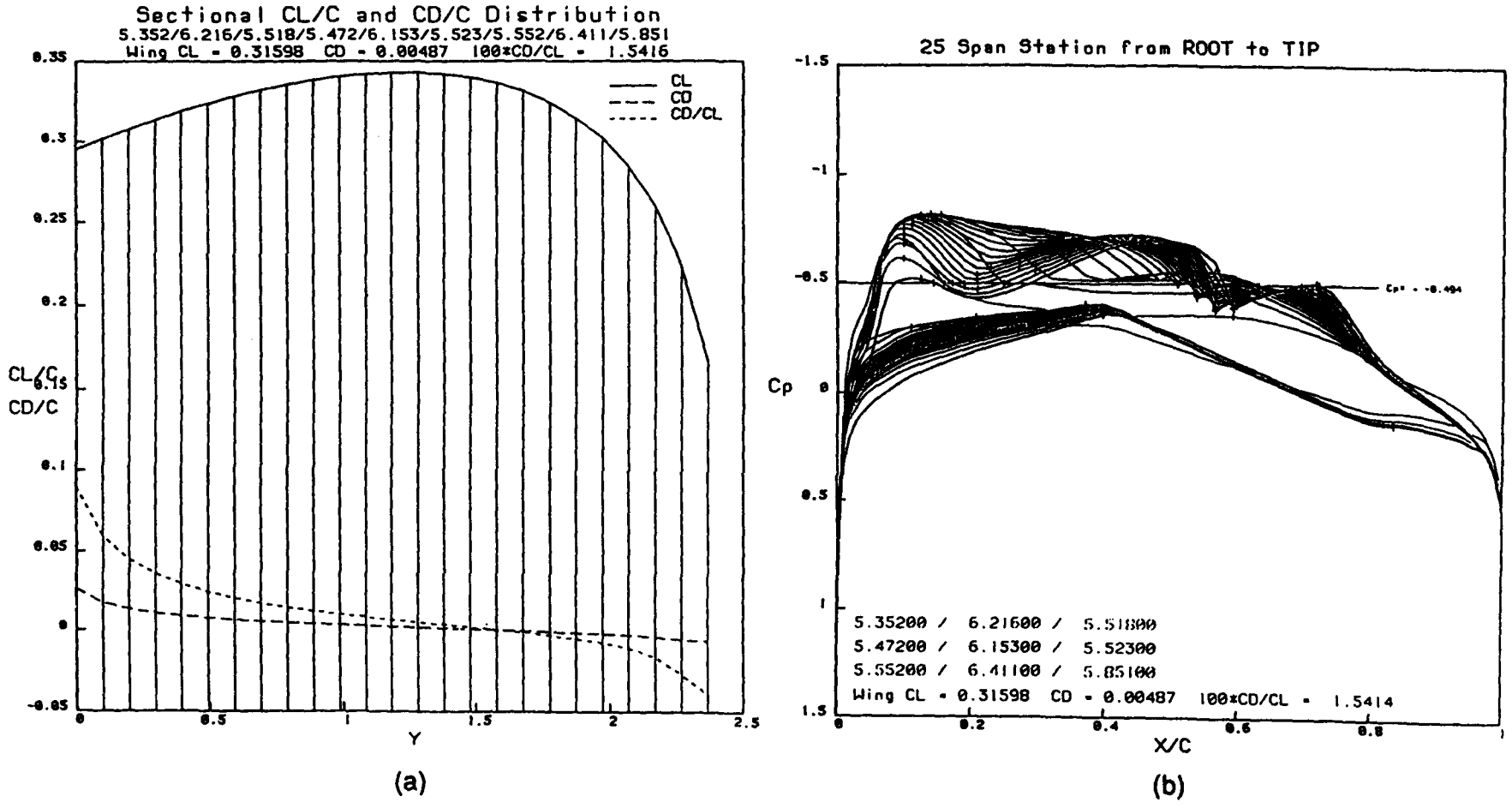

Figure 28. Illustration of the spanwise sectional lift, drag, and drag/lift ratio at each of the 25 spanwise locations along the 3-D profile for the surface pressure distribution shown as obtained at the end of the 9th optimization cycle for the benchmark case study

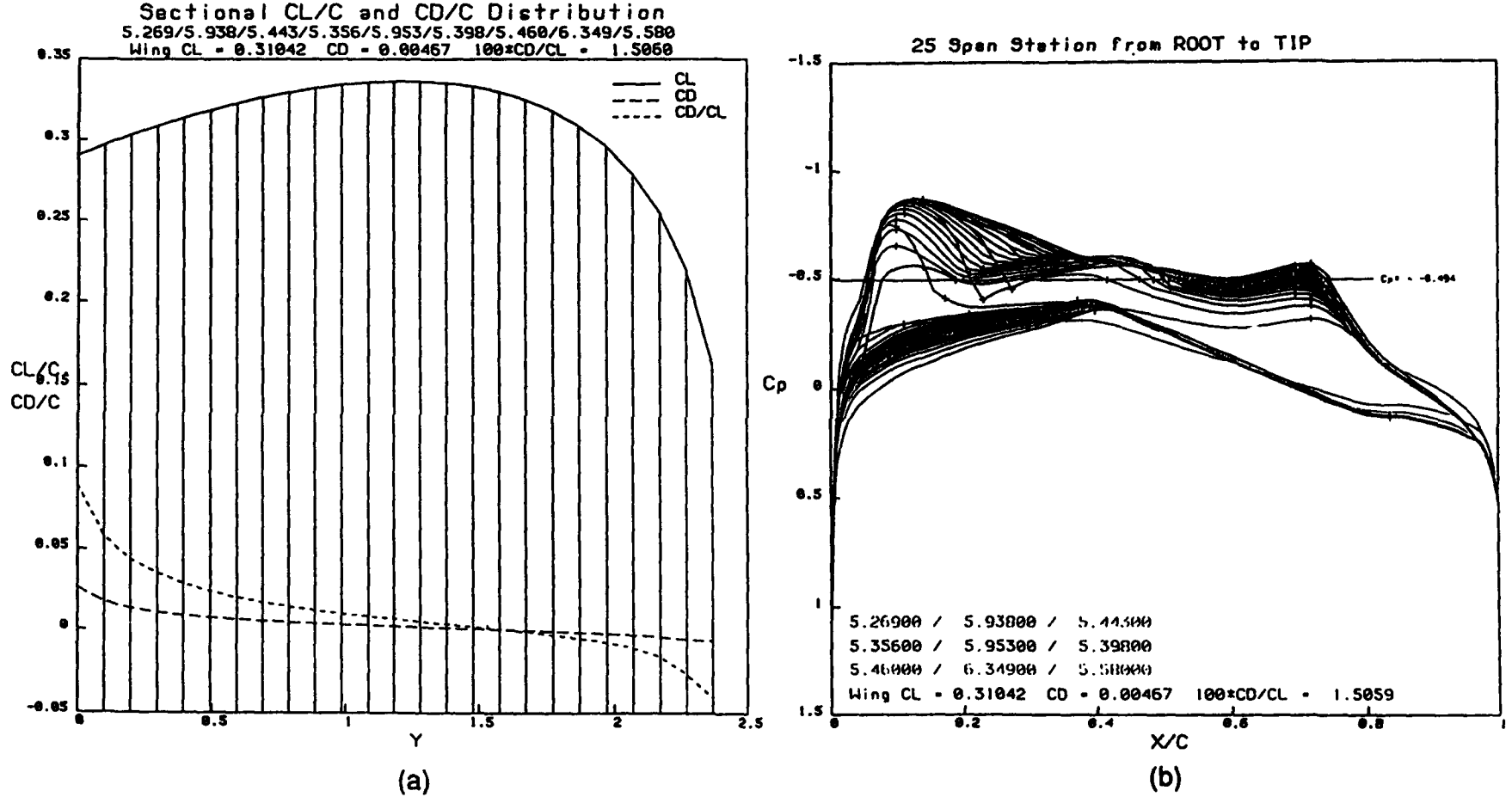

Figure 29. Illustration of the spanwise sectional lift, drag, and drag/lift ratio at each of the 25 spanwise locations along the 3-D profile for the surface pressure distribution shown as obtained at the end of the 10th optimization cycle for the benchmark case study

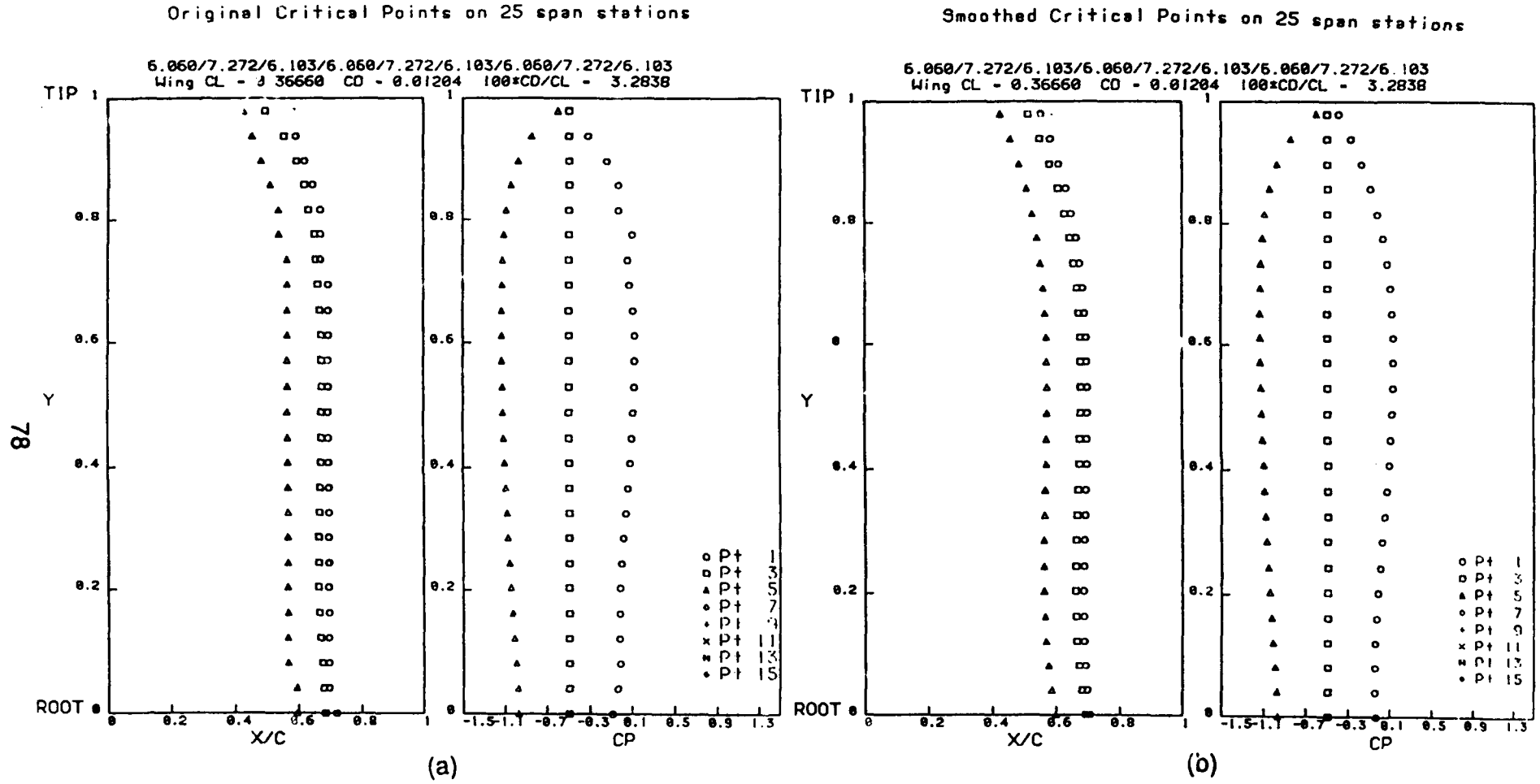

Figure 30. Illustration of improvement in spanwise invariant point location and invariant point C_p values provided by invariant point relocation procedure incorporated in 3-D approximation method for baseline 3-D surface pressure distribution for benchmark case study

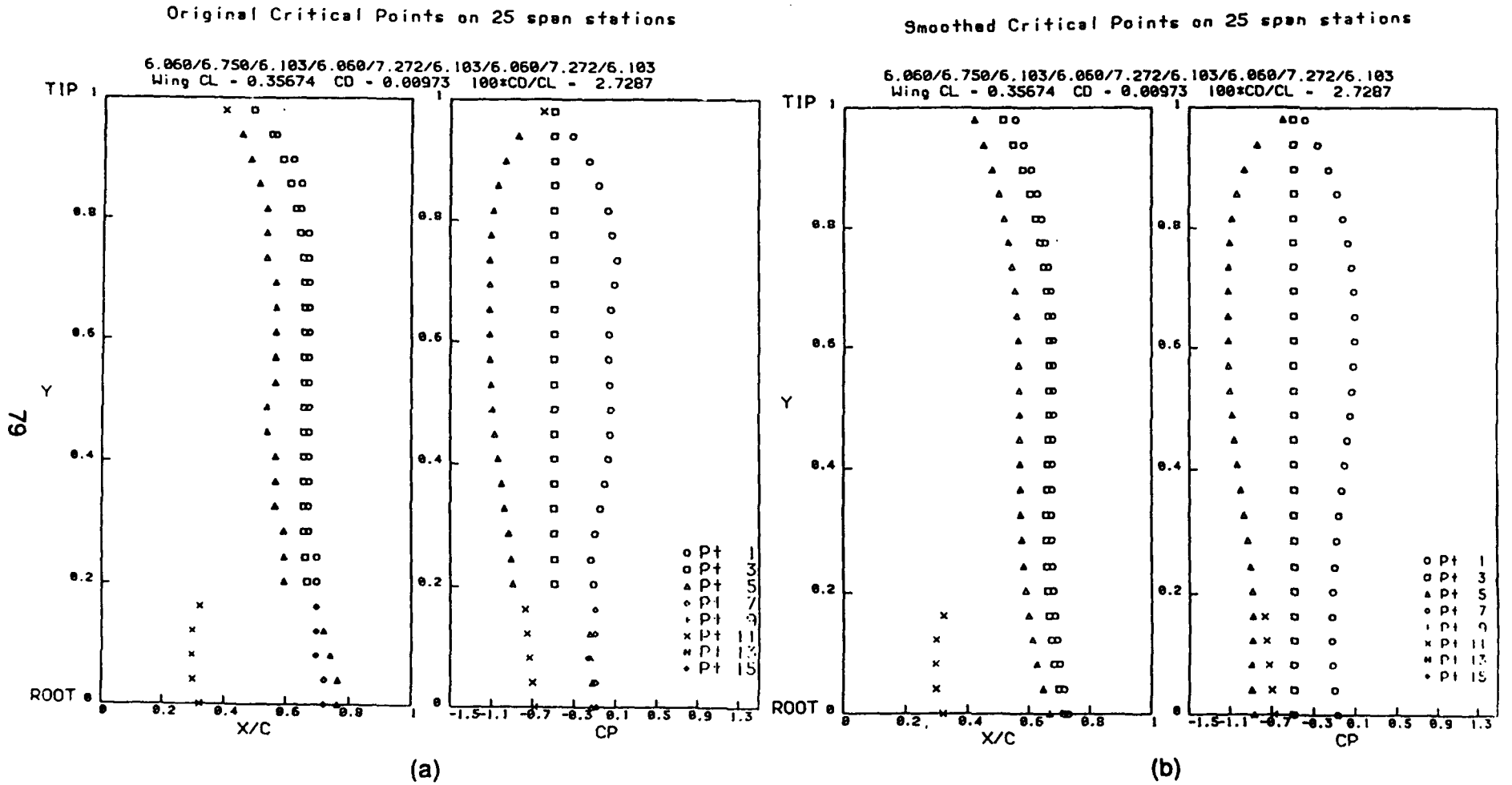

Figure 31. Illustration of improvement in spanwise invariant point location and invariant point C_p values provided by invariant point relocation procedure incorporated in 3-D approximation method for 3-D surface pressure distribution calibration associated with calibration solution for 2nd design variable for benchmark case study

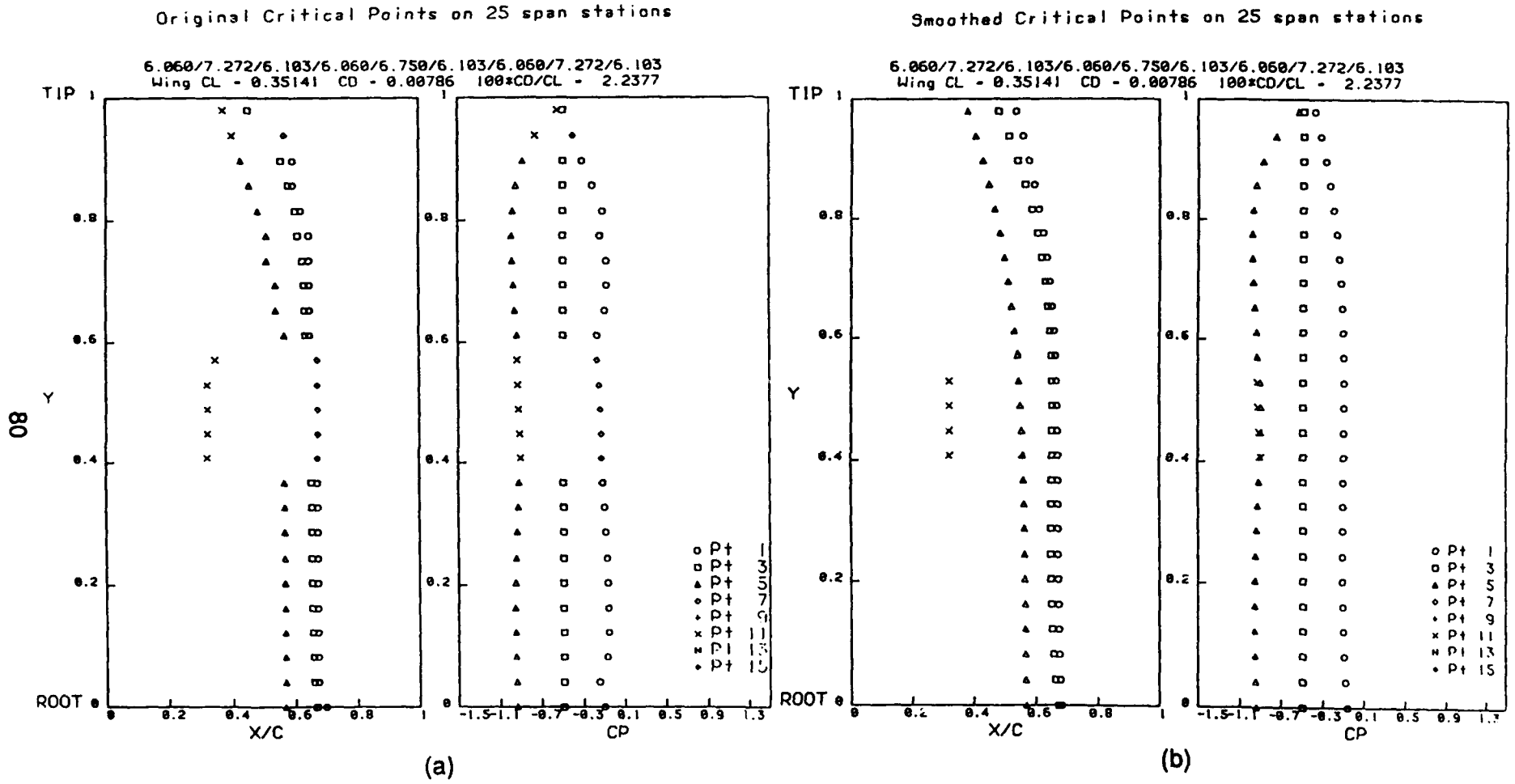

Figure 32. Illustration of improvement in spanwise invariant point location and invariant point C_p values provided by invariant point relocation procedure incorporated in 3-D approximation method for 3-D surface pressure distribution calibration associated with calibration solution for 5th design variable for benchmark case study

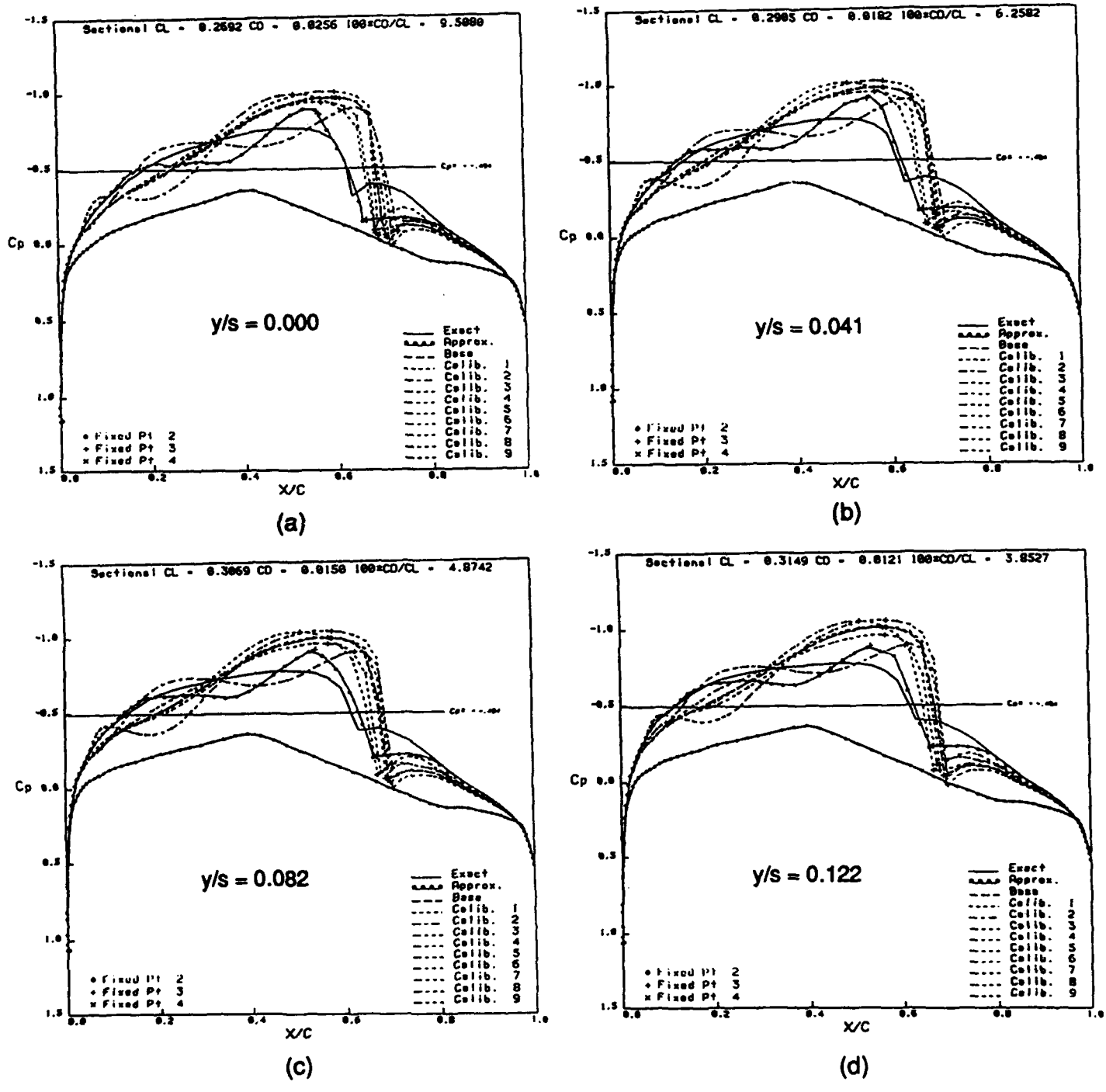

Figure 33. Comparison of 3-D approximation predicted and exact nonlinear chordwise surface pressure distributions at all 25 spanwise stations for the pressure distribution associated with the 7th optimization cycle design result for the benchmark case study

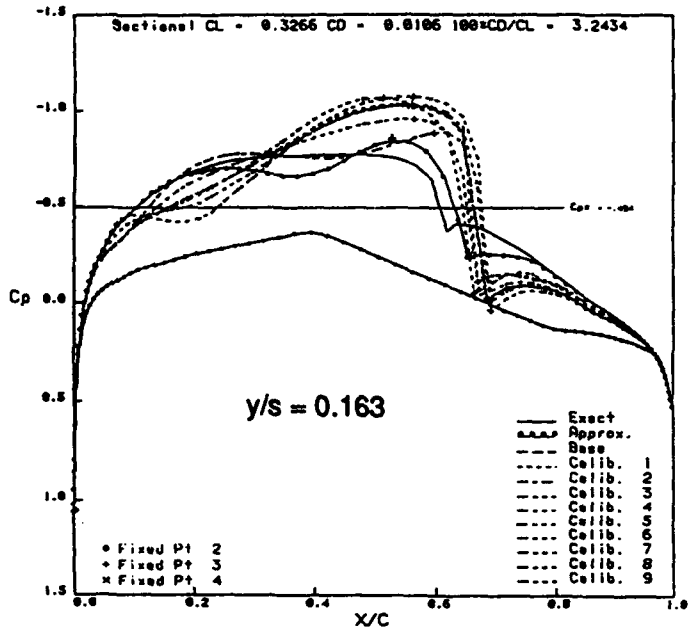

(e)

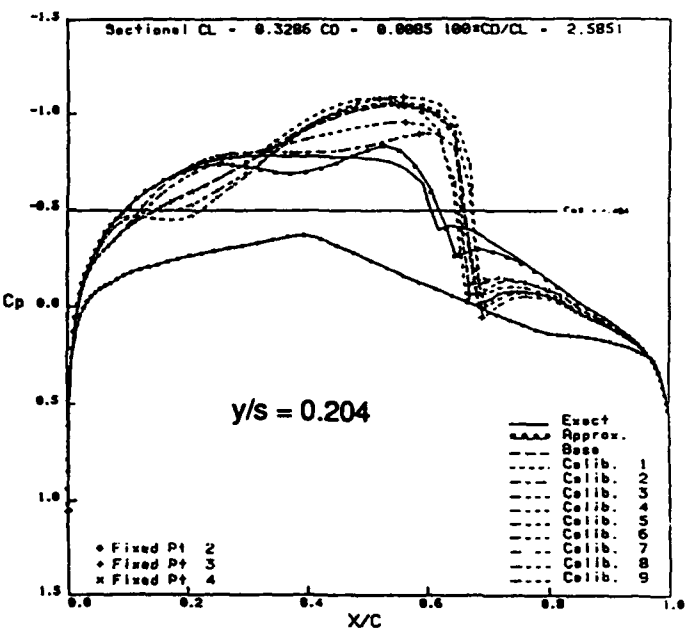

(f)

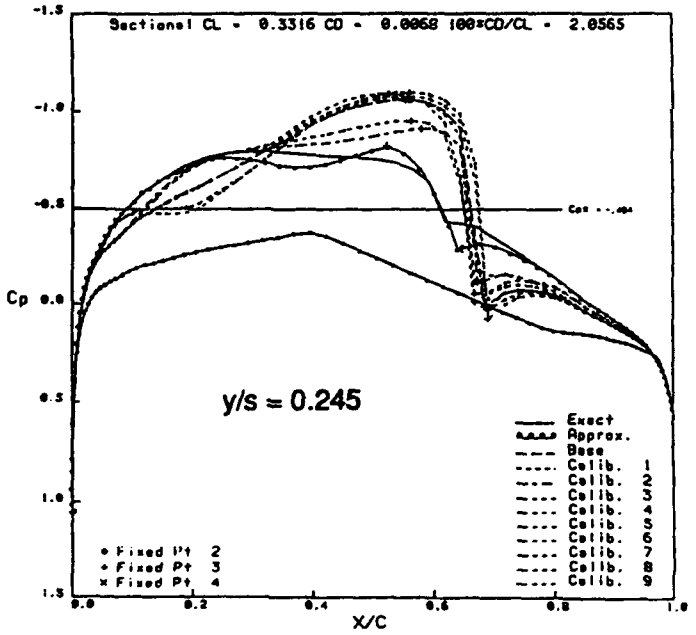

(g)

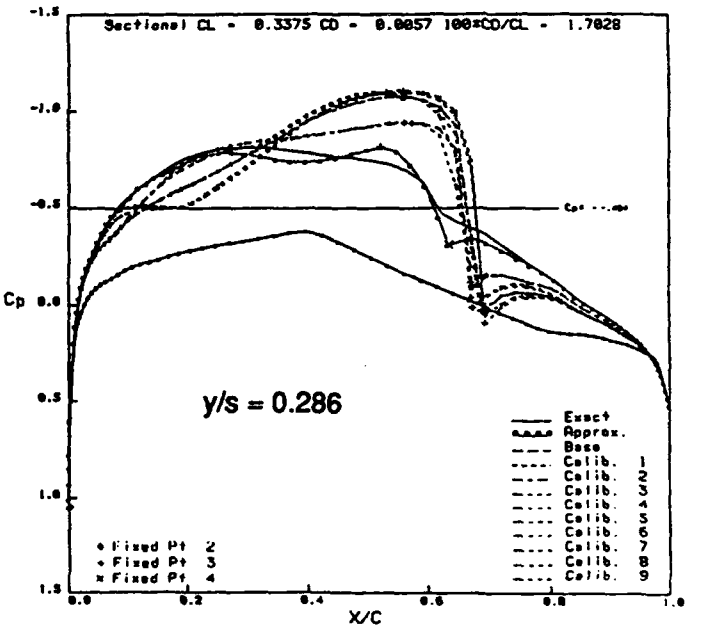

(h)

Figure 33. - Continued

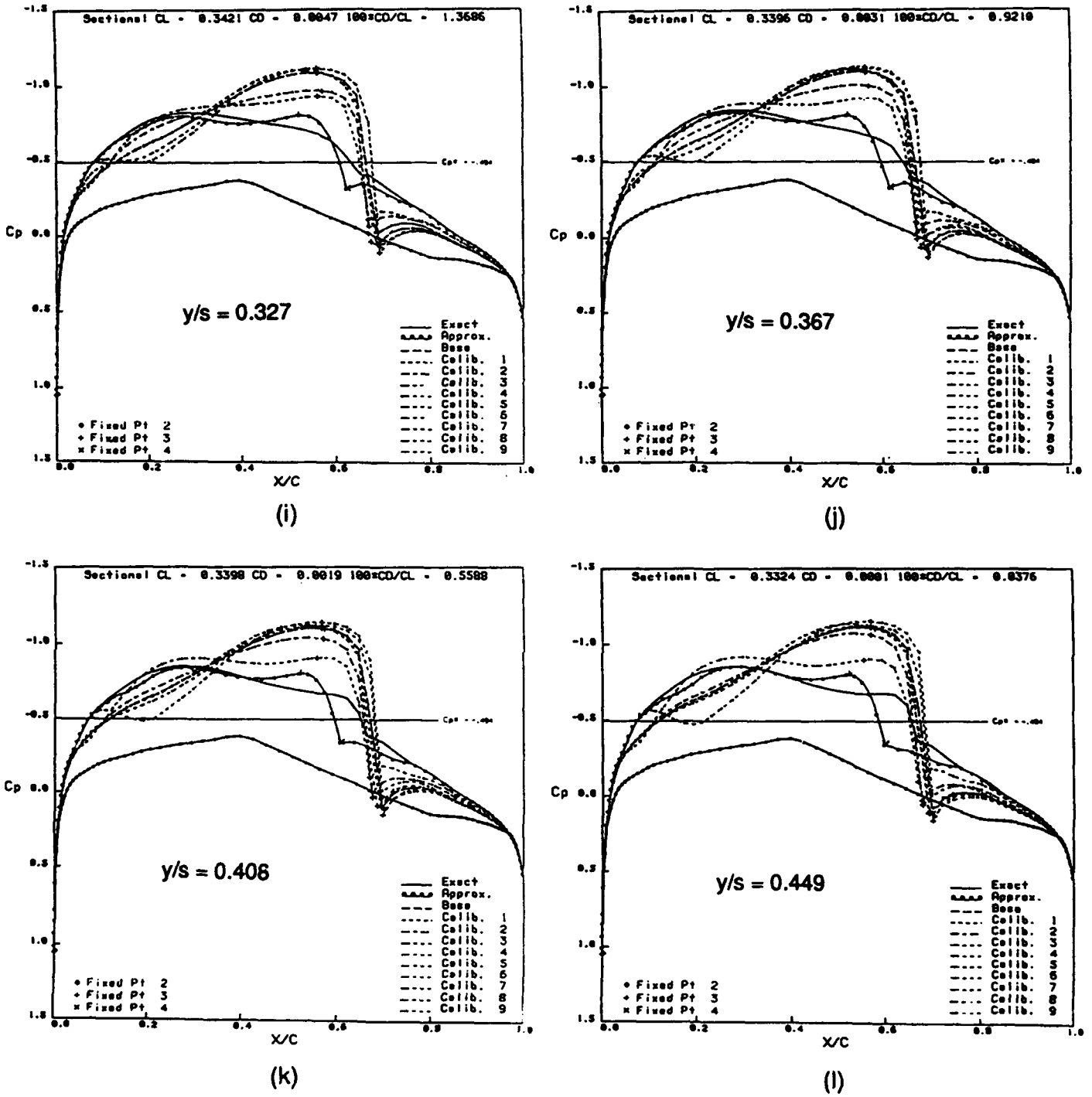

Figure 33. - Continued

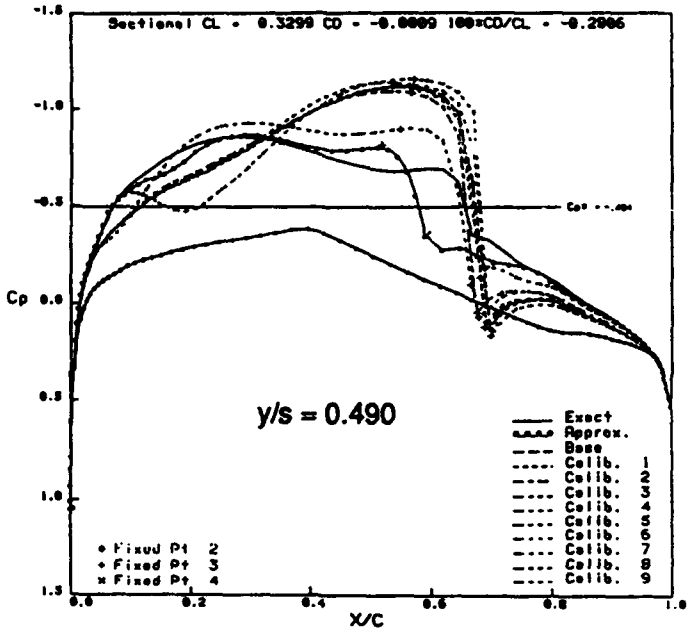

(m)

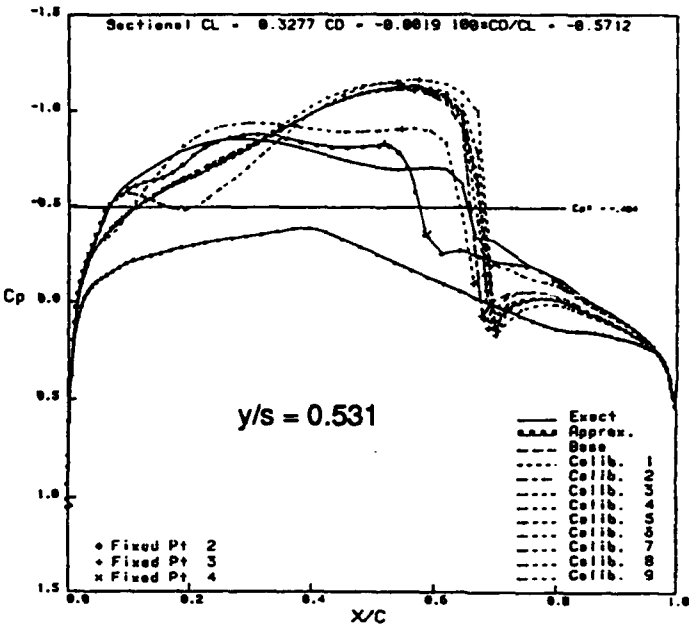

(n)

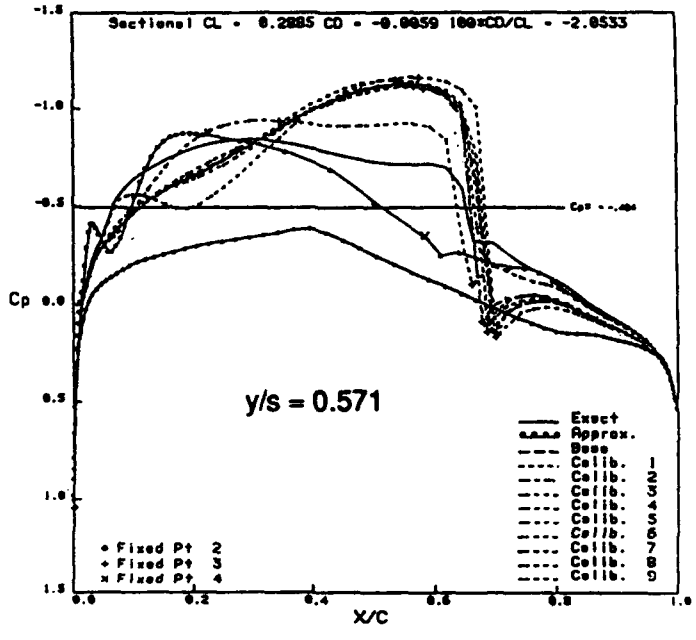

(o)

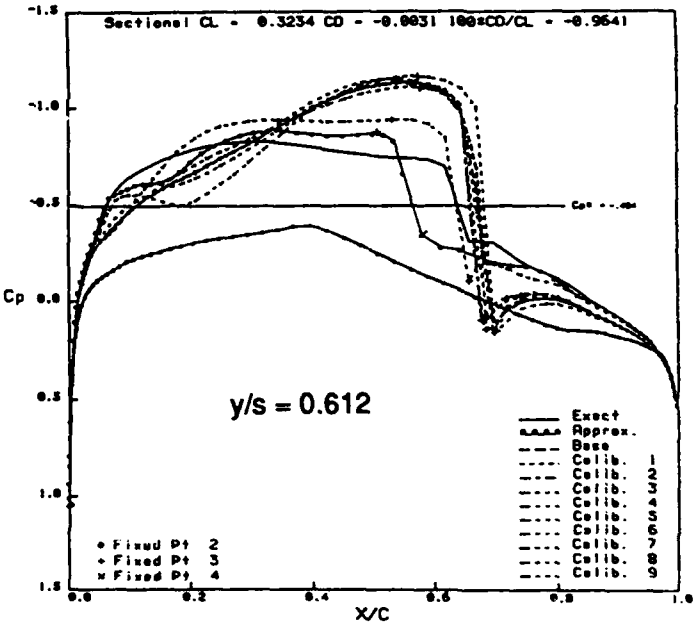

(p)

Figure 33. - Continued

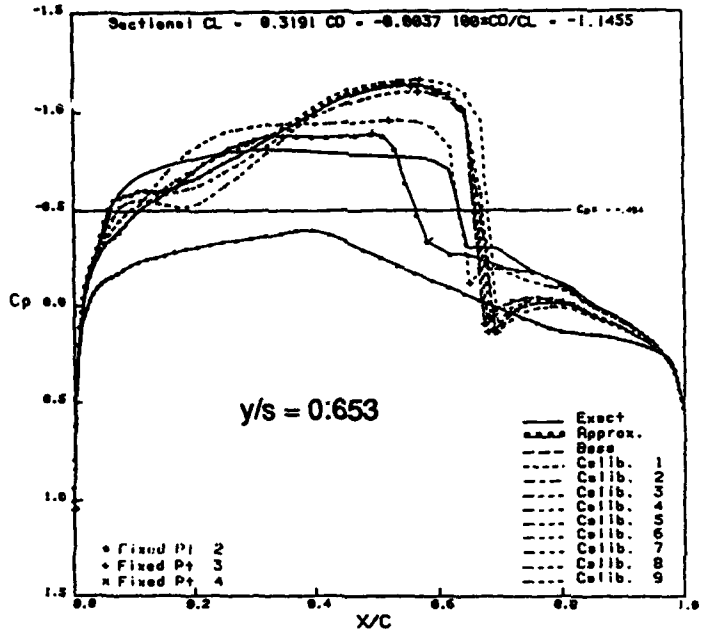

(q)

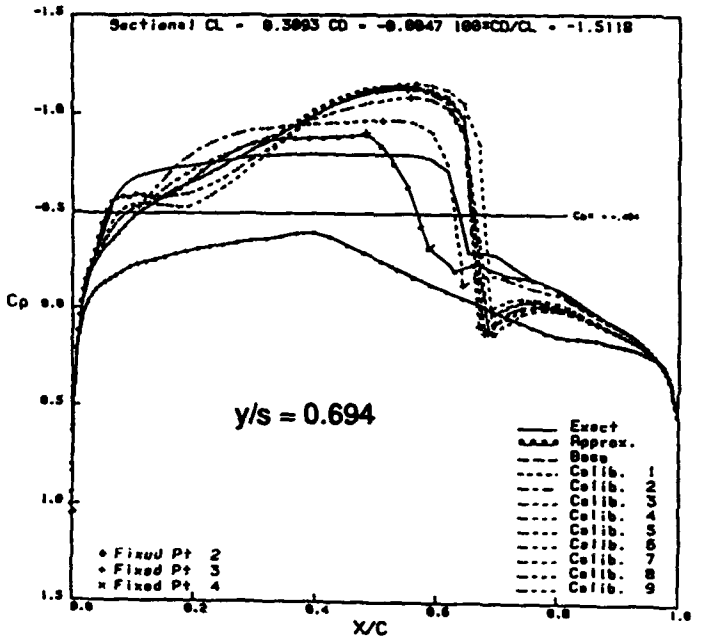

(r)

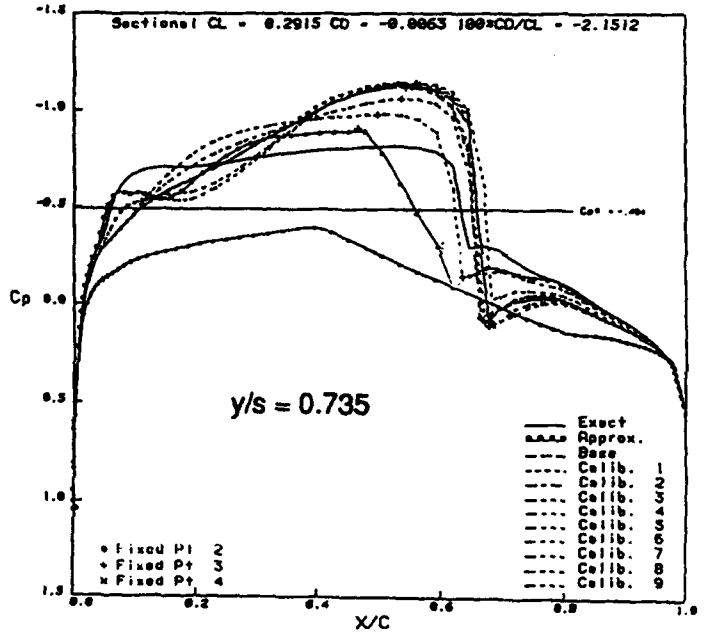

(s)

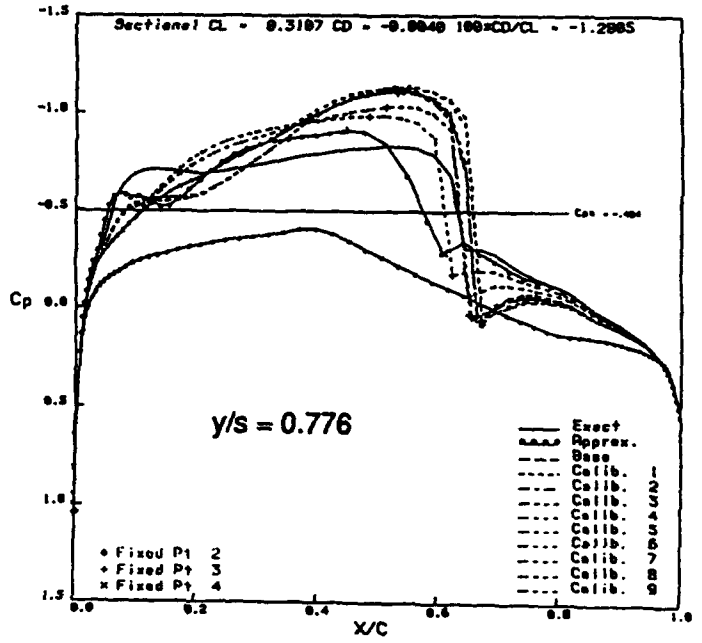

(t)

Figure 33. - Continued

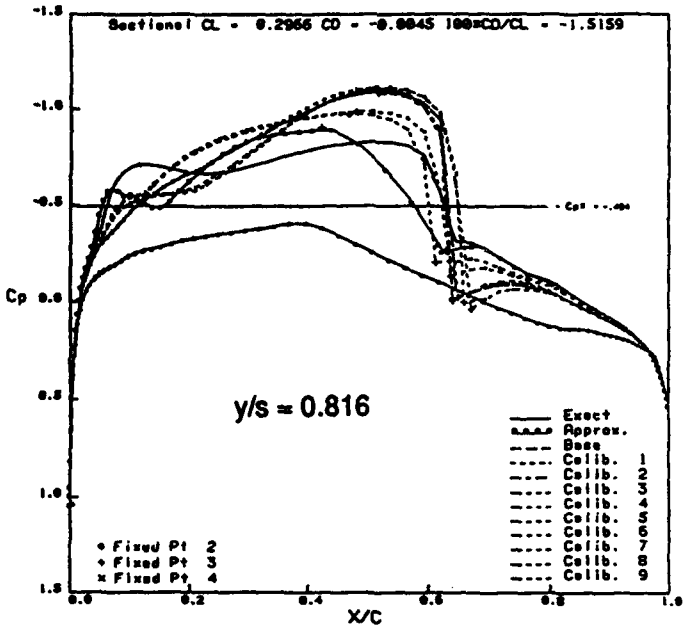

(u)

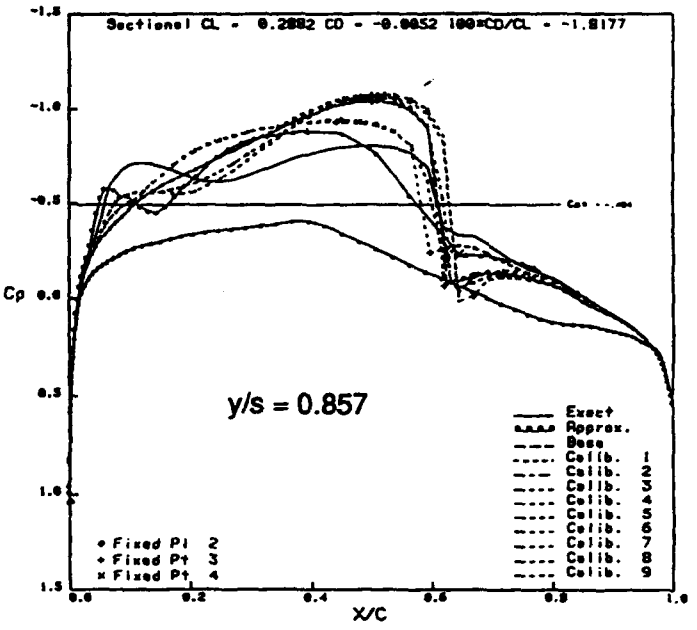

(v)

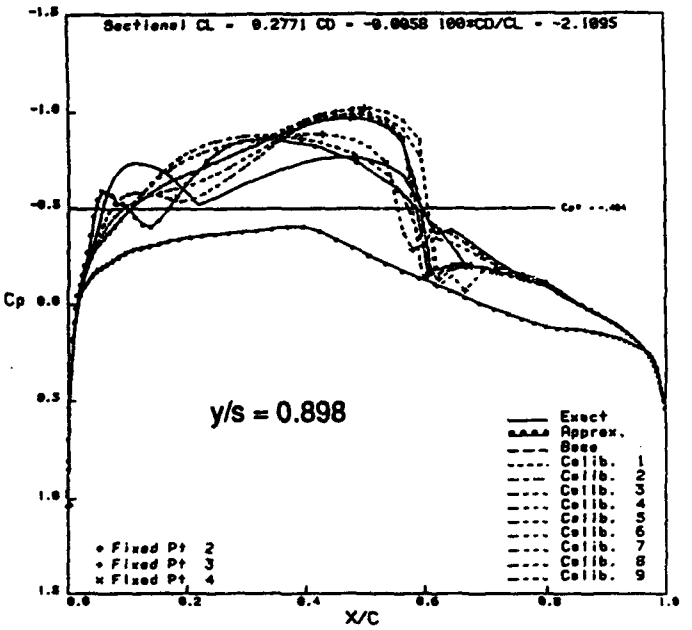

(w)

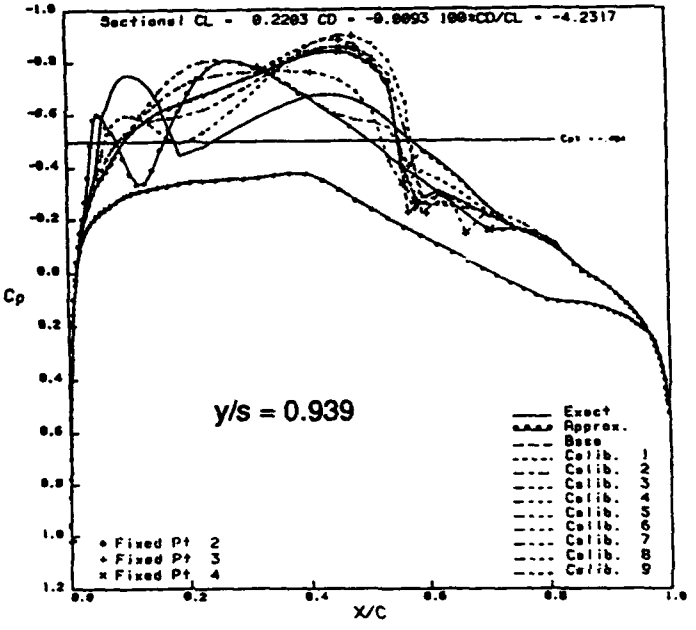

(x)

Figure 33. - Continued

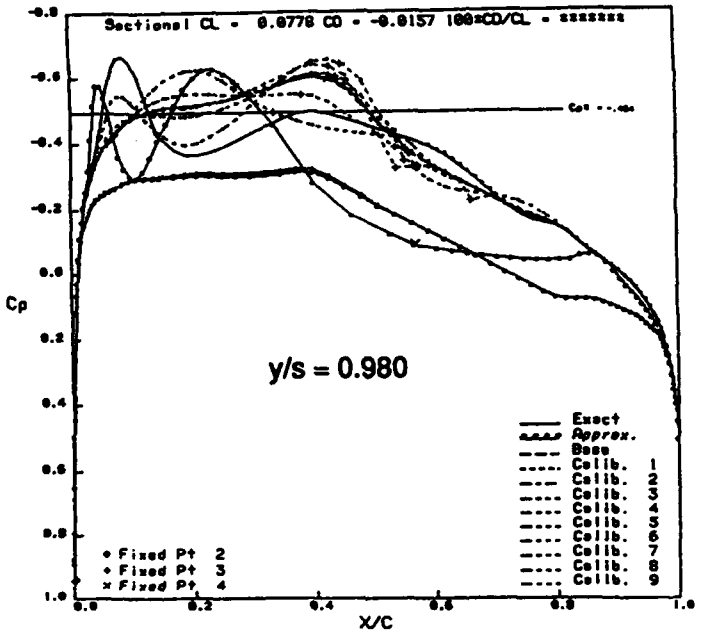

(y)

Figure 33. - Concluded

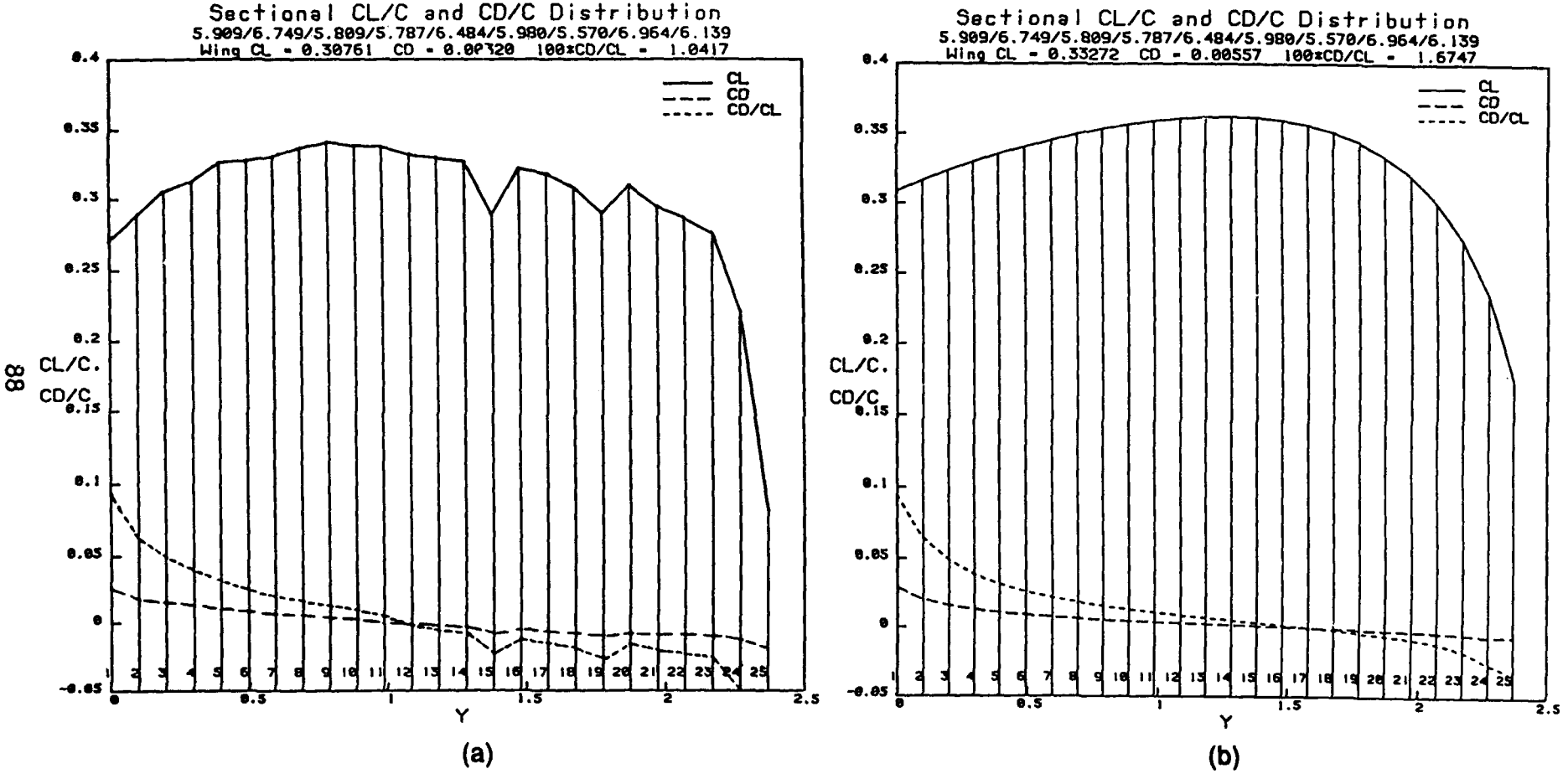

Figure 34. Comparison of 3-D approximation predicted and exact nonlinear spanwise distributions of the sectional lift, drag, and drag/lift ratio associated with the 7th optimization cycle design result for the benchmark case study

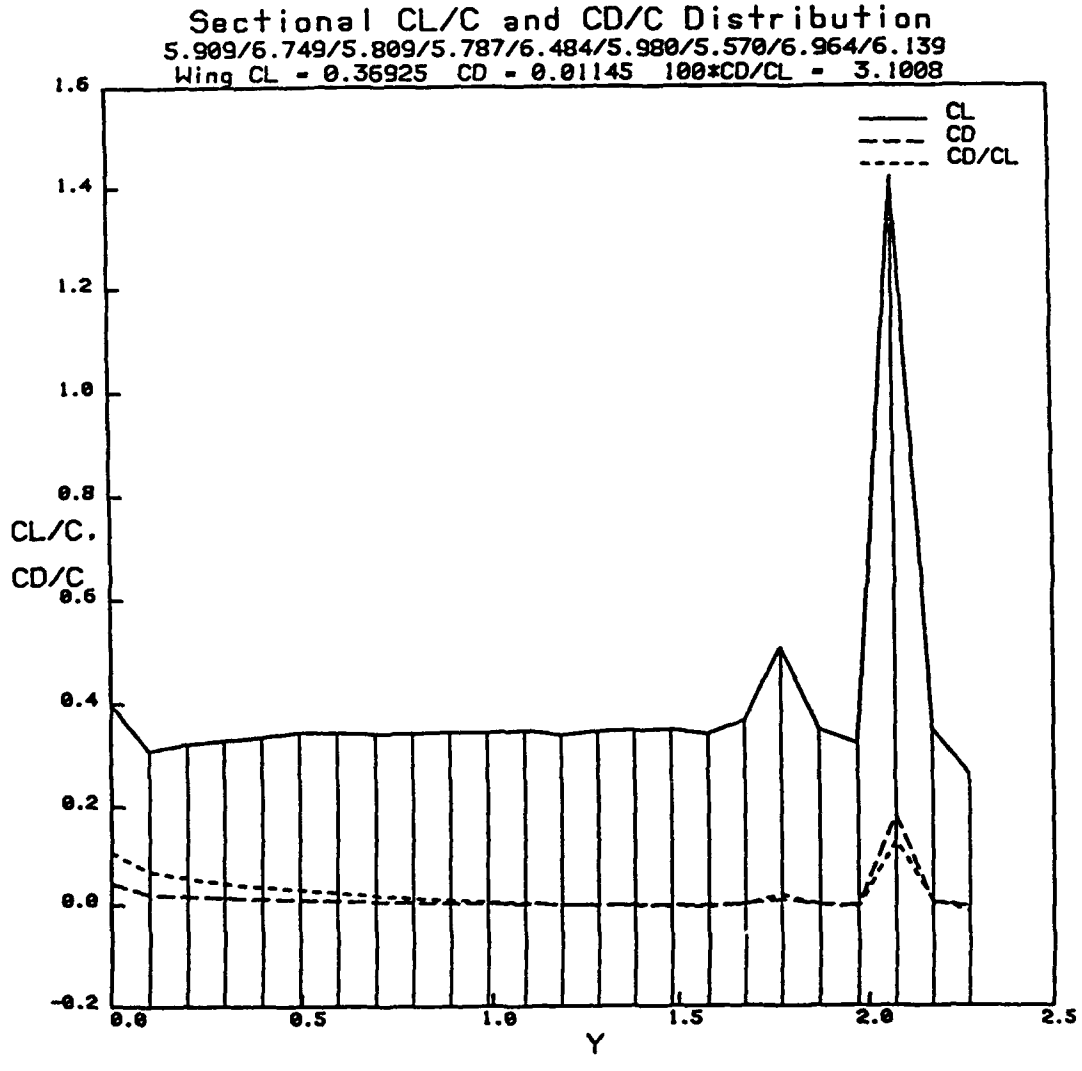

Figure 35. Illustration of the approximation predicted spanwise distributions of the sectional lift, drag, and drag/lift ratio based on post-processed invariant point surface pressure distributions

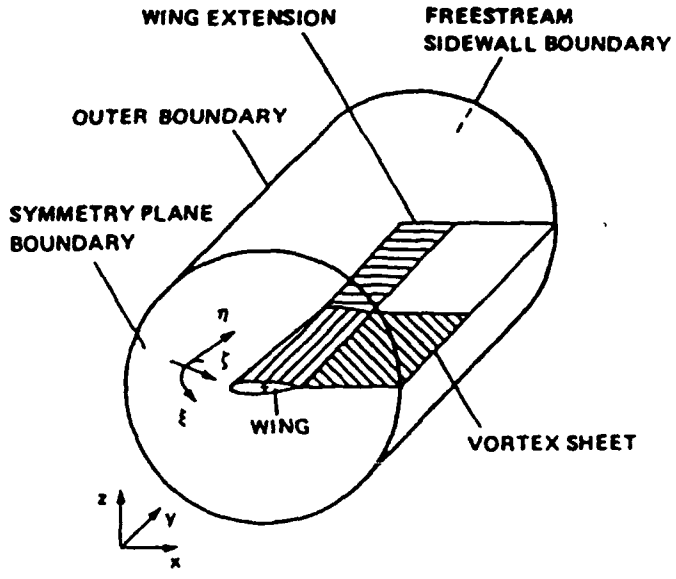

a) physical domain

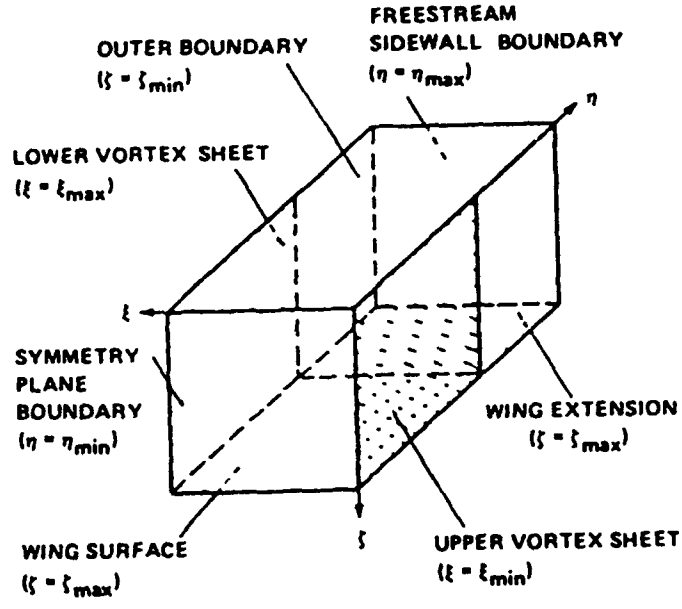

b) computational domain

Figure 36. Ilustration of the physical and computational computational domains embodied in the 3-D TWING flow field solver

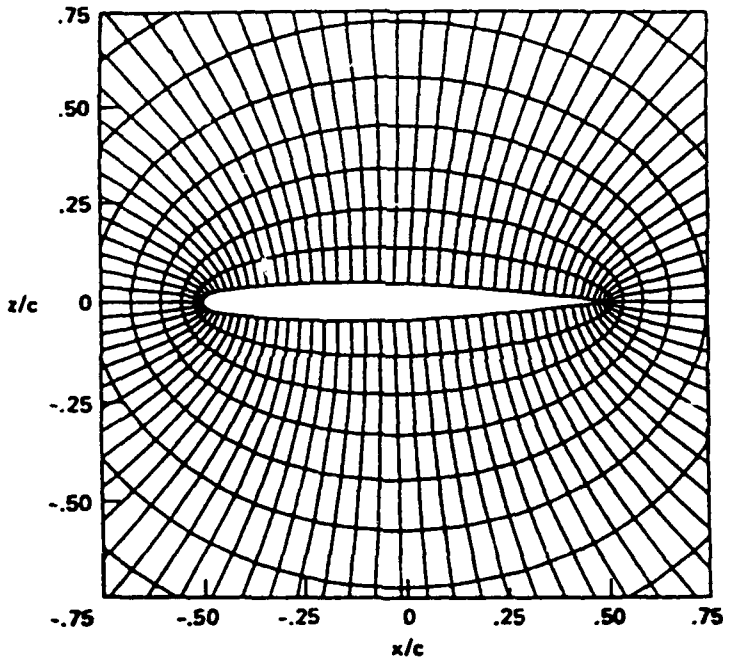

Figure 37. Illustration of the two-dimensional (X,Z) O-type grid at the first spanwise station (symmetry plane) along wing

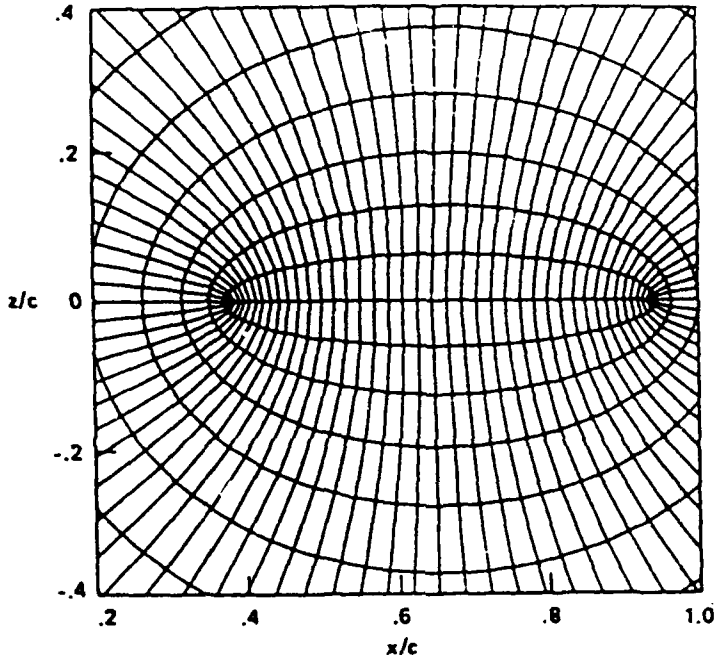

Figure 38. Illustration of the two-dimensional (X,Z) O-type grid at the first spanwise station beyond the wing tip

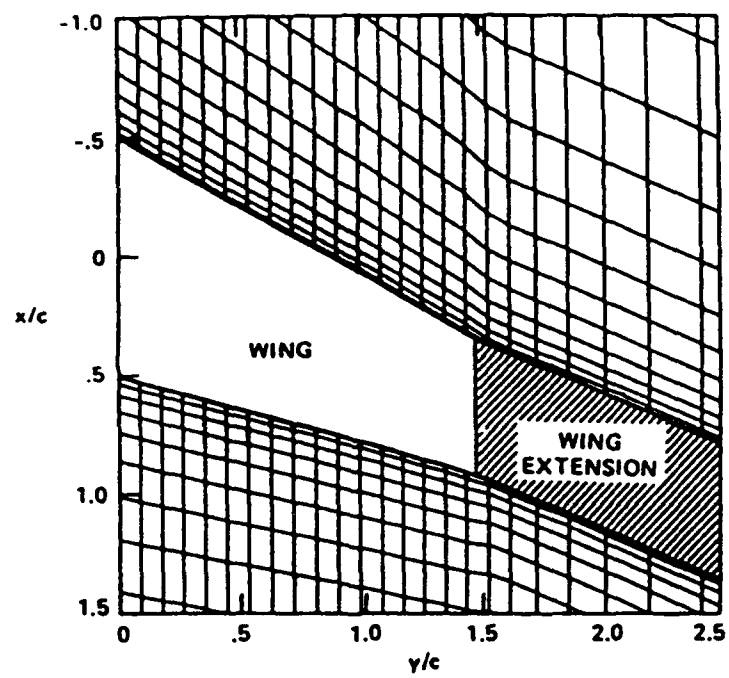

Figure 39. Planform view of TWING grid in Z = 0 plane illustrating grid tapering and clustering near leading and trailing edges and ficticious wing extension

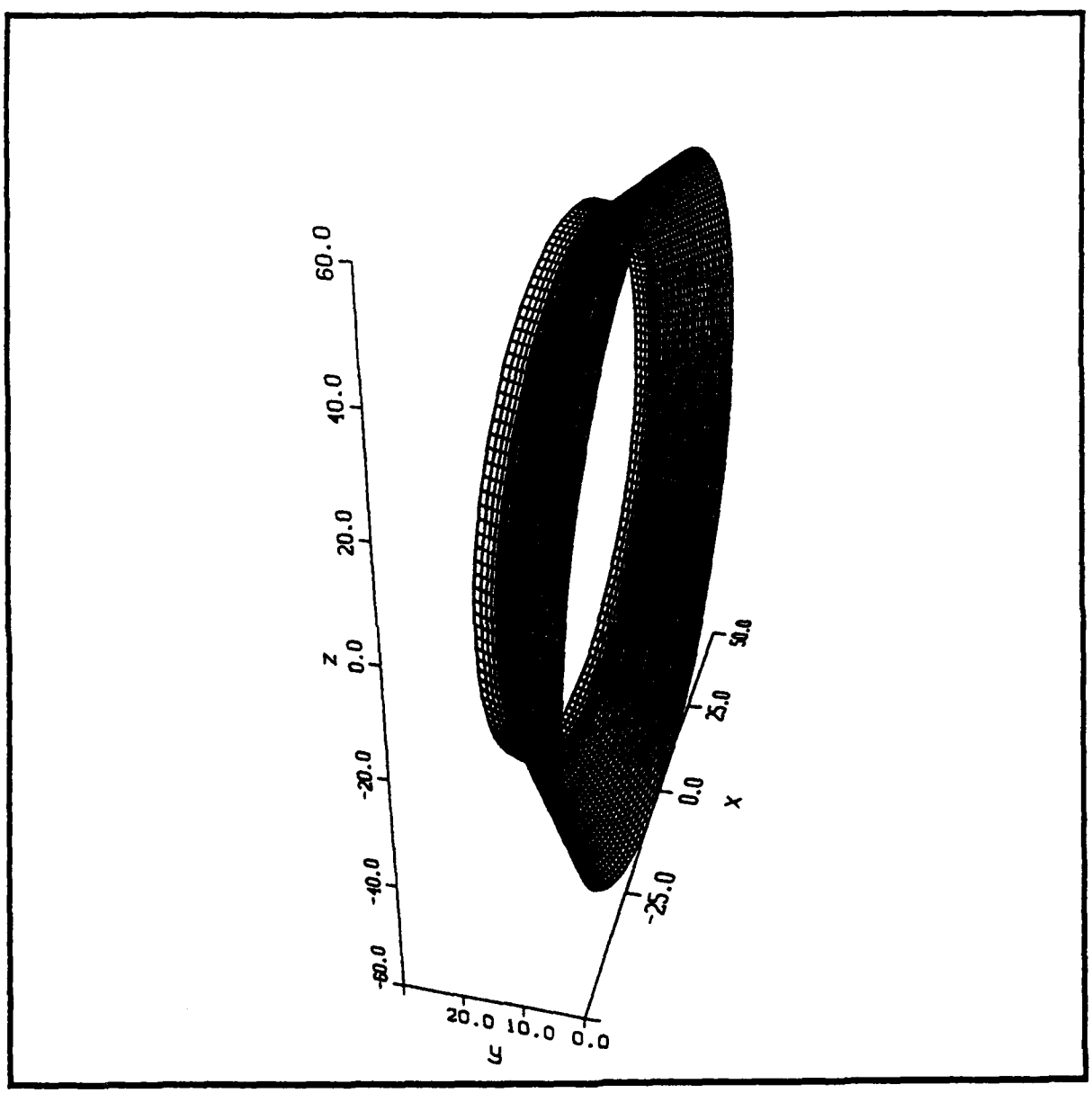

Figure 40. Perspective view of outer boundary of 3-D TWING grid; K = 1 computational grid shell in physical coordinates

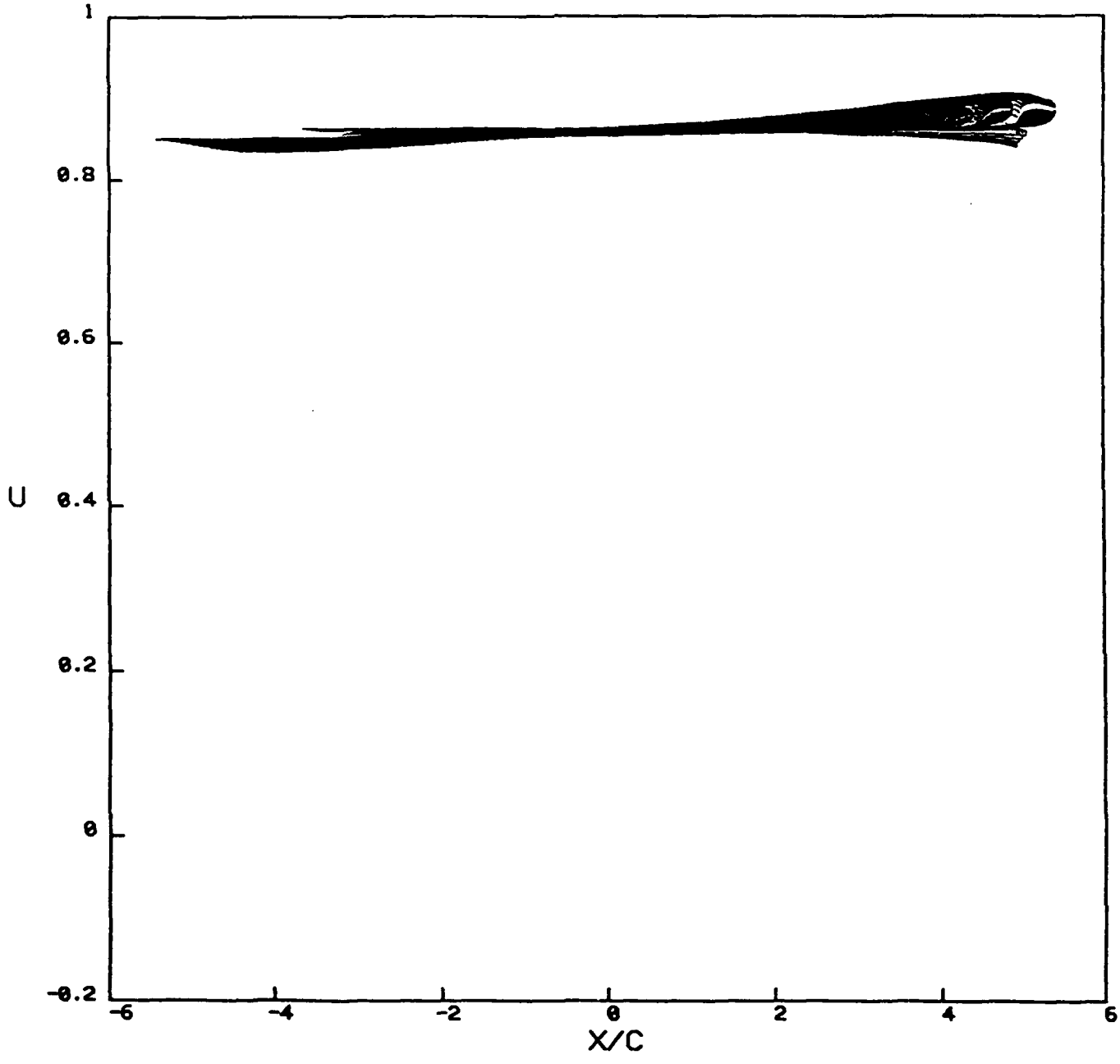

Figure 41. Distribution of U velocity component at the 30 spanwise locations from wing root to sidewall boundary on the K = 2 grid shell

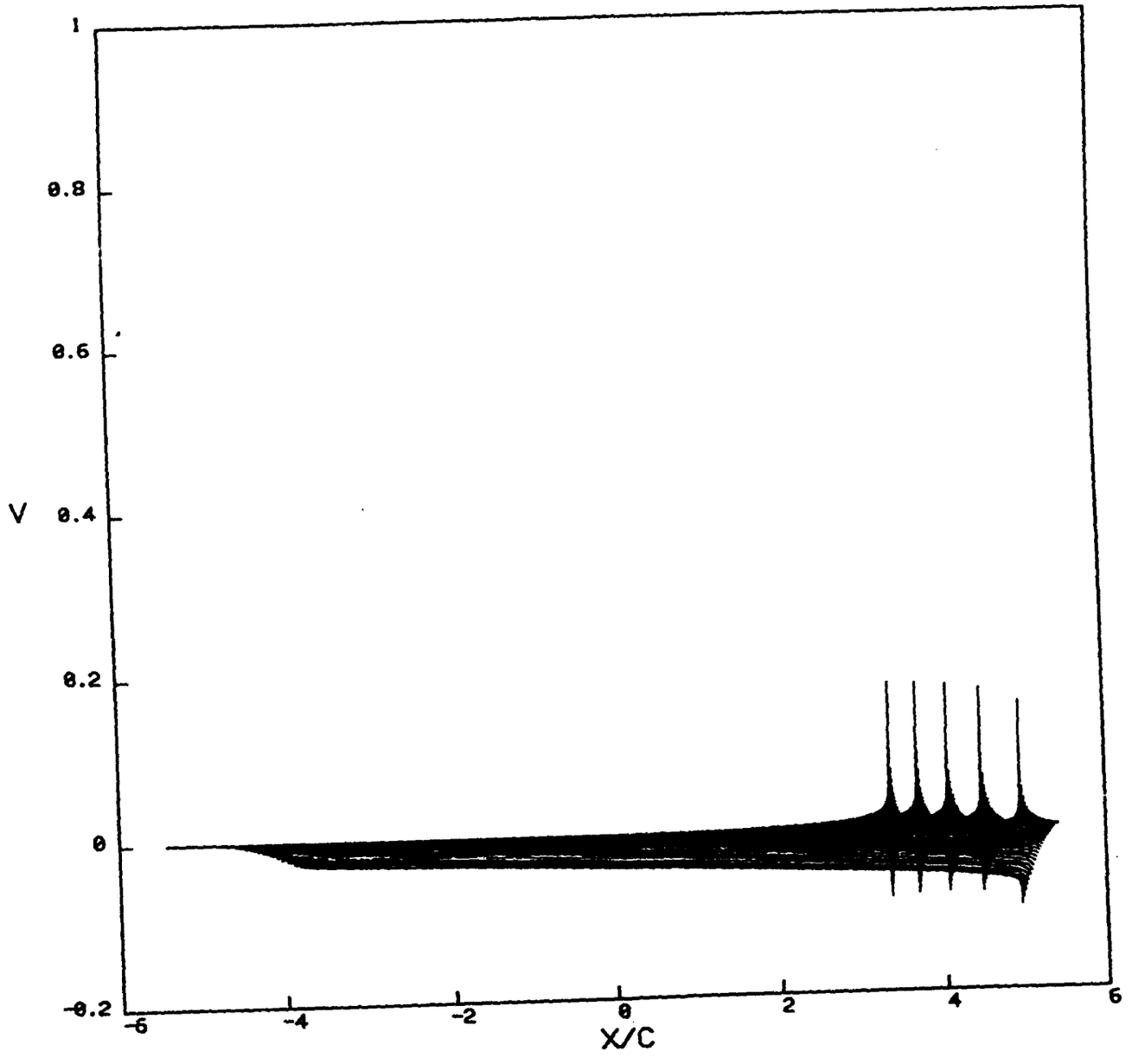

Figure 42. Distribution of V velocity component at the 30 spanwise locations from wing root to sidewall boundary on the K = 2 grid shell

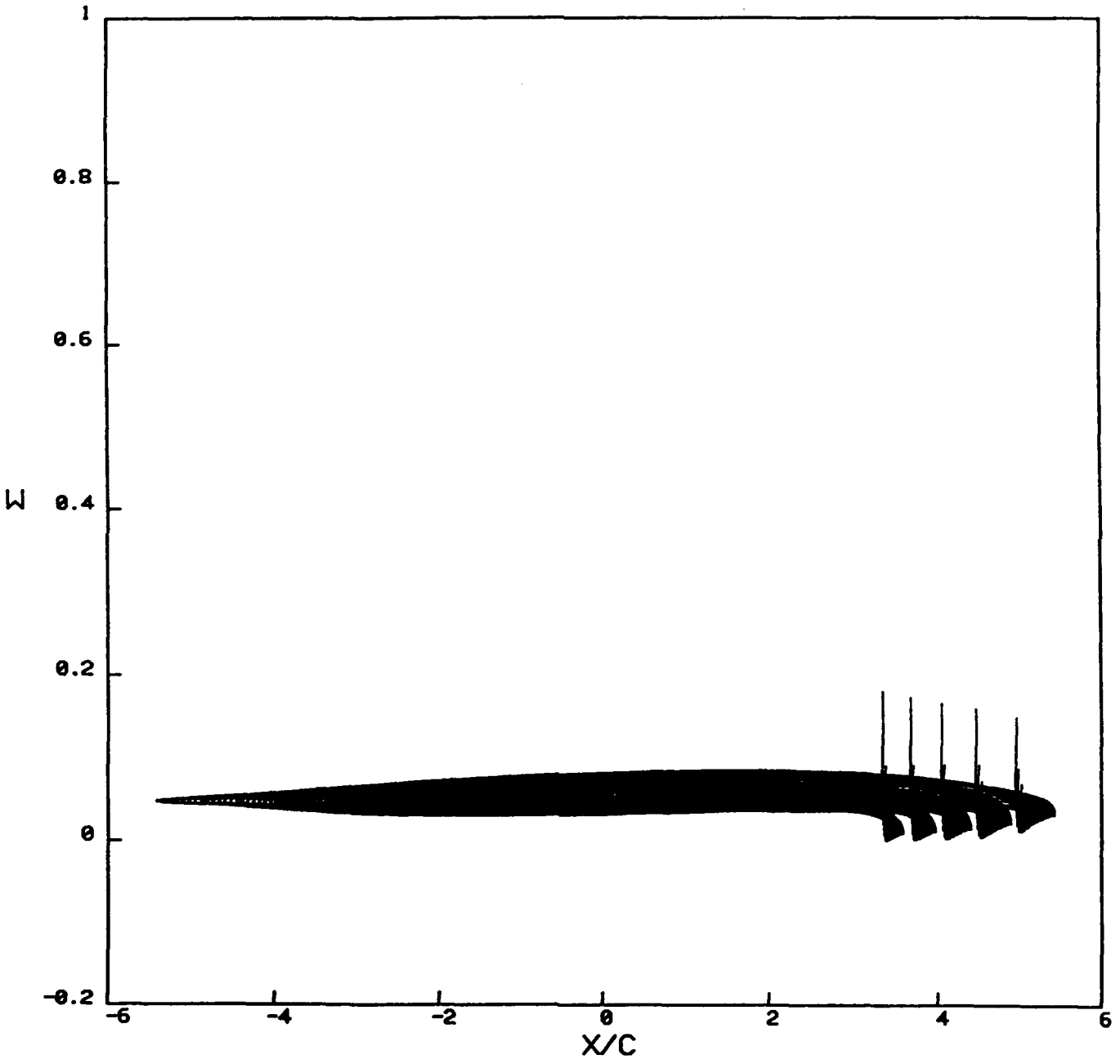

Figure 43. Distribution of W velocity component at the 30 spanwise locations from wing root to sidewall boundary on the K = 2 grid shell

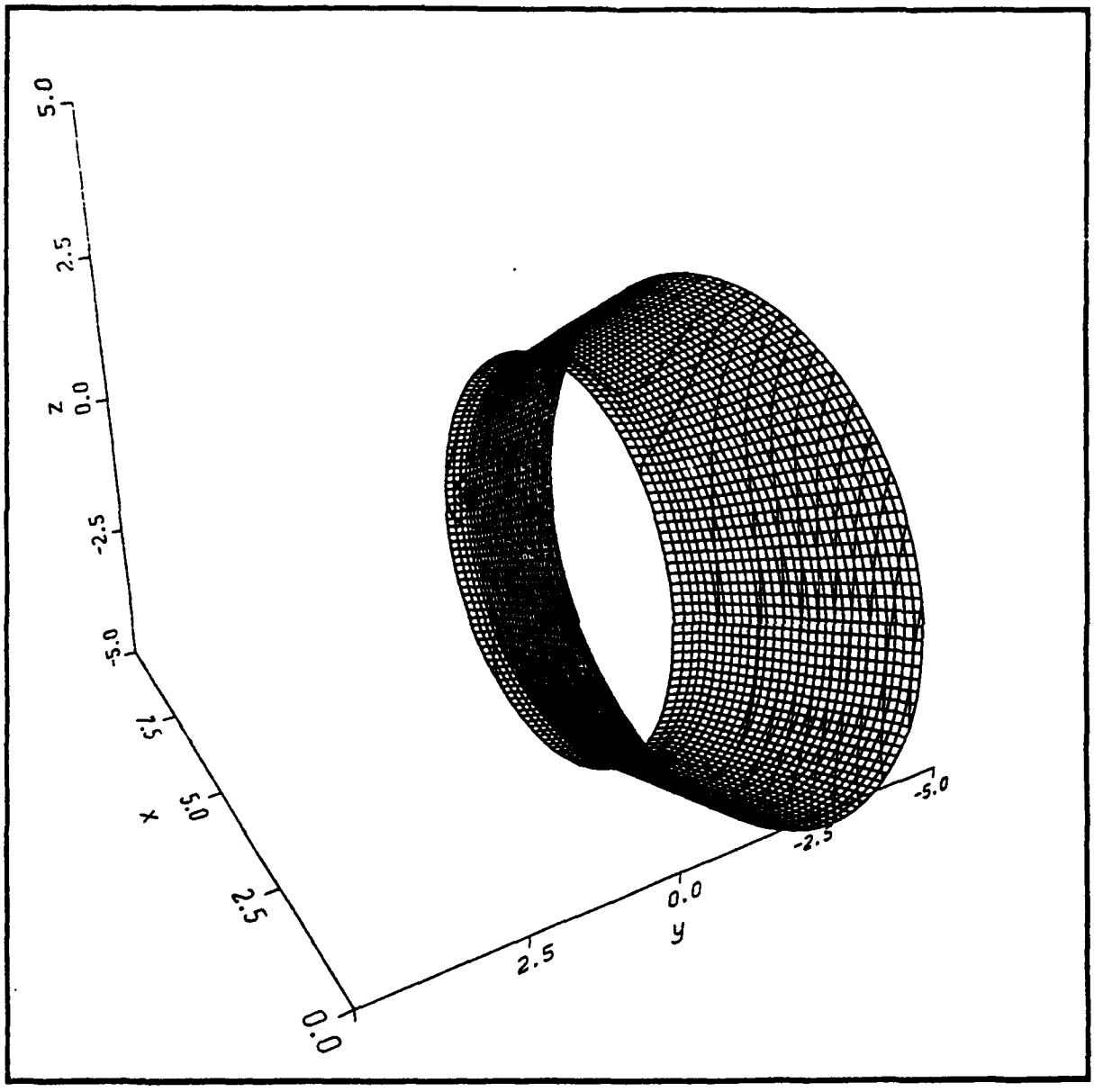

Figure 44. Density contours on the K = 2 computational grid shell illustrating the effect of the wing tip trailing vortex

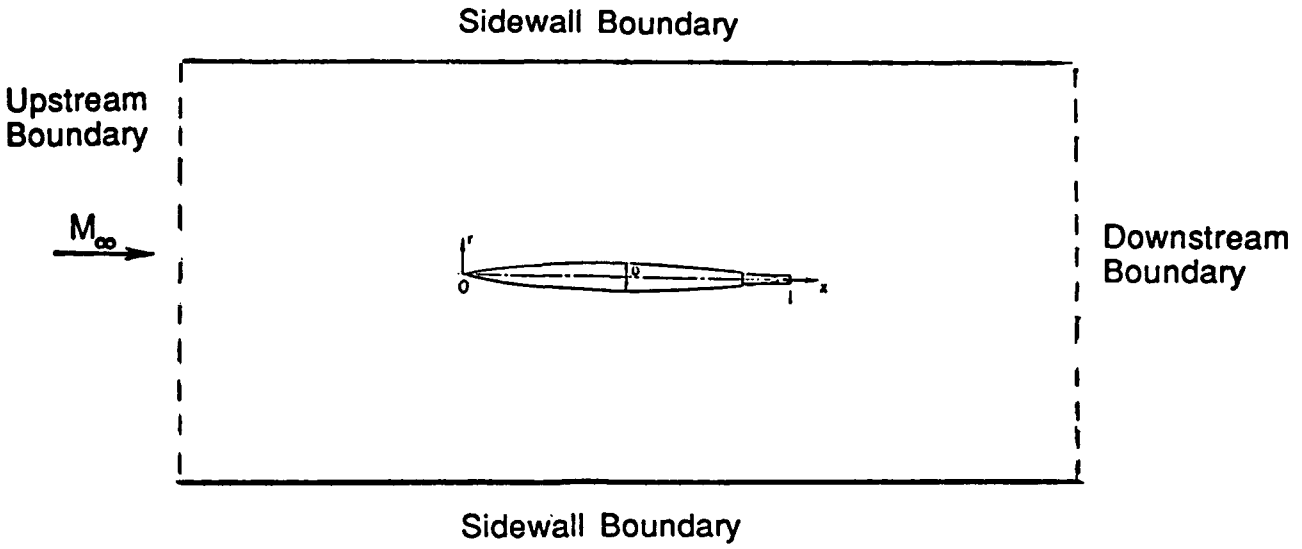

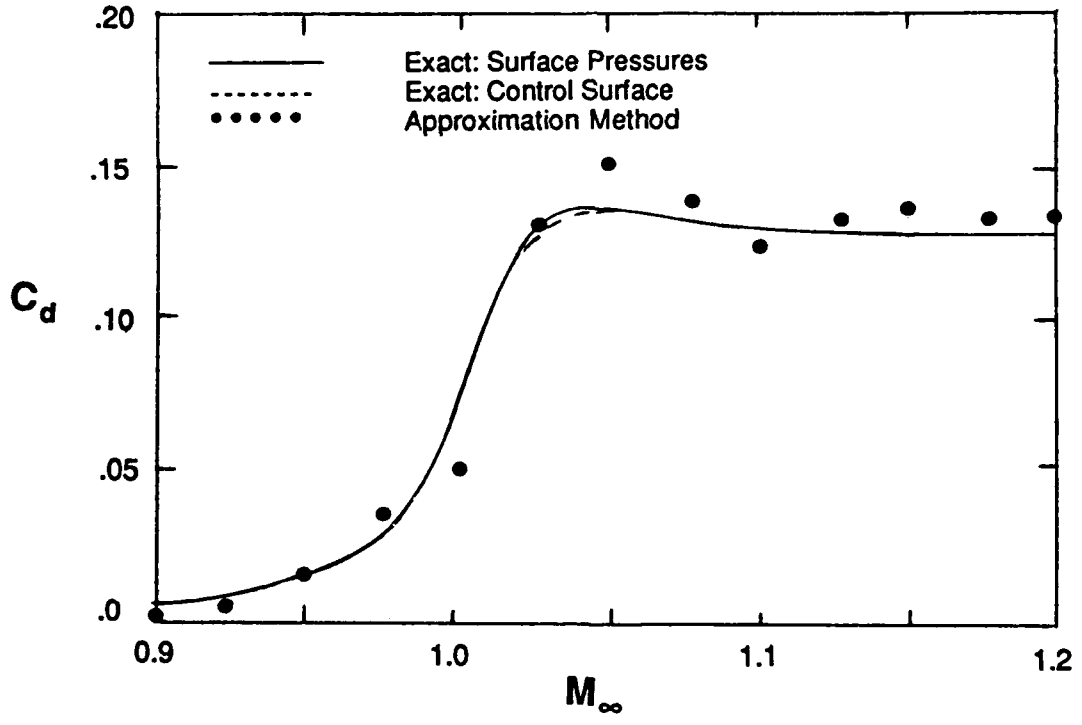

Figure 45. Illustration of test case formulation for approximation method based on using flow field rather than surface properties; axisymmetric transonic flow past a body of revolution with a solid wall outer boundary ; comparison of wave drag predictions

☆U.S. Government Printing Office:1991—648-127/62028